The Dissertation Committee for Stefan Vincent Eccles
certifies that this is the approved version of the following dissertation:

Holographic complexity: bulk tests and implications

Committee:

Willy Fischler, Supervisor

Elena Caceres

Can Kilic

Sonia Paban

Paul Shapiro

Holographic complexity: bulk tests and implications

by

Stefan Vincent Eccles, B.S.Phy.

DISSERTATION

Presented to the Faculty of the Graduate School of

The University of Texas at Austin

in Partial Fulfillment

of the Requirements

for the Degree of

DOCTOR OF PHILOSOPHY

THE UNIVERSITY OF TEXAS AT AUSTIN

May 2021

Acknowledgments

It has been a great privilege to learn and work at UT Austin for my graduate studies. My stay in this town has taught me many things about life and physics. Reflecting on this time period, I am struck by my indebtedness to a great many individuals who offered advice, knowledge, encouragement, and friendship in many forms along the way.

Thanks to my advisor, Willy Fischler, for countless instances of advice and lessons on physical problem solving: reminding me, among other things, to keep the physical question in sight in the midst of a mathematical problem, to leverage numerous approaches against each other in search of mutual consistency and intuition, to take an observer's perspective as a starting point for many problems in cosmology, gravity, and quantum gravity.

Thanks to my committee members. To Elena Caceres for much-needed encouragement and for facilitating the holography journal club. To Sonia Paban and Can Kilic, for many interesting brown bag talks and for their role in making the theory group a pleasant place. To Paul Shapiro for teaching me much of what I know about astrophysics and cosmology. To all members of the UT theory group for passing on aspects of their deep knowledge.

Thanks to the other research collaborators on the projects represented in this thesis: Ming-lei Xiao, Phuc Nguyen, and Ted Jacobson. Special thanks

to Josiah Couch, who has been an invaluable friend and collaborator from the beginning. Thanks to the graduate students who came before me and took a special role in my early training: Dustin Lorshbough, Dan Carney, Aditya Aravind, and Phuc Nguyen. For feedback pertaining specifically to the works in this dissertation, I and my collaborators are indebted to Jacques Distler, Hugo Marrochio, Robert Myers, Cesar Agón, Juan Pedraza, Adam Brown, Shira Chapman, Matt Headrick, Eliezer Rabonovici, Henry Stoltenberg, Netta Engelhart, Veronika Hubeny, Aron Wall, and Brian Swingle.

Thanks to the administration members who have been so helpful to me at various times, especially Janice Duffy, A.J. Bunyard, and Matthew Ervin.

Infinite thanks to my family for unwavering support through times good and bad, without which I don't know where I'd be.

Thanks to my high school physics teacher Drew Neilson and my undergraduate advisor Charles Kankelborg for physics mentorship.

Thanks to my dear friends Abhranil, Josiah, Georgios, George, Ben, Guarav, "the Sarahs," Rustam, Tess, Stacey, James, Garrett, Jaimie, Jared, Eleni, Maria Jose, Behnam, Tyler, and all others who played an indispensable role in my journey thus far, teaching me much about the world and helping me feel at home within it.

Thanks to Jorge Luis Borges, Ray Douglas Bradbury, and Naomi Shihab Nye for placing beauty and inspiration always within arm's reach throughout my studies.

The work in this dissertation was supported by National Science Foundation through grants PHY-1407744, PHY-1620610, PHY-1708139 and PHY-1820712.

Holographic complexity: bulk tests and implications

Publication No. _____

Stefan Vincent Eccles, Ph.D.
The University of Texas at Austin, 2021

Supervisor: Willy Fischler

This dissertation consists of four chapters. The first broadly and briefly orients the reader through an introduction to holographic complexity within the AdS/CFT correspondence. The next three chapters correspond to distinct lines of research conducted during my time as a graduate student, chosen for their thematic relation to holographic complexity, and particularly the two conjectures known as “complexity equals volume" (CV), and “complexity equals action" (CA). Chapter two is based on work conducted with Josiah Couch, Willy Fischler, and Ming-Lei Xiao, studying the holographic complexity of noncommutative field theories under the CA conjecture [1]. Chapter three is based on work with Josiah Couch, Phuc Nguyen, and Ted Jacobson, studying general aspects of the CV conjecture, and addressing certain challenges to that proposal [2]. Chapter four is based on work with Elena Caceres, Josiah Couch, and Willy Fischler, testing proposed extensions of both CA and CV that apply them to subsystem complexity [3].

Table of Contents

Acknowledgments **iv**

Abstract **vii**

List of Figures **xi**

Chapter 1. Introduction: orientation and background **1**
1.1 What complexity? 2
1.2 What bulk quantity? 7
1.3 Tests of the conjectures: evidence and challenges 10
1.3.1 Late-time growth 10
1.3.2 Switchback Effect 11
1.3.3 Early time dependence 14
1.3.4 Subsystem complexity 16
1.4 Summary of remaining chapters 17

Chapter 2. CA and noncommutative gauge theory **21**
2.1 Motivation for this study 22
2.2 Holographic Complexity of 4d $\mathcal{N} = 4$ NCSYM 25
2.2.1 The holographic dual to noncommutative SYM 25
2.2.2 Wheeler-DeWitt Patch Action 28
2.3 Non-Commutativity Enhancement of Complexification Rate . . 33
2.4 Finite Time behavior 38
2.5 Other noncommutative systems 44
2.5.1 Supergravity solutions and decoupling limit 44
2.5.2 Complexification Rates 47
2.5.3 Summary of Results 51
2.6 Conclusion 53

2.7 Appendix I: Calculation of $\dot{S}_{WDW}$ 56
2.7.1 Bulk Contribution 57
2.7.2 Boundary Contributions 59
2.7.3 Joint Contributions 59
2.7.4 Combined Contributions 61
2.8 Appendix II: Thermodynamics and the Lloyd Bound 62

Chapter 3. Complexity as Volume **64**
3.1 Introduction 65
3.2 Volume inside and outside the horizon 70
3.3 Volume current 75
3.3.1 Second law of complexity 77
3.3.2 Complexity flow from UV to IR 78
3.3.3 Asymptotic late time flows on stationary spacetimes . . 80
3.3.4 Asymptotic volume growth and complexity 82
3.3.5 Maximal time from horizon to final slice 83
3.3.5.1 Schwarzschild-AdS black holes 84
3.3.5.2 Upper bound to τ_f set by the AdS scale 85
3.4 Global volume inequality and complexification rate monotonicity 86
3.4.0.1 Monotonicity on a boost-symmetric background 89
3.5 Quenches, rotation and AdS-Rindler: further probes of CV duality 91
3.5.1 AdS-Vaidya: event horizon vs apparent horizon 92
3.5.1.1 Single quench 93
3.5.1.2 Two quenches 99
3.5.2 Rotating BTZ black hole 102
3.5.3 Kerr black hole 104
3.5.4 Rindler wedge complexity growth 108
3.6 Conclusion 110
3.7 Appendix I: Boundary foliation induces maximal bulk foliation 112
3.8 Appendix II: Techniques to evaluate the maximal volume . . . 117
3.8.1 Direct evaluation of flux 118
3.8.2 Flux across a null surface 121

3.9 Appendix III: Stationarity of maximal foliation and volume flow in the late-time regime 123
3.10 Appendix IV: Maximal slices in Vaidya: a closer look 125

Chapter 4. Holographic Purification Complexity **127**
4.1 Introduction 128
4.2 Purification Complexity: Quantum Expectations 132
4.2.1 Definition and Refinements 133
4.2.2 Additivity Properties 135
4.2.3 Basis and Spectrum decomposition 138
4.2.4 Expectations for Holographic States 143
4.3 Holographic Purification Complexity 145
4.3.1 Motivation from Entanglement of Purification 146
4.3.2 Purification Complexity 151
4.3.3 Adding a boundary term 155
4.4 Superadditivity 158
4.4.1 Maximal volumes of subregion wedges 160
4.4.2 CV 2.0 163
4.4.3 Additivity in CA? 164
4.5 Additional Purifications 165
4.5.1 Multisided Black Holes 166
4.5.2 Two sided BTZ black hole: detailed treatment 169
4.5.3 Subregions of pure AdS_3 174
4.6 Conclusion 178
4.7 Appendix I: Calculation of two-sided BTZ Action 180
4.7.1 Setup 181
4.7.2 Bulk contribution 184
4.7.3 Joint contribution 185
4.7.4 Counterterm 185
4.7.5 $\mathcal{A}^T$: full WdW patch action 186
4.7.6 Subregion Action 188

Bibliography **190**

List of Figures

1.1 A Penrose diagram for a two-sided black hole in AdS. With time flowing upward, the growth of the interior region (as indicated by the blue arrows) is the curious feature that motivated the holographic complexity conjectures. 3

1.2 Left: Under the CV conjecture, the boundary state $|\Psi(t_L, t_R)\rangle$ has a circuit complexity proportional to the volume of the maximal codimension-1 bulk surface homologous to the boundary Cauchy surface at times t_L, t_R. Right: Under the CA conjecture, the state complexity is proportional to the action evaluated on the Wheeler-DeWitt (WDW) patch, which is shaded in blue. Both the volume and action are divergent quantities, presumably reflecting the UV-divergence of the CFT state complexity. Usually, a cutoff at finite bulk radius is employed, though for certain discussions (e.g., time-rate change of complexity) are cutoff-independent. 8

1.3 A schematic representation of a circuit implementing the composite operator $U(t)WU^\dagger(t)$. Each horizontal line represents a qubit, and vertically linked dots represent gates which couple the corresponding qubits. Gates are applied in sequence from right to left. In the absence of the simple operator W, the $U(t)$ and $U^\dagger(t)$ would simply cancel. In the presence of the simple operator, some cancellation still occurs at early times (represented by the black gates), but after a time of order the scrambling time it prevents this cancellation minimally for small t, until at a time of order the scrambling time its effect has reached all degrees of freedom and no more cancellation occurs. 13

1.4 A Penrose diagram schematically illustrating the effect of a boundary perturbation in the distant past on the right hand side. A shock localized near the horizon (blue line) quantifies the gravitational back-reaction, thereby altering the maximal volume slice (solid red line), and likewise the WDW patch action (not pictured) in accordance with the switchback effect. . 15

2.1 Two WDW patches separated by δt. Although the boundary of each patch is really at some large but finite r_b, the choice of r_b drops out in the differences we consider and we do not indicate it explicitly in this graphic. 30

2.2 Late time action growth rate normalized by $C = \frac{\alpha^4 \Omega_5 V_3}{\hat{g}_s^2}$ and extra r_H dependence, versus ar_H, which is the Moyal scale measured in units of thermal length. It is observed that the complexification rate under the CA conjecture increases significantly when the Moyal scale is comparable to the thermal scale, and saturate a new bound which is $5/4$ of the commutative value when the Moyal scale is much larger than the thermal scale. . 32

2.3 This circuit represents the end of one copy of a circuit Q_U implementing a hypothetical unitary U and the beginning of a second copy of Q_U. In this plot horizontal lines are qubits, and the dots connected by vertical lines are gates acting on the pair of qubits they connect. For this illustration, we will consider gates to be their own inverse. Gates from two copies may cancel (illustrated here with dashed blue lines connecting the gates), reducing the complexity of the circuit and providing a more efficient way to compute U^N. This cancellation relies, however, on the ability of gates to commute past each other, so that gates which could cancel can meet. We argue that in the noncommutative case, fewer gates commute and so there are fewer cancelations of this type. In this illustration, we see on the third line that a gate which can commute to cancel in the commutative case is prevented from doing so in the non-commutative case due to mild non-locality. Cartoon inspired by one used in a talk by Adam Brown. 36

2.4 Normalized complexification rate versus time in thermal units for $\gamma = 80$ and $b = 0$. 39

2.5 normalized complexification rate versus time in thermal units. γ is held fixed at 80 while $b = ar_H$ is varied. 41

2.6 The vertical axis is the ratio between the local maximum and the asymptotic late time value of the complexification rate. The black, orange and blue curves correspond to $\gamma = 1, 2, 3$. 42

2.7 normalized complexification rate versus time in thermal units. γb^2 is held fixed at 1 while $b = ar_H$ is varied. 43

3.1 Shockwave geometry dual to a perturbed thermofield double state, with a maximal volume hypersurface anchored at late time on the left and early time on the right. 75

3.2 Left: Illustration of the boundary foliation $\Sigma(\tau)$ with 3 slices in the foliation. Right: Illustration of the corresponding bulk foliation by maximal slices, and the volume flow. 77

3.3 Plot of the flow lines of the BTZ volume current (in solid green) on a quarter of a Penrose diagram. Left: the flow lines are shown together with the Schwarzschild coordinate grid lines (dotted black), and the final slice (solid blue). Right: the flow lines are shown together with the maximal slices (dashed red). 81

3.4 An SSA-like inequality is obeyed between the four maximal slices shown (solid red and dashed orange). 87

3.5 On the left are two Cauchy slices, σ_1 (in continuous blue) and σ_2 (in dashed blue), on the boundary of the Poincaré patch of an asymptotically AdS spacetime. On the right the corresponding σ_+ and σ_- are in dashed blue and continuous blue, respectively. 89

3.6 Conformal diagram for the BTZ-Vaidya spacetime in the thin-shell limit for three representative choices of the horizon radius r_+ (left: $r_+ = 5L$, center: $r_+ = L$, right: $r_+ = L/5$). For all three panels, the center of AdS, the infalling shell and the boundary are in continuous black, the horizon is in dashed black and the singularity is in red. Moreover, on the left panel, we depict a maximal slice anchored at a boundary time to the past of the infalling shell in blue. The portion inside the event horizon is in continuous blue, and the portion outside the horizon is in dashed blue. 95

3.7 The region inside the apparent horizon is shaded in blue. . . . 96

3.8 Plot of volume versus boundary time, for a large black hole (left) with $r_+ = 5\ell$ and a small black hole (right) with $r_+ = \ell/5$. In both panels, the blue curve is the volume inside some large cutoff, the red curve is the volume inside the event horizon and the brown curve is the volume inside the apparent horizon. The boundary time is measured in units of ℓ. 97

3.9 Eddington-Finkelstein diagram of the BTZ-Vaidya solution with two infalling shells. The abscissa and ordinate for the plot are $\rho = \arctan(r)$ and $t = v - \rho$, respectively. The two infalling shells, the center of AdS, and the boundary are in thick black, the singularity is in solid red, the constant radius portion of the apparent horizon between the shells is in dashed blue, the event horizon is in short-dashed red, and the maximal slice anchored at late boundary time is shown in continuous blue. The apparent horizon is the boundary of the grey shaded region. . 101

3.10 Plot of the maximal slice volume inside the apparent horizon in a Vaidya spacetime with two shells. The kinks occur when the maximal slice crosses the points where the first and second shells meet the apparent horizon. 102

3.11 Plot of (rate of change of final slice volume ÷ longest time from the horizon to the final slice) :$(T_{\rm H} S_{\rm BH})$, versus the spin parameter for a Kerr black hole in four spacetime dimensions. The ratio is roughly constant over the entire range from nonspinning to maximal spin. 108

3.12 A plot of the final slice of AdS-Rindler embedded into global AdS. Here we use global coordinates for AdS, in which the metric reads $ds^2 = L^2(-\cosh^2\rho d\tau^2 + d\rho^2 + \sinh^2\rho d\phi^2)$, except that we have compactified the radial coordinate by applying the *arctan* function (in other words, the boundary of the cylinder is at radius $\pi/2$). The line running across the cylinder is the bifurcation line of the Rindler horizon. 110

3.13 Hypothetical situation where two maximal slices anchored on different boundary Cauchy slice intersect. 113

3.14 Illustration of the derivation of (3.53). 122

4.1 Entanglement of purification between two interval subregions with non-zero mutual information. The minimal surface whose area gives the entanglement of purification is shown in green. . 148

4.2 We may purify the state on AB to states with different course grainings, corresponding to different cutoffs, shown here as a dashed line. The optimal purification will correspond to cutoff which hugs the RT surface, shown here as a red dashed line. . 150

4.3 A two sided black hole, with different cutoff surfaces on the right side. For each cutoff surface, we have draw the corresponding regulated WDW patch. 154

4.4 The dashed lines in this figure represent the stretched horizon. The purification complexity in CV of the left (right) reduced state is given by the volume of the left (right) green segment plus the red segment. The complexity of the total state is given by the volume of both green segments plus the volume of the red segment. We thus have that $C_L + C_R - C_T$ is given by the volume of the red segment, and as such is positive definite. We may identify the green segments with the basis complexity, and the red segment with the spectrum complexity, as per the discussion in section 3.3 of [4]. 156

4.5 Similarly to CV, we may decompose the action in CA, CV2.0, or CA-2 by associating different parts of the WDW patch to the spectrum, basis, and degeneracy complexity. Roughly speaking, we suggest the green regions should correspond to the basis complexity, the blue regions to the degeneracy complexity, and the red to the spectrum complexity. 159

4.6 A slice through entanglement wedges who share an HRT surface, as in the case of a two-sided BH, or the wedges of two halves of the boundary of pure AdS. 161

4.7 On the left is a spatial slice showing the wedge of a region A, the wedge of a region B, and a 'bridge region.' Here there is clearly a gap between a spatial slice on the A wedge and a spatial slice in the B wedge, as shown in the cross-section on the right. We can however always bridge this gap by an arbitrary spatial slice of the bridge region which meets the slices associated to A and B respectively at their boundaries 162

4.8 The WDW patch for a two-sided black hole, outlined with dashed lines. If we consider subregion A to be the left boundary and subregion B to be the right boundary, then the entire outside of the horizon on the left side, w_L, is the entanglement wedge of A, and likewise for the right side and B. The entanglement wedge of AB is the whole spacetime. 164

4.9 The above plots show the difference between the total state complexity $C_T = C_{LR}$ and the sum of left and right subregion complexities $C_L + C_R$ for the BTZ black hole at $t_L = t_R = 0$, computed using the complexity=action prescription. Positive values indicate that the left and right factors behave superadditively, and negative indicates subadditivity. The cutoffs are constant z surfaces $z_R = \delta_R$, $z_L = \delta_L$ and various choices of $\tilde{L}/L_{AdS}$ are displayed. Positivity in the strict UV limit ($\delta_L \to 0$ and $\delta_R \to 0$) requires that the lengthscale $\tilde{L}$ be chosen greater than L_{AdS}, so only such lines are displayed. The dashed portions of each line are excluded if we demand positivity of the total state complexity as well as both subregion complexities at the corresponding cutoffs. We find that in the remaining parameter space the system always behaves superadditively: $C_T > C_L + C_R$. 171

4.10 A conformal diagram for the two-sided BTZ spacetime is shown in the left panel. The Wheeler-DeWitt patch corresponding to the total state is shaded in light red, while dark red indicates the subregion of interest for the right subregion computation. Both regions are "diamond shaped" so we adopt a shared labeling scheme for the joints and null boundaries, as illustrated in the right panel. 182

4.11 The cutoff prescription utilized in this work is that of the left diagram. 183

Chapter 1

Introduction: orientation and background

The AdS/CFT correspondence [5–7] provides a remarkable duality between gravitational theories living in asymptotically anti-de Sitter spacetimes and non-gravitational quantum conformal field theories defined in one lower dimension. It currently provides the most rigorous instantiation of the holographic principle, and as such has been a continual source of insight into questions of quantum gravity for the last two decades.

At a high level, the AdS/CFT equivalence is often stated as an equality between the gravitational partition function in asymptotically AdS spaces and the generating functional of correlators in the CFT. Even accepting this equivalence in full, the precise mapping or "dictionary" between physical quantities in the two languages is highly nontrivial. Understanding this dictionary and identifying its useful entries[1] is an overarching goal of ongoing AdS/CFT research.

The holographic complexity conjectures of Susskind and collaborators [8–12] posit that one entry, or a family of related entries, into the AdS/CFT

[1] "Useful" means different things to different researchers, depending on how they wish to utilize the correspondence. For our purposes, understanding the mapping itself is of interest, as it elucidates how gravitational physics can emerge from a purely quantum theory.

dictionary should relate the quantum circuit complexity of the boundary state to a bulk analog in one of several variables. The conjecture initially emerged from a question about black holes: what, on the boundary side of AdS/CFT, corresponds to the continual growth of the behind-the-horizon region of black hole spacetimes? Consider a two-sided, eternal black hole solution, dual to the thermofield double state [13, 14]. From the perspective of either boundary density matrix, the state is thermal and static: no interesting dynamics occur in the entropy or associated quantities of black hole thermodynamics. Yet something about the way these two density matrices are "glued" together encodes the ever-growing spacetime region behind the horizon, indicated schematically by the blue arrows in figure 1.1. That such behavior must be captured by a more fine-grained notion than the entanglement entropy is apparent [9], but what sort of quantum mechanical quantity could do the job? The answer, according to the conjecture, is the quantum circuit complexity of the boundary state.

1.1 What complexity?

As employed in holography, the quantum circuit complexity[2] [15–17] can be thought of as an answer to the following question: how many simple operations are necessary to prepare a given state or unitary? As phrased, this question is imprecise. But before stating a more rigorous definition we

[2]Throughout this work the terms quantum circuit complexity, quantum complexity, and complexity will be used synonymously.

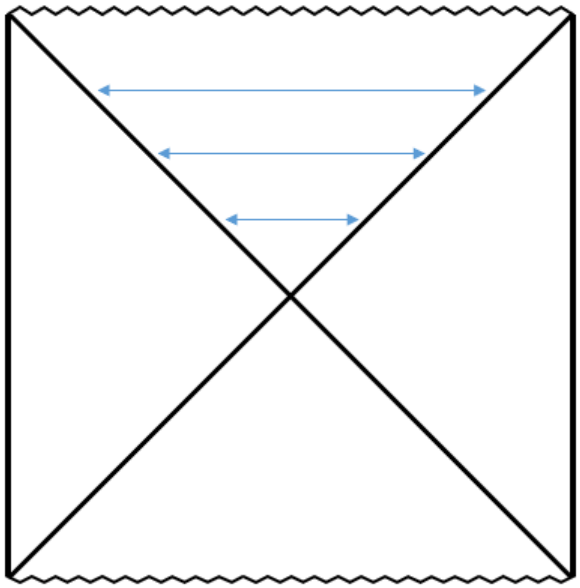

Figure 1.1: A Penrose diagram for a two-sided black hole in AdS. With time flowing upward, the growth of the interior region (as indicated by the blue arrows) is the curious feature that motivated the holographic complexity conjectures.

consider the following example, which intuitively captures how the concept is employed in holography. Consider three states of an N-qubit system in the computational basis:

$$|\Psi_1\rangle = |000000000\ldots0000\rangle$$

$$|\Psi_2\rangle = |000000000\ldots0001\rangle$$

$$|\Psi_3\rangle = |110010001\ldots1100\rangle$$

How close to each other are these states? We could define a notion of closeness on the Hilbert space via the Fubini-Study metric [18, 19] or a similar

metric based on the inner product:

$$d_{FS}(\Psi_i, \Psi_j) = \arccos(\langle \Psi_i | \Psi_j \rangle).$$

By this measure, all of the states above are as far apart from each other as possible, by virtue of being orthogonal. However there is an intuitive notion of closeness not captured by this metric: states Ψ_1 and Ψ_2 differ by a single qubit flip, while Ψ_3 is relatively scrambled. This apparent difference is entirely basis-dependent, but it is this intuition that quantum complexity can codify and capture.

To define quantum complexity precisely requires several choices. First pick a reference state $|\Psi_{ref}\rangle$ in the relevant Hilbert space $\mathcal{H}$. [3] Also choose a small tolerance parameter ϵ. Lastly, choose a set of allowed gates $G = \{g_i\}$, where each gate g_i is a unitary on the Hilbert space. These gates define what we mean by simple operations. The choice of gates is arbitrary except for the following restrictions. For any gate g_i in G, its inverse g_i^{-1} must also be in G. The gate set must also be universal, meaning that any unitary can be approximated (to within ϵ, in a sense indicated in the forthcoming definition) by a finite, ordered set of gates, which we call a quantum circuit. Finally, define the quantum complexity of state $|\Psi\rangle$ to be the minimum number of gates that can build a quantum circuit which takes the reference state to the target state, to within the tolerance:

[3] For now we consider a finite-dimensional Hilbert space.

$$C(|\Psi\rangle) = \min(N) : d_{FS}\left(\left(\prod_{i=1}^{N} g_i\right)|\Psi_{ref}\rangle, |\Psi\rangle\right) < \epsilon. \tag{1.1}$$

Likewise, the operator complexity of a unitary U is the minimum number of gates required to implement a circuit (a string of gates) which approximates a given unitary to within the desired tolerance:[4]

$$C(U) = \min(N) : \left|\left|\prod_{i=1}^{N} g_i - U\right|\right| < \epsilon. \tag{1.2}$$

Based on this definition, it is apparent that a quantum complexity measure is far from unique. The appropriate generalization to infinite-dimensional Hilbert spaces and CFT states in particular is also far from settled. See [20–25] for a selection of work on this topic, and see [26, 27] for nice discussion of "complexity geometry", an effort to replace the discrete counting problem of quantum complexity with a related notion that is manifestly continuous and more geometric, by defining a related metric on the Hilbert space [28, 29]. Despite these difficulties, the features of quantum circuit complexity that recommend it for consideration in holography are quite general, particularly its scaling properties and its time-dependence. To gain intuition about these behaviors, we again look to N-qubit systems. For generic k-local Hamiltonians exhibiting chaotic behavior, states very quickly thermalize in the sense that any small subsystem quickly becomes approximately maximally mixed with its complement on a time scale of order $log(N)$. This is indicated by the

[4]Here $||A|| = \sqrt{\rho(A^\dagger A)}$ and ρ the spectral radius.

subsystem reaching near-maximal entanglement entropy, and it corresponds to the de-localization of information initially associated with any local perturbation. Yet long after thermalization, the quantum complexity continues to grow linearly. This continues for a time that is exponential in the number of degrees of freedom. Eventually, complexity saturates and fluctuates near it's maximal value, at least before quantum recurrence occurs on time scales doubly-exponential in the size of the system. For any state that is not close to maximal complexity, it is overwhelmingly likely that Hamiltonian evolution carries it to increasing complexity, in a manner analogous to the entropy increase of the second law of thermodynamics. This is dubbed the second law of complexity [27].

The systems just described correspond in several ways to black hole physics. Black holes are known to be "fast scramblers", in the sense that localized perturbations spread throughout the system on a time scale known as the scrambling time $t_* \sim \beta \log(S)$. Such a process is also referred to as thermalization because it rapidly takes the dynamical black hole system to a static or stationary black hole end state, with its corresponding thermal properties. Meanwhile, under the holographic complexity conjecture, the state complexity's continual linear growth is thought to correspond to the continual linear growth of the region behind the horizon. Saturation and recurrence are not expected to be captured in the static black hole spacetimes, as the relevant timescales would require that quantum processes such as evaporation ought to be considered.

1.2 What bulk quantity?

To have a meaningful correspondent in the states of the CFT, this behind-the-horizon growth must be captured by a gauge-invariant variable, which in this context means a bulk quantity that is invariant under diffeomorphisms leaving a given boundary state fixed. The first bulk quantity postulated for this purpose was the maximal volume among codimension-one hypersurfaces ("slices") that are homologous to a fixed boundary Cauchy surface [8–10]:

$$C_V(\sigma) = \max_{\sigma=\partial\Sigma}\left[\frac{\mathrm{Vol}(\Sigma)}{G_N l}\right] \tag{1.3}$$

.

Here σ is a boundary Cauchy surface on which the CFT state is defined, and Σ is a codimension-one bulk hypersurface with boundary σ. The length scale l is necessary to make the right-hand side dimensionless, and it is usually taken to be the AdS scale L. This gives the expected late-time growth rate for large black holes, while for small black holes the same criterion would require $l \sim r_h$, the horizon radius. The choice of lengthsale l will be discussed extensively in chapter 3, where we suggest that it be chosen to correspond with a particular length scale that is intrinsic to the black hole geometry. Regardless, the apparent lack of universality in the choice of length scale was a motivating factor behind the follow-up conjecture, known as complexity equals action [12, 30]:

$$C_A(\sigma) = \frac{I_{WDW}}{\pi\hbar} \tag{1.4}$$

.

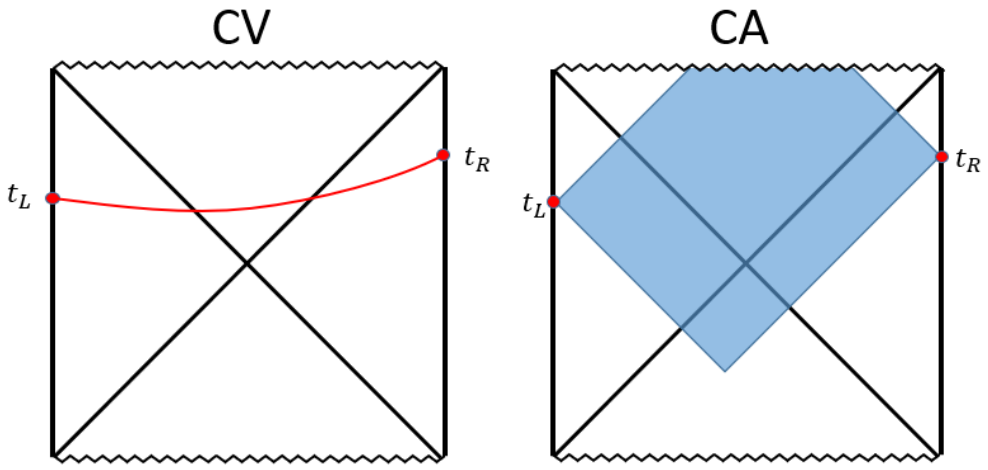

Figure 1.2: Left: Under the CV conjecture, the boundary state $|\Psi(t_L, t_R)\rangle$ has a circuit complexity proportional to the volume of the maximal codimension-1 bulk surface homologous to the boundary Cauchy surface at times t_L, t_R. Right: Under the CA conjecture, the state complexity is proportional to the action evaluated on the Wheeler-DeWitt (WDW) patch, which is shaded in blue. Both the volume and action are divergent quantities, presumably reflecting the UV-divergence of the CFT state complexity. Usually, a cutoff at finite bulk radius is employed, though for certain discussions (e.g., time-rate change of complexity) are cutoff-independent.

The complexity in this proposal is simply proportional to the action computed on the Wheeler-DeWitt (WDW) patch, the union of bulk points that are timelike or null separated from the boundary Cauchy slice σ (the boundary of which is obtained by following future and past-directed null rays inward from the boundary slice). The computation of the action also includes

some ambiguities associated with the contributions of null boundaries and codimension-2 "joints", though these choices do not affect the late time growth rate. It has been suggested that the freedom associated with these parameters could be associated with freedom in gate choices [20].

In addition to these conjectures, several modified proposals have been made utilizing related bulk quantities, including the spacetime volume on the WDW patch (CV 2.0, see [31]) and the action without kinetic terms (CA-2, see [32]). These succeed in passing some of the general tests described below but differ in detailed behavior. The proliferation of bulk quantities supposedly dual to a quantum complexity may not be too surprising, considering that the latter is far from unique. However, it also certainly indicates that much remains to be understood before the conjecture can be made precise. The bulk quantities in question are all sensible, gauge-invariant variables, so they must have a corresponding notion in the boundary theory. Action and volume are fundamental bulk quantities, irrespective of their relationship to complexity; investigating their behavior in holographic systems to understand their emergence from the dual theory is an interesting goal in its own right. In this spirit, most of the work in the following chapters restricts focus to the original CV an CA proposals, though in chapter 4 we also discuss CV 2.0.

1.3 Tests of the conjectures: evidence and challenges

1.3.1 Late-time growth

The most suggestive correspondence between these bulk quantities and quantum circuit complexity is already mentioned as motivation: the indefinite linear growth that follows any transient effects. For thermal systems, the complexity growth rate is expected to be proportional to $T * S$ [8], with the temperature T setting the timescale on which gates operate, and the entropy S indicating the number of active degrees of freedom.

Early statements of the conjecture also hoped that the late-time complexification rate[5] for black holes would precisely saturate a speed limit on computation known as the Lloyd bound [33], which was used to set the precise coefficient in the CA conjecture. The bound states that the maximal rate of computation for a system is $2E/\pi\hbar$, with E being the system's energy. However, this use of the Lloyd bound has been called into question based on more general models of quantum computation [34] and by noting that its application to holographic states assumes that time evolution occurs as a series of transitions between orthogonal states [35]. Regardless, holographic computations indicate that the proposed bulk quantities do not obey this bound universally. For instance, in [36] it was noted that Schwarzschild-AdS black holes at late times actually saturate this bound from above. Similar behavior is observed in the noncommutative systems explored in chapter 2, where it is also found

[5] We will often refer to the time-rate change of complexity as complexification rate.

that the presence of noncommutativity enhances the late-time complexification rate beyond any bound that might have been supposed saturated in the commutative limit.

As already mentioned, the CV proposal requires a length scale l in the statement of the conjecture. The expectation that $\dot{C} \sim TS$ entails that for large black holes, l should be the AdS scale, up to a dimension-dependent numerical factor. On the other hand, for small black holes this would require l be of order the horizon radius. Chapter 3 proposes that this length scale may be understood as the maximum proper time for an observer to fall from the horizon to a particular slice that determines the late-time growth rate in CV. This choice achieves the correct scaling $\sim TS$, though the precise coefficient differs depending on spacetime dimension and other details of the black hole[6]. By contrast, the Action achieves $\lim_{t\to\infty} \dot{C} = 2M/\pi\hbar$ for a wide class of black holes, regardless of dimension. Though, as already stated, the action approaches this late time growth rate from above, so it cannot be understood as a straightforward saturation of the Lloyd bound.

1.3.2 Switchback Effect

An interesting and nontrivial test of the correspondence comes from the switchback effect [10], which considers the change in complexity of a state after evolution due to a "precursor" operator $\mathcal{P}(t) = U(t)WU^{\dagger}(t)$. Here W

[6]It is not necessarily expected that the overall coefficient is the same for all systems, and identifying the appropriate notion of complexity (gate set, ..., etc.) may clarify these factors.

is a simple operator (low complexity), and U is the time evolution operator. To understand how the complexity of such an operator depends on time, note that for all times, we have

$$C(\mathcal{P}) < C(U) + C(W) + C(U^\dagger) = 2C(U) + C(W) \approx 2C(U).$$

Here we're using the fact that any circuits that build the individual operators can be stacked sequentially to build the total operator (and W is a low complexity operator). However, this may be far from optimal. For instance, if the operator W were the identity, or more generally if $[U, W] = 0$, then the time evolution operators cancel and do not contribute anything to the complexity. For a simple operator W, the expectation in a circuit model is that immediately after its application, it only prevents such cancellation minimally as its effect is restricted to a region of the circuit that is localized in the relevant basis (see figure 1.3). However as its effect propagates throughout the system, less cancellation between $U$and $U^\dagger$ occurs, and after the scrambling time t^* the effect of W has spread throughout the entire system, and no such cancellation occurs. After that, the total complexity grows linearly at twice the rate of the time evolution unitary. Correspondingly, the complexity of a state that is acted upon by a precursor operator is expected to be, at least for $t >> t^*$

$$C(\mathcal{P}(t)\,|\psi\rangle) \propto 2E(t - t^*). \tag{1.5}$$

We can generalize this expectation to include multiple simple operators placed in arbitrary time sequence and with arbitrary time offsets be-

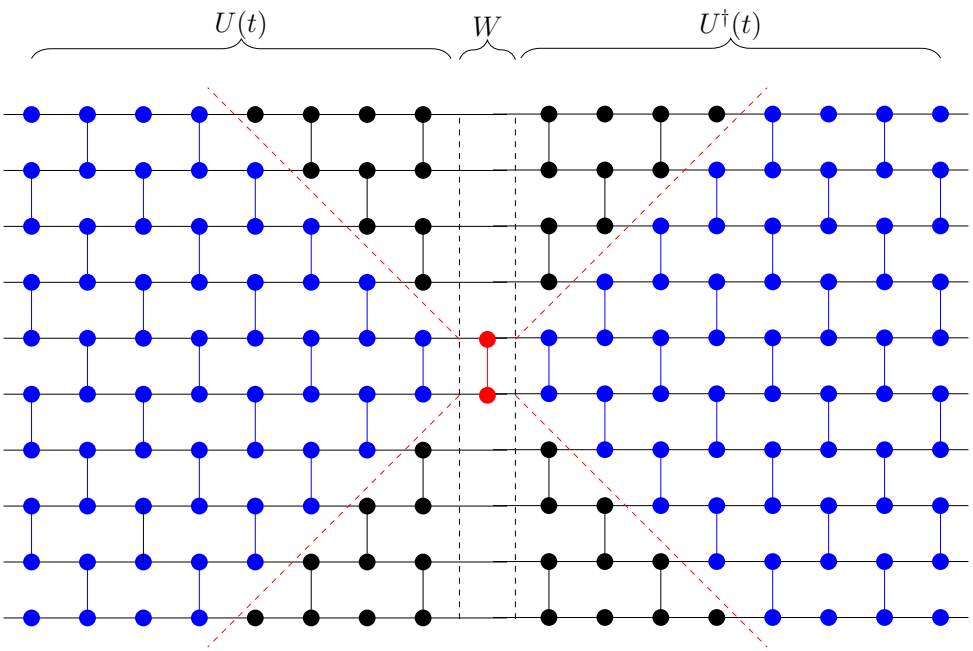

Figure 1.3: A schematic representation of a circuit implementing the composite operator $U(t)WU^\dagger(t)$. Each horizontal line represents a qubit, and vertically linked dots represent gates which couple the corresponding qubits. Gates are applied in sequence from right to left. In the absence of the simple operator W, the $U(t)$ and $U^\dagger(t)$ would simply cancel. In the presence of the simple operator, some cancellation still occurs at early times (represented by the black gates), but after a time of order the scrambling time it prevents this cancellation minimally for small t, until at a time of order the scrambling time its effect has reached all degrees of freedom and no more cancellation occurs.

tween each. The expectation is then that the complexity of the total operator is proportional to the sum of the absolute value of the time offsets, minus $2t^* n_{textsb}$, where $n_{\rm sb}$ is the number of "switchbacks" or reversals of time ordering. This is because each switchback allows some cancellation of the adjacent time-evolution operators, but the complexities simply add linearly after scrambling has occurred.

This intuition has a corresponding story in the bulk physics of black hole spacetimes. A simple operator applied in the distant past in the boundary theory corresponds to a small injection of energy, which then grows in influence as it falls toward the black hole. The effect of such an injection on the bulk spacetime can be approximated analytically using null shockwave geometries, which effectively glue together two vacuum solutions across a null surface containing the stress tensor contribution of the infalling stress-energy. In these geometries, both the WDW patch action and the max volume computations are altered by the presence of the shock, with the result that the complexity matches equation 1.5 (e.g. figure 1.4).

1.3.3 Early time dependence

Most of the preceding discussion focuses on the late-time limit (or at least times past any transient effects) of the bulk quantities, where the behavior ought to match the linear growth regime of quantum complexity. The finite-time behavior also provides an interesting lever by which to distinguish the various bulk quantities. For a thorough discussion of time-dependence, see [37], where many of the following results were worked out for the first time.

The action and the volume do, in fact, behave quite distinctly at early times in Schwarzschild dS spacetimes. For instance, the action has a period over which it is constant, followed by a brief negative divergence in the complexification rate which then grows to slightly exceed the expected late time value, and then approach this limit from above. These behaviors seem at

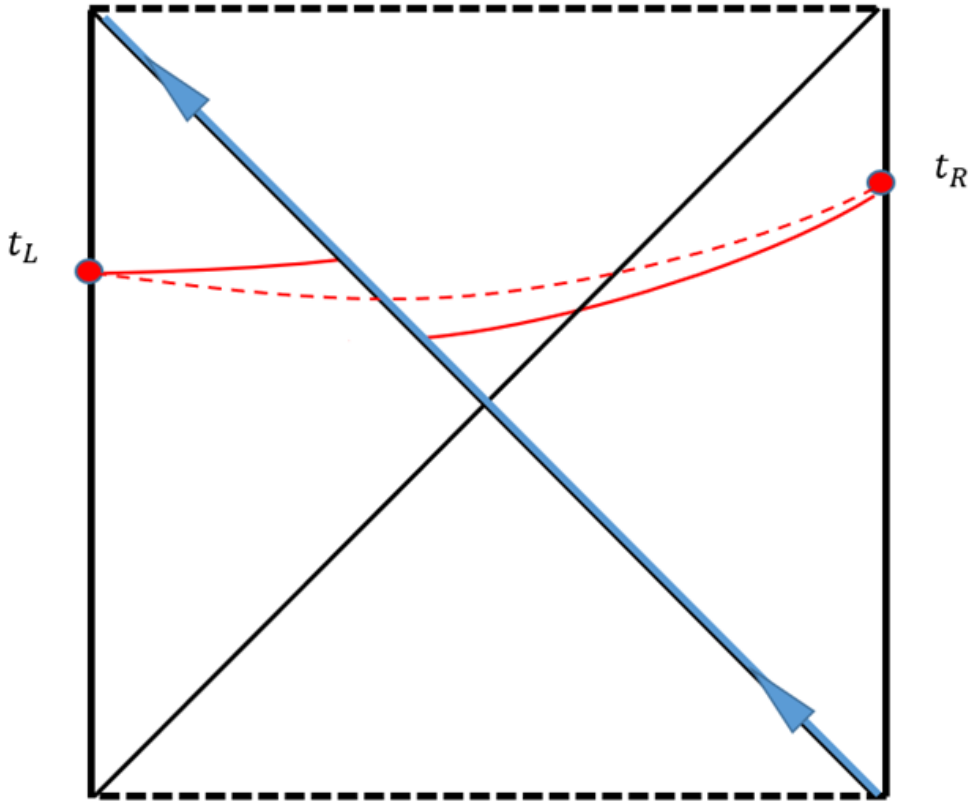

Figure 1.4: A Penrose diagram schematically illustrating the effect of a boundary perturbation in the distant past on the right hand side. A shock localized near the horizon (blue line) quantifies the gravitational back-reaction, thereby altering the maximal volume slice (solid red line), and likewise the WDW patch action (not pictured) in accordance with the switchback effect.

odds with a complexity interpretation, though it has been argued that one should time-average over a few thermal times scales to eliminates the negative divergence since the conjecture should not be taken seriously on sub-thermal timescales.

By contrast, the volume is a positive definite quantity, and as we show

in chapter 3 the complexification rate under CV can be shown to increases monotonically in spacetimes with a boost symmetry.

1.3.4 Subsystem complexity

The original complexity conjectures concerned the state complexity of the full boundary state. A natural generalization is to consider the corresponding bulk quantities when restricted to subregions. The action or volume computed on an arbitrary bulk subregion is not expected to have particular meaning in the boundary theory (recall our restriction to gauge-invariant variables). However, a particular bulk subregion known as the entanglement wedge is thought to be uniquely dual to the density matrix on a corresponding boundary subregion [38–40]. Perhaps the action or volume restricted to an entanglement wedge corresponds to the complexity of the corresponding boundary theory density matrix. There is an immediate problem with this generalization of the complexity conjecture(s); the complexity of a density matrix does not have an established definition. In fact, there are multiple plausible definitions, but if the bulk subregion correspondence computes any one of them it is not immediately clear which it is. Regardless, such extended conjectures for holographic subsystems refer to the "subregion complexity" [4, 41–43], and try to compare the behavior of the bulk quantities to expectations from various notions of quantum subsystem complexity. Chapter 4 of this thesis focuses on one proposal known as the "purification complexity," which defines the complexity of a density matrix as the minimal state complexity

among states which purify the density matrix.

1.4 Summary of remaining chapters

The remainder of this work details three independent lines of research into various aspects of holographic complexity. These chapters are largely independent, and can therefore be read in a standalone manner, and each contains its own conclusions and appendices.

In chapter 2 we undertake a detailed investigation of the CA proposal in spacetimes that are dual to noncommutative gauge theories. We compute the action in such spacetimes and investigate both its finite-time and late-time dependence. We find that maximal noncommutativity has the effect of increasing the late-time complexification rate by a simple improper fraction beyond the commutative value. The precise fraction differs depending on the brane dimension and the number of noncommuting directions. We then provide a heuristic explanation, using a simple circuit model, for why the noncommutativity might affect the complexity in this way. At finite times, we find that the complexification rate exhibits behaviors analogous to those found in [36], in particular that there is a negative logarithmic divergence at early times followed by a quick rises to a maximum positive value before approaching the late-time complexification rate from above. The negative divergence must be eliminated by averaging over a thermal time scale or some other method if the complexity interpretation is to make sense. The occurrence of a maximum rate prior to the late time limit is not a strict a violation of the complexity

correspondence, though it is surprising and does contradict the claim that the late time rate is saturating an upper bound such as the Lloyd bound, which we discuss this in some detail.

In chapter 3 we revisit the CV conjecture. We first attempt to address one of the main shortcomings of the original proposal: volume does not yield a late time complexification rate proportional to T times S for all black hole systems using any fixed length scale to define the conjecture. We propose that a particular length scale intrinsic to black hole geometries should be used, eliminating this problem. However, the use of this length scale seems to render the CV conjecture ill-defined outside the context of black hole spacetimes. We argue that this is not as restrictive as if first appears if one considers, for example, Rindler horizons. Regardless, a generalization to fully dynamical and non black hole spacetimes may exist, though we do not propose any full generalization. In fact, we argue that it might be appropriate to restrict the conjecture to thermal contexts where certain ambiguities associated with complexity can be easily eliminated. We also argue that the appropriate cut-off prescription may be at the thermal scale itself (i.e. count only the volume behind the horizon). We also employ a "volume current," a particular vector field uniquely associated with a foliation of the bulk spacetime by maximal slices. Such a current gives an alternative view on the CV duality, where it is the flux of this current that is dual to the circuit complexity. This picture suggests that complexity flows from the UV to the IR. It also provides a simple proof that the volume behind a future horizon is always increasing,

entailing a “second law of complexity" for the volume behind a horizon. We prove some other geometric results. First we demonstrate the monotonicity of complexification rate in boost invariant spacetimes. Then we turn to the question of whether a boundary foliation by Cauchy slices (i.e. a choice of boundary time coordinate) induces a unique bulk foliation, and therefore a unique volume flow current. We establish that, given minimal assumptions about the spacetime's causal structure, the strong energy condition, and the Einstein equations, there is such a unique foliation.

In chapter 4, we study subregion complexity in CA, CV, and CV 2.0. We test the idea that the action, volume, or spacetime volume computed on the entanglement wedge subregion may correspond to the complexity of the corresponding boundary density matrix. In particular, we test the conjecture that the relevant notion of mixed state complexity is the purification complexity. A well-defined notion of purification complexity includes a specification of the allowable auxiliary (purifying) Hilbert space. Suppose we assume that the allowed purifications include purifications by holographic states. Then we have a bulk geometric method to test the conjecture: any holographic geometry which geodesically completes a given entanglement wedge corresponds to a valid purifying boundary state, and the total state complexity so computed must be greater the subregion complexity for the entanglement wedge if the purification complexity conjecture is to remain viable. This is demonstrably true under the CV and CV 2.0 prescriptions. If it is to remain true under the CA prescription, we find that this imposes nontrivial constraints on the arbi-

trary constants associated with the action computation and on the allowable cutoff prescriptions. Carrying this line of reasoning further, we consider varying the cutoff surface in the region complementary to the entanglement wedge to provide valid purifications under variable course grainings. We are led to conclude that the CV conjecture is, in fact, computing a certain minimization over the complexity of purifications. With the action proposal, on the other hand, we encounter problems for such a duality. We focus on many-sided black hole solutions in three dimensions, which can be considered as a family of holographic purifications for the density matrix on any one side. The action computation for these states can be made arbitrarily negative by increasing the genus of the behind-the-horizon topology. In this way, we can find a purifying geometry with complexity that is less than that of the subregion complexity for one side. This poses a problem for the purification complexity interpretation of subregion complexity in CA, or imposing nontrivial constraints on the allowed genus which were not previously apparent.

Chapter 2

CA and noncommutative gauge theory

[1] In this chapter we study the holographic complexity of noncommutative field theories based on the "complexity equals action" (CA) conjecture. In particular, the four-dimensional $\mathcal{N} = 4$ noncommutative super Yang-Mills theory with Moyal algebra along two of the spatial directions has a well known holographic dual as a type IIB supergravity theory with a stack of D3 branes and non-trivial NS-NS B fields. We start from this example and find that the late time holographic complexity growth rate, according to the CA conjecture, experiences an enhancement when the non-commutativity is turned on. This enhancement saturates a new limit which is exactly 1/4 larger than the commutative value. We suggest a qualitative quantum mechanical explanation of the enhancement, and then investigate the finite time behavior of the complexity growth rate. Inspired by the non-trivial result, we then consider a more general setup in string theory where we have a stack of Dp branes and also turn on the B field. Multiple noncommutative directions are considered

[1] This chapter is based on [1] with Josiah Couch, Willy Fischler, and Ming-lei Xiao. Willy Fischler provided expertise on noncommutative gauge theories. Josiah Couch was the primary author of the arguments of section 2.3. I performed all computations either independently or in collaboration with Ming-lei Xiao, and otherwise contributed to all aspects of the paper.

in higher p cases.

2.1 Motivation for this study

A thorough test of the CA conjecture would compute the quantum complexity of a boundary CFT state and compare this corresponding bulk action calculation. Unfortunately, relatively little can be said about the quantum complexity in the boundary field theory. The task of actually computing the relative complexity between states in general quantum systems is notoriously difficult. What is more, in the definition one has to make several choices, including a gate set, reference state, and tolerance parameter. Where these choices appear in the holographic prescription is as of yet unclear. There has been considerable effort defining complexity in holographic quantum field theories [20, 21, 44–47], but they are weakly related to the holographic complexity at this point.

Therefore, at this stage we aim to investigate the behavior of the bulk action in novel contexts, and compare to available constraints on complexity and general intuition from quantum mechanics. Among the constraints considered is the Lloyd bound [33]. This bound was derived from the Margolus-Levitin theorem [48] under the assumption that each gate will evolve a generic state into an orthogonal state. It states that the time rate change of complexity, or "complexification," is constrained by the energy:

$$\dot{\mathcal{C}} \leq \frac{2M}{\pi}, \tag{2.1}$$

where M is the energy of the system. In [12, 30] it was conjectured that neutral black holes should saturate this bound, an assumption which was utilized in order to set the constant of proportionality between complexity and action. This conjecture originated from the fast scrambling nature of black holes and the related notion that black holes act as the fastest possible quantum computers. However, one finds that for neutral black holes, the Lloyd bound is saturated from above [36], which makes the conjecture somewhat suspicious. One can also argue that the Lloyd bound is not applicable because it is based on an idealized model of quantum computation. Therefore, whether this assumption applies in the case of holographic complexity has been further questioned in [35].

In light of these difficulties with the Lloyd bound, it is desirable to test the CA conjecture against additional pieces of intuition in novel contexts. One context which provide an interesting testbed is the noncommutative field theories. The study of such theories has a long history and has produced many profound results, see for example [49–54].

One feature of noncommutative field theory which might have interesting implications for complexity is that it adds a degree of non-locality. This has been shown to lead to other interesting effects, e.g. an increase relative to the commutative case in the dissipation rate of scalar modes [55]. Likewise, the holographic entanglement entropy has also been studied in this context [56, 57], where non-trivial behavior was found in the limit where the Moyal scale is much larger than the thermal scale. For our holographic studies we

therefore consider geometries obtained in a string theory context by turning on the NS-NS B fields on Dp branes. The non-vanishing B field then induces Dirichlet boundary condition for open strings, and non-zero commutator of the end point coordinates [49]. After decoupling the closed strings, the Dp brane worldvolume becomes a noncommutative space. It was shown that in such setup, although space is coarse-grained by the Moyal scale, which might indicate a reduction in the number of degrees of freedom, it turns out that all thermodynamical quantities are unchanged [50, 52]. This can be understood by looking at the thermal boundary state in the large N limit, which consists of only planar diagrams without external legs. Such diagrams are insensitive to the non-commutativity of the spacetime [58]. This thus provides a perfect arena for testing quantum complexity, a primary characteristic of which is that it is more than thermodynamics. If the holographic complexity can see the difference caused by non-commutativity, it is a sign that we are on the right track.

The remainder of this chapter is organized as follows: In section 2.2 we construct the holographic dual of a noncommutative super Yang-Mills (NC-SYM) theory and compute the holographic complexity of a state on the boundary using the CA proposal. The complexity growth rate is given as a function of the Moyal scale a, the horizon radius r_H and time t, and at late times its monotonic enhancement with a is shown. In section 2.3, we attempt to give a quantum mechanical explanation of the enhancement of late time complexity growth rate. In section 2.4, we discuss the finite time behavior of our result

and compare to the recent independent studies [36]. To make our result more convincing, we explore more examples with non-commutativity in section 2.5. We have a similar setup as in section 2.2 in various dimensions and we have various numbers of pairs of noncommutative directions. In 2.6, we conclude with a brief discussion of our results and make a few remarks of possible directions for future studies. In the appendix 2.7, we show the explicit calculation for the WDW patch action. Appendix 2.8 talks about the thermodynamic property of the Dp brane solutions.

2.2 Holographic Complexity of 4d $\mathcal{N} = 4$ NCSYM

2.2.1 The holographic dual to noncommutative SYM

We consider the noncommutative field theory widely studied in the context of string theory. It was shown that the non-vanishing NS-NS B field will induce a noncommutative space on the D brane that decouples from the closed string excitations [49]. The B field is turned on by performing a T duality, in D3 brane for instance, along x_3 direction, assuming the x_2, x_3 are compatified on a torus. The torus becomes tilted after the T duality, indicating a D2 brane smearing along the x_3 direction. Then one performs another T duality along x_3, to get the following solution ([50, 51]):

$$
\begin{aligned}
ds^2 &= \alpha' \Bigg[\left(\frac{r}{R}\right)^2 \left(-f(r)dt^2 + dx_1^2 + h(r)(dx_2^2 + dx_3^2)\right) + \left(\frac{R}{r}\right)^2 \left(\frac{dr^2}{f(r)} + r^2 d\Omega_5^2\right) \Bigg], \\
f(r) &= 1 - \left(\frac{r_H}{r}\right)^4, \quad h(r) = \frac{1}{1 + a^4 r^4},
\end{aligned}
\tag{2.2}
$$

$$
\begin{aligned}
e^{2\Phi} &= \hat{g}_s^2 h(r), \\
B_{23} &= B_\infty (1 - h(r)), \quad B_\infty = -\frac{\alpha'}{a^2 R^2}, \\
C_{01} &= -\frac{\alpha' a^2 r^4}{\hat{g}_s R^2}, \quad F_{0123r} = \frac{4\alpha'^2 r^3}{\hat{g}_s R^4} h(r).
\end{aligned}
\tag{2.3}
$$

The $\{t, x_1, x_2, x_3\}$ are the D3 brane coordinates, while $\{x_2, x_3\}$ are non-commuting with Moyal algebra

$$
[x_2, x_3] = i a^2. \tag{2.4}
$$

The radius coordinate r has units of inverse length[2], and a is the Moyal scale with units of length. r_H denotes the location of the event horizon, and $\hat{g}_s$ denotes the closed string coupling, which is related to the S^5 radius as $R^4 = \hat{g}_s N$.

Note that the geometry becomes degenerate at $r \to \infty$; thus we have to put the boundary theory on some cutoff surface $r_b < \infty$. It was shown that this natural cutoff plays an important role in the divergent structure of entanglement entropy [56]. However, as will be explained later, our computation is cutoff independent; therefore we don't specify a cutoff prescription.

[2]In the literature, the coordinate denoted here by 'r' is typically denoted 'u' in order to emphasize that it does not have dimensions of length. We have however chosen to denote it by 'r' to avoid confusion with the Eddington-Finkelstein like null coordinate

As explained in [50], all the thermodynamic quantities of this solution are the same as in the commutative case. In particular, the temperature and entropy is independent of a, given by

$$\begin{aligned} E &= \frac{3r_H^4\Omega_5 V_3}{(2\pi)^7\hat{g}_s^2} \\ T &= \frac{r_H}{\pi R^2}, \\ S &= \frac{4\pi R^2 r_H^3\Omega_5 V_3}{(2\pi)^7\hat{g}_s^2} \end{aligned} \tag{2.5}$$

It is then interesting to ask whether the complexity is affected by the non-commutativity because complexity is fine-grained information that "knows more" than thermodynamics.

We adopt the Complexity equals Action (CA) approach to compute the holographic complexity of the boundary state. It involves evaluating the action in a bulk subregion called the Wheeler-deWitt (WDW) patch. Recent work on evaluating gravitational action [59] provided a toolkit that deals with null boundary contributions in the context of Einstein gravity. Hence we are interested in the Einstein frame action of type IIB supergravity:

$$ds_E^2 = \exp(-\Phi/2)ds^2, \tag{2.6}$$

$$\begin{aligned} 2\kappa^2 S_E = &\int d^{10}x\sqrt{-g_E}\left[\mathcal{R} - \frac{1}{2}|d\Phi|^2 - \frac{1}{2}e^{-\Phi}|dB|^2 - \frac{1}{2}e^{\Phi}|F_3|^2 - \frac{1}{4}|\tilde{F}_5|^2\right] \\ &- \frac{1}{2}\int C_4 \wedge dB \wedge F_3, \end{aligned} \tag{2.7}$$

where the notation $|F_p|^2 = \frac{1}{p!}F_{\mu_1\ldots\mu_p}F^{\mu_1\ldots\mu_p}$ is understood. One should keep in mind that the 5-form $\tilde{F}_5$ is self dual while evaluating this action. This

requirement actually always makes the term $|\tilde{F}_5|^2 = 0$. [3]

2.2.2 Wheeler-DeWitt Patch Action

The WDW patch is defined to be the union of all spatial slices anchored on a boundary time slice Σ. Regarding representing the boundary state, the WDW patch differs from the entanglement wedge at two points: first, it specifies a specific time slice on the boundary, instead of a covariant causal diamond; second, it probes behind the horizon. It was conjectured in [12, 30] that the action evaluated in the WDW patch is dual to the relative complexity of the quantum state living on Σ. This conjecture is referred to as 'complexity = action' or CA duality. In our noncommutative geometry setup, we will be interested in the WDW patch for the two-sided black hole, which intersects the left boundary at time t_L, and the right boundary at time t_R. According to CA quality, the action evaluated on such a patch will compute the complexity of the quantum state of the boundary CFT living on the (t_L, t_R) slice as

$$\mathcal{C}(t_L, t_R) = kS_{WDW}, \tag{2.8}$$

with the coefficient set to $k^{-1} = \pi\hbar$ by the assumption that AdS-Schwartzchild black hole saturates the Lloyd bound. The complexity computed this way is

[3] We point it out that due to the famous subtlety about type IIB action, that the self-duality condition should be imposed by hand, the treatment we use for the action is only plausible. There are other ways to impose self-duality, for example the PST formulation, but the action computation and the holography there will be subtle.

cutoff dependent, but its time derivative

$$\dot{\mathcal{C}}(t_L, t_R) := \frac{d}{dt_L}\mathcal{C}(t_L, t_R), \tag{2.9}$$

in which we are interested, is cutoff independent. Notice that our choice to differentiate with respect to the left time is arbitrary, as the geometry should be symmetric between left and right. It will prove convenient to utilize radial advanced/retarded null coordinates:

$$dr^* = \frac{R^2 dr}{r^2 f(r)}, \quad u = t + r^*, \quad v = t - r^*. \tag{2.10}$$

Notice that unlike r, r^* has units of length. Suppressing all but the bulk and timelike direction, the contributions to the time rate change of the WDW patch can be visualized in the conformal diagram represented in Figure 2.1.

The calculation of the time rate change of the action is detailed in Appendix 2.7. It is convenient to express the result in terms of the radial coordinate r_B of the pastmost joint of the WDW patch (joint B_2 in the diagram 2.1, which coincides with joint B_1 as $\delta t \to 0$.) Note that r_B increases monotonically with t_L from $r_B = 0$ to $r_B = r_H$ as $t_L \to \infty$, and so we will use it to parameterize the time dependence of the complexification rate. [4] We find the following combined result:

$$\begin{aligned}\dot{S}_{WDW} = \frac{\Omega_5 V_3}{(2\pi)^7 \hat{g}_s^2}\Bigg(&\frac{-2\log(1+a^4 r_B^4)}{a^4} + 4r_B^4 + 6r_H^4 \\ &+ 3(r_H^4 - r_B^4)\log\Big|\frac{c\bar{c}\sqrt{\hat{g}_s}R^2 r_B^2}{\alpha(1+a^4 r_B^4)^{1/4}(r_H^4 - r_B^4)}\Big|\Bigg)\end{aligned} \tag{2.11}$$

[4] We consider only $t_L > 0$, and fix t_R so that this corresponds to when the joint B has left the past singularity.

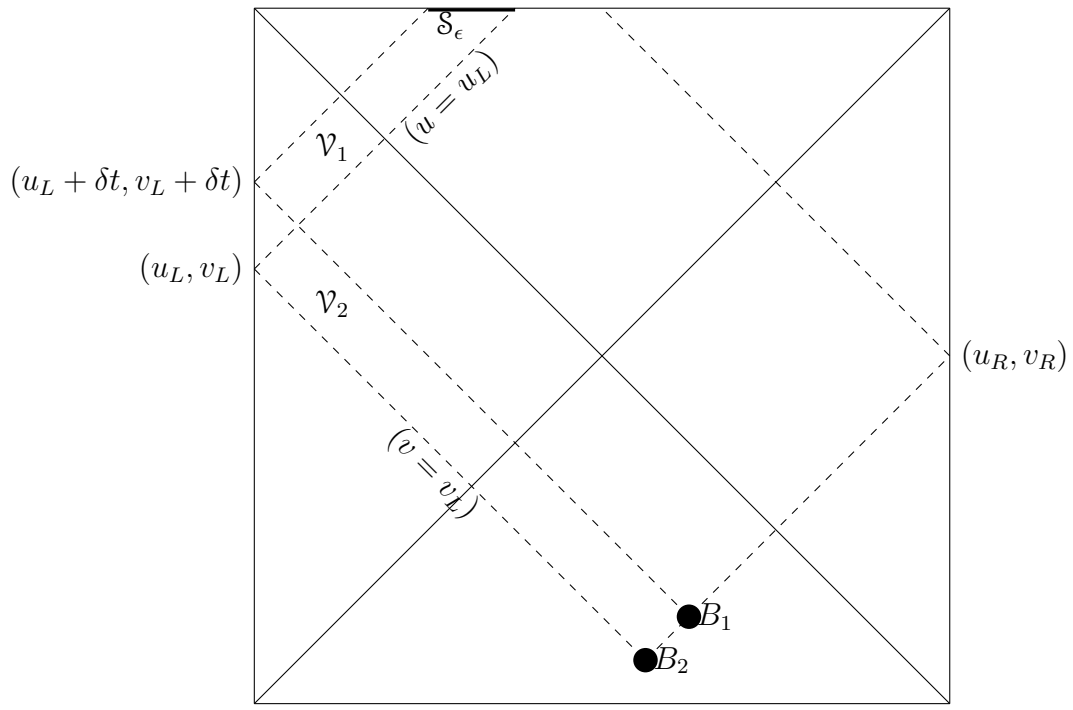

Figure 2.1: Two WDW patches separated by δt. Although the boundary of each patch is really at some large but finite r_b, the choice of r_b drops out in the differences we consider and we do not indicate it explicitly in this graphic.

where c and $\bar{c}$ are arbitrary constants associated with the normalization of boundary null generators entering the computation of δS_{joint}. See Appendix 2.7.3, as well as [59], [20] for discussion.

Various aspects of the time dependence (or r_B dependence) of equation 2.11 are unusual in light of the conjectured CA duality. Similar features have been seen in other systems [36]. We discuss the finite time behavior in Section 2.4.

The late time complexification rate is achieved by sending $r_B \to r_H$:

$$\dot{S}\big|_{t\to\infty} \approx \frac{\Omega_5 V_3 r_H^4}{(2\pi)^7 \hat{g}_s^2}\left(10 - 2\frac{\log(1+a^4 r_H^4)}{a^4 r_H^4}\right) \tag{2.12}$$

One can immediately see that if we assume the standard relationship, $\mathcal{C} = kS$ with $k = 1/\pi$, then the system violates the Lloyd bound (2.1) at late times: the ratio $\frac{\dot{S}}{2M}$ should be less than or equal to 1, but at late times it saturates values between $4/3$ to $5/3$ as we vary a. The relevance of the bound to holographic complexity has been disputed [35], and violations have been found in many other systems. But for purposes of comparison we find it interesting that, even if we had not assumed the standard $k = 1/\pi$, but instead used the logic that commutative black holes should saturate the Lloyd bound, we would set $k = 3/(4\pi)$. Clearly, the associated bound would fail immediately upon considering highly noncommutative black holes. Rather than proposing some different k in the relationship $\mathcal{C} = kS$, we find it plausible that such a choice does not generalize to all systems, at least under the current conventions for computing bulk action.

Overlooking the Lloyd bound for now, the dependence of the late time complexification on the noncommutativity parameter a is rather striking.

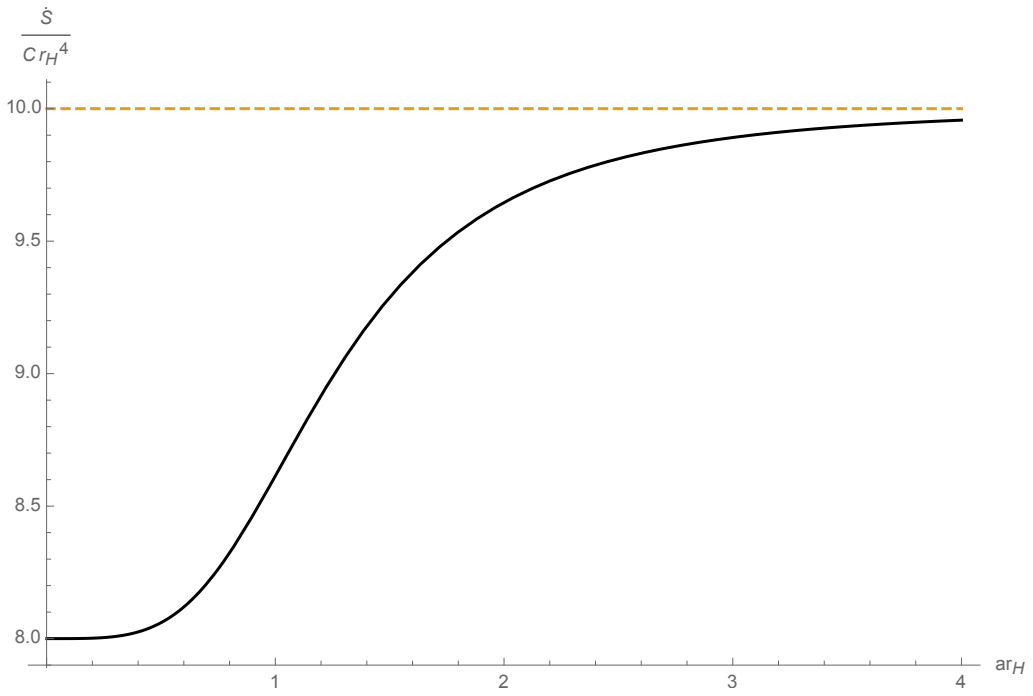

Figure 2.2: Late time action growth rate normalized by $C = \frac{\alpha^4 \Omega_5 V_3}{\hat{g}_s^2}$ and extra r_H dependence, versus ar_H, which is the Moyal scale measured in units of thermal length. It is observed that the complexification rate under the CA conjecture increases significantly when the Moyal scale is comparable to the thermal scale, and saturate a new bound which is 5/4 of the commutative value when the Moyal scale is much larger than the thermal scale.

As one can see from Figure 2.2, the complexification rate increases with the non-commutativity parameter a. It's also intriguing that a always appears in the combination ar_H, indicating that the only reference scale in the theory that the Moyal scale is sensitive to is the thermal scale $T^{-1} \sim r_H^{-1}$. When $a \ll$

T^{-1}, the complexification rate does not change much. It noticeably changes when a becomes comparable to T^{-1}. When $a \gg T^{-1}$, the complexification rate stops growing and saturates a new bound. It is inspiring to see that it does not grow indefinitely because that would violate the Lloyd bound in any possible sense. On the other hand, the ratio that it increases is an interesting rational number $5/4$. It may imply that this enhancement could be understood in terms of some kind of counting problem. With these interesting features in mind, we want to answer two questions:

1. How might we explain the enhancement from non-commutativity?

2. Are there other examples of noncommutative theories that corroborate these results?

These will provide the content for the next few sections.

2.3 Non-Commutativity Enhancement of Complexification Rate

Why the above enhancement should be exactly 25% is as of yet unclear. We do, however, have a conceptual argument for why there should be a noncommutative enhancement at all.

Consider the following problem: We have a unitary operator U, whose complexity is known to be $\mathcal{C}(U)$, and we want to know what can be said about the complexity of $\mathcal{C}(U^N)$ for some integer N. We can immediately say that

$$\mathcal{C}(U^N) \leq N\mathcal{C}(U) \tag{2.13}$$

Because given an optimal circuit Q implementing U, U^N can be implemented by N successive applications of Q, namely Q^N. [5] The bound above need not be saturated, however, as there might be a few gates at the beginning of Q which can cancel with some at the end of a successive copy of Q , resulting in a new circuit which (a unitary identical) to Q^N, but which is less complex. If we suppose that every time a new copy of U is added (after the first one of course), we get a cancellation of χ gates, and we suppose that χ doesn't depend on N (or at least asymptotes to a constant as N becomes large), then we have

$$\mathcal{C}(U^N) \approx N\mathcal{C}(U) - (N-1)\chi \tag{2.14}$$

It's easy to show that this formula holds for any $U \to U^n$ with the same χ.

If we are then interested in the (time evolution of the complexity of a family of operators) generated by some hamiltonian H

$$U(t) = e^{iHt}, \tag{2.15}$$

[5] There is a subtlety here in that Q only need implement a unitary that is within some small number ϵ of U, but if this is the case, there is no guarantee that Q^N will be within ϵ of U^N. It is also possible that for particular choices of gate set, some power of Q, say Q^M, may itself be a gate. This would result in "saw tooth" growth in complexity and periodically discontinuous time derivatives. It may be hoped that such concerns are rendered obsolete in an appropriate continuum limit (as in the "geometry of complexity" program [60, 61]), and we ignore these subtleties for the present discussion.

then we may use the above to write

$$\mathcal{C}(t) \equiv \mathcal{C}(U(t)) = \mathcal{C}[U(\delta t)^{t/\delta t}] \approx \frac{t}{\delta t}\left[\mathcal{C}(\delta t) - \chi\right] + \chi. \tag{2.16}$$

This will be true for any t and δt. Therefore we can compute the complexification rate

$$\frac{d}{dt}\mathcal{C}(t) \approx \frac{1}{\delta t}\left[\mathcal{C}(\delta t) - \chi\right]. \tag{2.17}$$

Now, what happens if we turn on non-commutativity in our theory? Let us suppose that our Hamiltonian $H = H_a$ varies continuously with the Moyal scale a, and suppose that our gates vary continuously as well so that the gates in the noncommutative theory can be identified with gates in the commutative theory. Suppose furthermore that for sufficiently small δt, $U_a(\delta t) = e^{iH_a \delta t}$ can be optimally approximated by the same circuit Q, but with each of the original gates g replaced with its noncommutative analog g_a (Call this circuit Q_a). Then it is still true that U_a^N can be implemented by Q_a^N. But now, because of the non-commutativity, it is likely that fewer of the gates at the beginning and end of Q will commute with each other (see figure 2.3). And so we can still write

$$\mathcal{C}_a(t) \approx \frac{t}{\delta t}\left[\mathcal{C}_a(\delta t) - \chi_a\right] + \chi_a \approx \frac{t}{\delta t}\left[\mathcal{C}(\delta t) - \chi_a\right] + \chi_a, \tag{2.18}$$

but because fewer gates cancel, χ_a will be smaller than the original χ. These mean that the complexifaction rate

$$\dot{\mathcal{C}}_a(t) \equiv \frac{d}{dt}\mathcal{C}_a(t) \approx \frac{1}{\delta t}\left[\mathcal{C}(\delta t) - \chi_a\right] \tag{2.19}$$

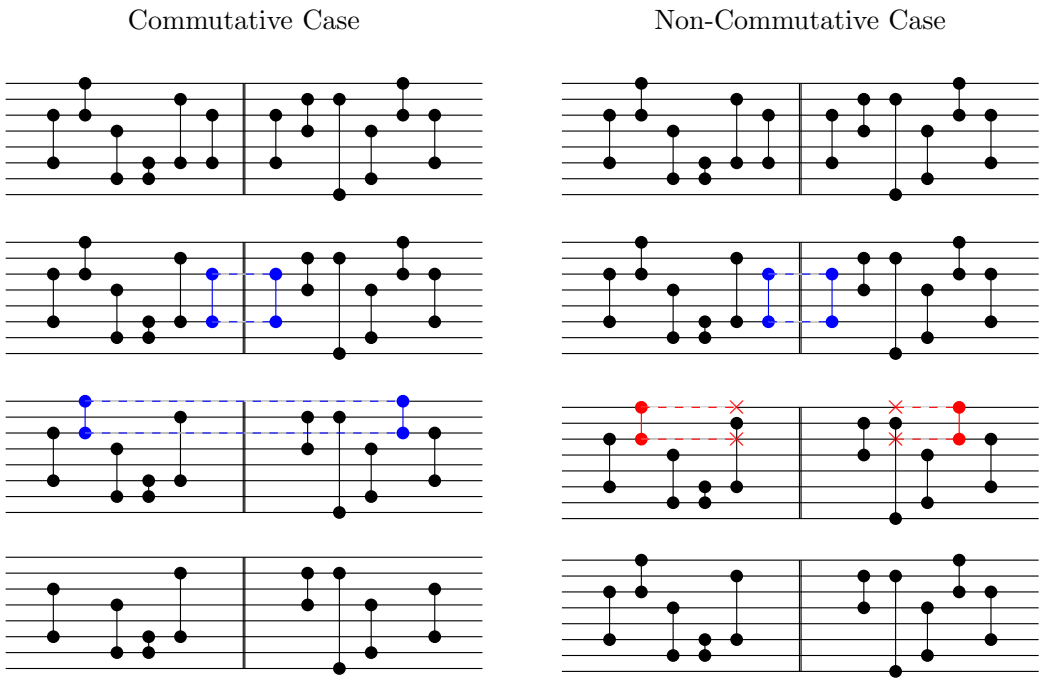

Figure 2.3: This circuit represents the end of one copy of a circuit Q_U implementing a hypothetical unitary U and the beginning of a second copy of Q_U. In this plot horizontal lines are qubits, and the dots connected by vertical lines are gates acting on the pair of qubits they connect. For this illustration, we will consider gates to be their own inverse. Gates from two copies may cancel (illustrated here with dashed blue lines connecting the gates), reducing the complexity of the circuit and providing a more efficient way to compute U^N. This cancellation relies, however, on the ability of gates to commute past each other, so that gates which could cancel can meet. We argue that in the non-commutative case, fewer gates commute and so there are fewer cancelations of this type. In this illustration, we see on the third line that a gate which can commute to cancel in the commutative case is prevented from doing so in the non-commutative case due to mild non-locality. Cartoon inspired by one used in a talk by Adam Brown.

gets an enhancement due to the suppression of χ_a. Finally we get an enhancement ratio of complexification rate as

$$\dot{\mathcal{C}}_a(t) \approx \frac{\mathcal{C}(\delta t) - \chi_a}{\mathcal{C}(\delta t) - \chi} \dot{\mathcal{C}}(t). \tag{2.20}$$

The same effect could be understood as arising from an increased non-locality due to the noncommutativity. The dependence of complexity growth on the locality of gates is explored in [12], where an extension of the Lloyd bound is studied by looking at the "k-locality" of the Hamiltonian and the gate set. A "k-local" operator is one that acts on at most k degrees of freedom: a k-local Hamiltonian consists of interactions coupling at most k degrees of freedom, and similarly a k-local gate set consists of at most k-local operators. [6] For convenience we let the Hamiltonian be "k-local" while the gate set is "j-local." Usually, the Lloyd bound should be satisfied if $j = k$, because one can choose the coupling terms as gates so that the time evolution could be easily implemented by the gates. However if one chooses a different j for the gate set, a bound of the following general form is to be expected

$$\dot{\mathcal{C}} \leq \frac{g(k)}{g(j)} \frac{2M}{\pi}, \tag{2.21}$$

where $g(k)$ is a monotonically increasing function. The interesting connection to our interpretation of non-commutativity is that the Moyal area introduced in non-commutative space can be thought of as an effective k for the Hamiltonian, meaning that non-local interactions couple wider range of degrees of

[6] To avoid dependence on the choice of basis, we would like to define k as the maximum rank of the coupling terms, or the maximum rank of the generators of the gates.

freedom than local interactions. On the other hand, we are not changing j because our holographic prescription is not changed. Then we have an extra factor $g(k)/g(j) > 1$ in the bound, hence an enhanced bound. A similar factor greater than 1 is hence obtained in eq(2.20).

2.4 Finite Time behavior

Up to now, we have only discussed the asymptotic behavior of the complexification rate at late times. It is plausible that the early time complexification rate is not as important as the late time limit because there is a thermal scale time resolution for this quantity. One might think of this resolution as the time scale for a new gate to act on the state. The finite time behavior of the complexification rate was studied in [36], where several interesting features were found. We will briefly outline the finite time behavior for noncommutative SYM, reproduce those features, and find new features introduced by the non-commutativity.

We first rewrite equation (2.11) using the dimensionless parameters

$$b = ar_H, \quad \rho = r_B/r_H, \quad \gamma = \frac{c\bar{c}\sqrt{\hat{g}_s}R^2}{\alpha' r_H^2}, \tag{2.22}$$

so that we get

$$\frac{\delta S}{\delta t} = \frac{\Omega_5 V_3 r_H^4}{(2\pi)^7 \hat{g}_s^2}\left(\frac{-2\log(1+b^4\rho^4)}{b^4} + 4\rho^4 + 6 + 3(1-\rho^4)\log\left|\frac{\gamma\rho^2}{(1+b^4\rho^4)^{1/4}(1-\rho^4)}\right|\right). \tag{2.23}$$

Note that since $T = r_H/\pi$, we have $b = \pi a T$.

Now normalize this by the late time commutative result at the same temperature to define (recall that ρ is implicitly our time parameter through r_B)

$$\dot{C}_{\rm n}(\rho) = \frac{-\log(1+b^4\rho^4)}{4b^4} + \frac{1}{2}\rho^4 + \frac{3}{4} + \frac{3}{8}(1-\rho^4)\log\Big|\frac{\gamma\rho^2}{(1+b^4\rho^4)^{1/4}(1-\rho^4)}\Big|. \tag{2.24}$$

We now display this normalized $\dot{C}_n$ vs time in thermal units at fixed b and γ. In the case where we take $b \to 0$ and $\gamma = 80$, this yields the plot in figure 2.4.

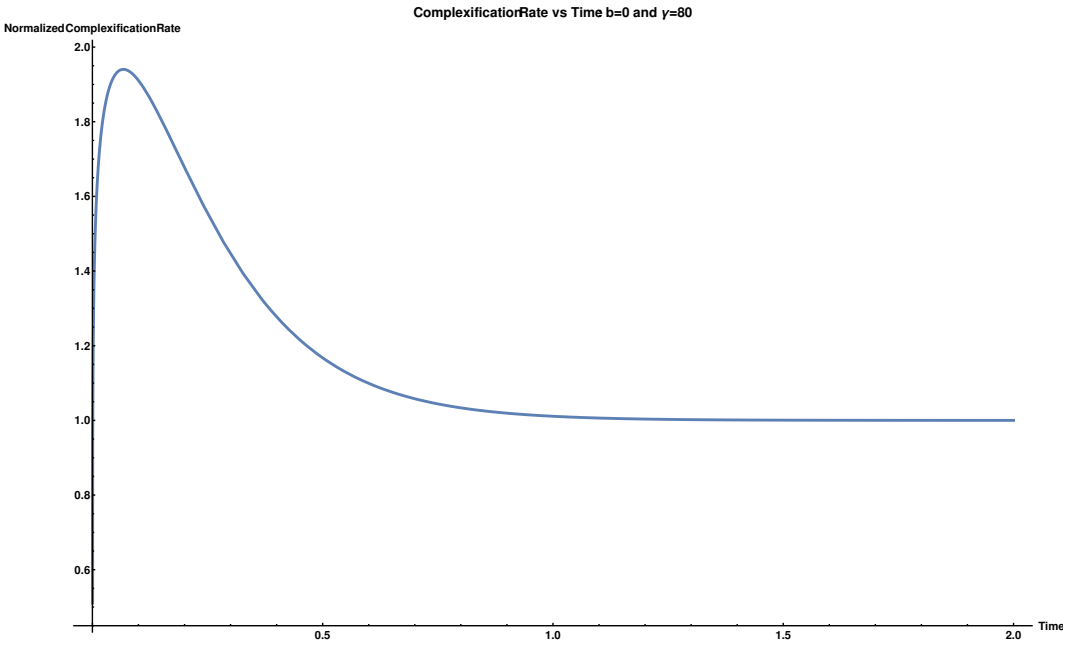

Figure 2.4: Normalized complexification rate versus time in thermal units for $\gamma = 80$ and $b = 0$.

It can be seen in this plot that there is a local maximum at early time (around $t = 0.1\beta$, β being the inverse temperature). Then at late times it approaches the smaller asymptotic value from above. There is also a logarithmic divergence as t goes to zero which comes from the log term in equation (2.24). Analogous features are also observed in [36], where they are discussed in great detail. The logarithmic divergence is not important in the sense that if you take the average complexification rate over a roughly thermal time scale, this divergence will be gone. A small period of decreasing complexity remains, but such behavior is not altogether prohibited. At early times the complexity is highly sensitive to the choice of the reference state, and only at late times is a constant growth rate expected for generic (time-independent) Hamiltonians. Regardless, the issues of the local maximum and the asymptotic approach to the "bound" from above are not resolved in any explanations here. One could average over an artificially long period of time to smooth out the local maximum, but doing so would never eliminate the approach from above, irrespective of the physicality of such a procedure.

Our primary interest here, however, is to discuss how these behaviors change with the noncommutative parameter b. To that end, we will consider what happens when we replot this curve fixing γ but varying b. The result is displayed in figure 2.5.

From figure 2.5 we see that as the non-commutativity is turned up, the local maximum decreases, and the asymptotic value increases. It is obvious that the change happens at $b \sim \pi$, which is when the Moyal scale a

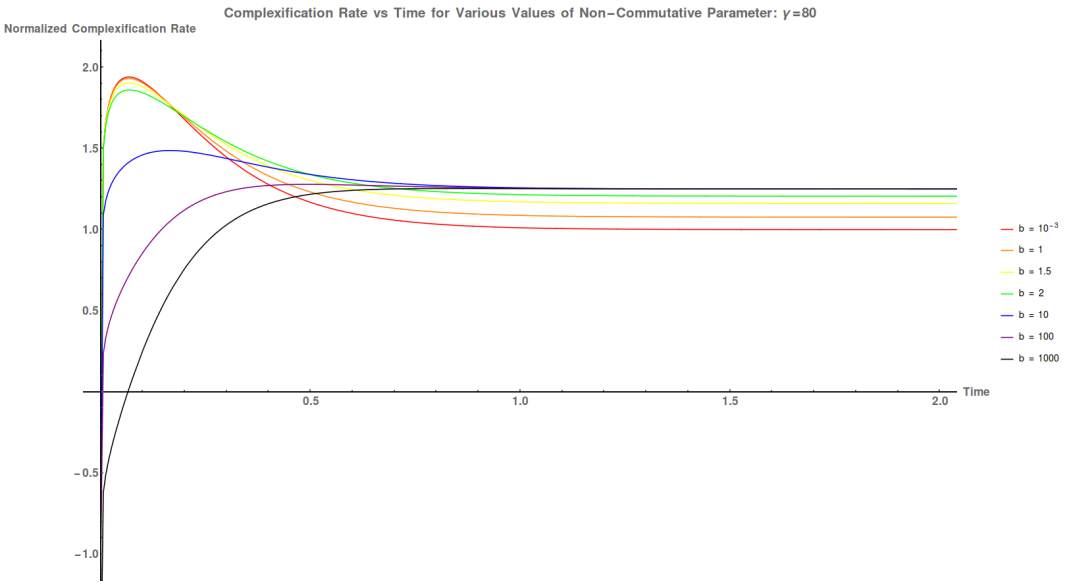

Figure 2.5: normalized complexification rate versus time in thermal units. γ is held fixed at 80 while $b = ar_H$ is varied.

is comparable to the thermal scale $T^{-1} = \pi/r_H$. For $b \gg \pi$, it seems that the asymptotic value is approached from below. Strictly speaking, it is not true, because the local maximum always exists, but has a diminishing relative height and is pushed to very late time. We can find the local maximum and plot its ratio to the asymptotic value versus b as in figure 2.6. The fact that the local maximum decays physically rather than by tuning some artificial choice is a sign that the noncommutative complexification rate at late time is a more qualified bound for a generic quantum system. We will discuss it in more details in the conclusion.

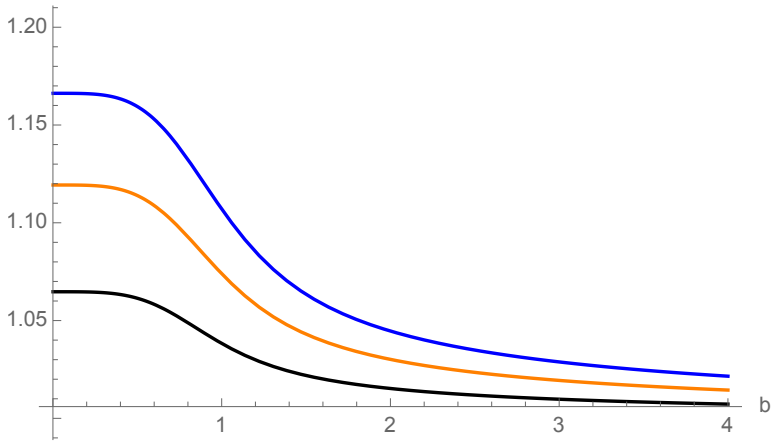

Figure 2.6: The vertical axis is the ratio between the local maximum and the asymptotic late time value of the complexification rate. The black, orange and blue curves correspond to $\gamma = 1, 2, 3$.

It is observed that the complexification rate mainly depends on temperature through the combination b, except an extra logarithmic contribution from γ. Therefore we expect that the variation with respect to temperature is

similar to figure 2.5. This can be implemented by varying b while fixing the combination γb^2, i.e., fixing a. When this is done with $\gamma b^2 = 1$ one gets figure 2.7, which is indeed similar to figure 2.5. This check shows that the only scale that the non-commutativity a is sensitive to is the thermal scale.

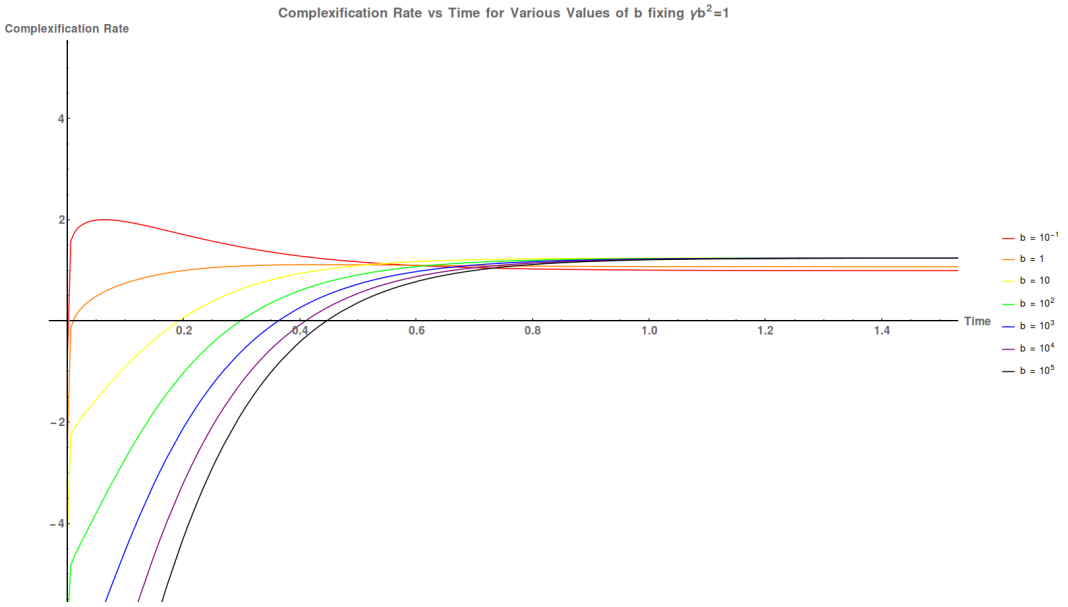

Figure 2.7: normalized complexification rate versus time in thermal units. γb^2 is held fixed at 1 while $b = ar_H$ is varied.

Finally, one may also be interested in the effect of γ, which at fixed AdS radius and temperature encodes information about the normalization of the generators of the null boundaries of the WDW patch. It has been suggested that this normalization, which is ambiguous in the action, should correspond to an ambiguity in the definition of complexity on the boundary such as the choice of reference state [20]. In our case, we observe that the dependence on

γ does not depend on the non-commutativity at all, which seems to support this idea for a broader class of theories.

2.5 Other noncommutative systems

As a test of the above argument, and to better understand the dependence of the enhancement on various factors, we would like to consider more examples of noncommutative field theories. It's easy to extend the D3 brane solution we discussed in Section 2.2 to other Dp branes, in which we are also able to put more noncommutative pairs of directions. For $p = 4, 5, 6$, we can turn on more than one B field component, making multiple pairs of directions non-commuting. Let us denote the number of non-vanishing B components as m so that B will be a rank-$2m$ matrix. In this section, we will investigate the dependence of late time complexification rate on the dimension of space p and the rank of the B field.

2.5.1 Supergravity solutions and decoupling limit

The general string frame metric for non-extremal Dp branes with m non-commuting pairs of directions are given as

$$\begin{aligned}\frac{ds^2}{\alpha'} = &\left(\frac{r}{R}\right)^{\frac{7-p}{2}} \left(-f(r)dx_0^2 + \sum_{i=1}^{p-2m} dx_i^2 + \sum_{i=1}^{m} h_i(r)(dy_{i,1}^2 + dy_{i,2}^2)\right) \\ &+ \left(\frac{R}{r}\right)^{\frac{7-p}{2}} \left(\frac{dr^2}{f(r)} + r^2 d\Omega_{8-p}^2)\right)\end{aligned} \tag{2.25}$$

where

$$f(r) = 1 - \frac{r_H^{7-p}}{r^{7-p}}, \tag{2.26}$$

$$h_i(r) = \frac{1}{1 + (a_i r)^{7-p}}. \tag{2.27}$$

In NS-NS sector we have

$$\begin{aligned} e^{2\Phi} &= \hat{g}_s^2 \left(\frac{R}{r}\right)^{\frac{(7-p)(3-p)}{2}} \prod_{i=1}^{m} h_i(r), \\ B^{(i)} &= -\frac{\alpha'}{(a_i R)^{\frac{7-p}{2}}}[1 - h_i(r)] dy_{i,1} \wedge dy_{i,2}. \end{aligned} \tag{2.28}$$

We also have many R-R fields turned on via the T-duality. One would expect them by looking at the Chern-Simons term in D brane action

$$S_{CS}^{Dp} = \mu_p \int \left(C \wedge \exp(B + kF)\right)_{p+1}. \tag{2.29}$$

Only rank-$(p+1)$ R-R potential C_{p+1} is turned on without any background field, whereas in the presence of B field, terms like $C_{p+1-2n} \wedge B^{(i_1)} \wedge \cdots \wedge B^{(i_n)}$ can also be sourced, where $n = 0, 1, \cdots, m$. In other words, when $m = 1$, we have C_{p-1} turned on; when $m = 2$, we have C_{p-3} turned on, and so on.

The general formulae for all these R-R fields are

$$\begin{aligned} C_{p+1} &= -\frac{(\alpha')^{\frac{p+1}{2}}}{\hat{g}_s} \left(\frac{r}{R}\right)^{7-p} \prod_i h_i(r), \\ C_{p-1}^{(j)} &= \frac{(\alpha')^{\frac{p-1}{2}}}{\hat{g}_s} \left(\frac{r}{R}\right)^{7-p} (a_j R)^{\frac{7-p}{2}} \prod_{i \neq j} h_i(r), \\ C_{p-3}^{(j,k)} &= -\frac{(\alpha')^{\frac{p-3}{2}}}{\hat{g}_s} \left(\frac{r}{R}\right)^{7-p} (a_j a_k R^2)^{\frac{7-p}{2}} \prod_{i \neq j,k} h_i(r), \\ C_{p-5}^{(j,k,l)} &= \frac{(\alpha')^{\frac{p-3}{2}}}{\hat{g}_s} \left(\frac{r}{R}\right)^{7-p} (a_j a_k a_l R^3)^{\frac{7-p}{2}} \prod_{i \neq j,k,l} h_i(r). \end{aligned} \tag{2.30}$$

We are omitting the basis here, but it's clear that these components are along all the directions on Dp brane except for the directions of the B fields indicated by their superscript. We also omitted their (inverse) hodge dual forms which may contribute to the action.

While these are all good solutions for supergravity in the bulk, one has to be careful with its world volume dual theory. The decoupling limit of the world volume theories for $2 \leq p \leq 6$ in the presence of B field is studied in [62], with the conclusion that there is no decoupling limit for D6 branes even for $m > 0$. For $p \leq 5$, decoupling limits do exist, and it's reasonable to talk about the complexity on the world volume theory. One may be worried that for D4 brane we have to up lift to 11 dimensions to compute the M theory action, but the effective string coupling at high energy is

$$e^{\Phi} \sim r^{\frac{(7-p)(p-3-2m)}{4}}, \tag{2.31}$$

which is suppressed by the non-commutativity when $m \geq 1$, indicating that at sufficiently high energy, we don't have to go to M theory.

As such, we will be using type IIB action for odd p and type IIA action for even p. The type IIA action is

$$\begin{aligned} S^{\text{IIA}}_{\text{string}} =& \frac{1}{2\kappa^2} \int dx^{10} \sqrt{-g} \left[e^{2\Phi} (\mathcal{R} + 4|d\Phi|^2 - \frac{1}{2}|H|^2) - \frac{1}{2}|F_2|^2 - \frac{1}{2}|\tilde{F}_4|^2 \right] \\ & - \frac{1}{4\kappa^2} \int B \wedge F_4 \wedge F_4, \end{aligned} \tag{2.32}$$

with the usual conventions:

$$F_2 = dC_1, \qquad F_4 = dC_3, \qquad \tilde{F}_4 = F_4 - C_1 \wedge H. \tag{2.33}$$

2.5.2 Complexification Rates

We report the action growth rates with the following p-dependent prefactor,

$$c_p \equiv \frac{\Omega_{8-p} r_H^{7-p}}{(2\pi)^7 \hat{g}_s^2}, \tag{2.34}$$

We also divide out the transverse volume V_p to give a "density of action." The complexification rate will be related to the action growth rate by eq(2.8), where the coefficient k is not specified yet. We will discuss the strategy of choosing k at the end of the section. Both the joint and boundary contributions to the late time complexification rate take a particularly simple form:

$$\begin{aligned} \dot{S}_{\text{joint}} &= (7-p)c_p \\ \dot{S}_{\text{boundary}} &= \frac{1}{8}(65 - 14p + p^2)c_p \end{aligned} \tag{2.35}$$

The bulk contributions exhibit more interesting dependencies on the size and number of noncommutativity parameters. These are here reported for each p.

D2 Brane

This is the simplest case, where we have fewest R-R fields and don't need to put the self-duality constraint. We have

$$F_2 = dC_{p-1}, \tag{2.36}$$

$$\tilde{F}_4 = dC_{p+1} - C_{p-1} \wedge H. \tag{2.37}$$

Plugging them in the type IIA action, we obtain the complexity growth rate. Including all contributions, the late time limit becomes

$$\dot{S}_{p=2,m=1} = 12c_p. \tag{2.38}$$

Surprisingly, we find that the late time complexification rate does not even depend on the non-commutativity parameter a. We may argue that it is the case where the bound is already saturated so that non-commutativity could not enhance it anymore.

D4 Brane

This is the minimal dimension that we can include two pairs of non-commutative directions, hence $m = 2$. The R-R field contents are

$$F_2 = dC_{p-3}^{(1,2)}, \tag{2.39}$$

$$\tilde{F}_4 = \sum_i \left[dC_{p-1}^{(i)} - C_{p-3}^{(1,2)} \wedge H^{(i+1)} \right] + *^{-1} \left[dC_{p+1} - \sum_i \left(C_{p-1}^{(i)} \wedge H^{(i)} \right) \right]. \tag{2.40}$$

Note that mod m is understood in the supercript of the forms.

The complexity growth rate including all contributions has late time limit

$$\dot{S}_{4,2} = \left(5 + \frac{3a_1^3 a_2^3 r_H^6}{(1 + a_1^3 r_H^3)(1 + a_2^3 r_H^3)} \right) c_p. \tag{2.41}$$

The $p = 4,\ m = 0, 1$ cases can be obtained by taking one or both of the a parameters to zero:

$$\dot{S}_{4,0} = \dot{S}_{4,1} = 5c_4 \tag{2.42}$$

It's striking that turning on a single pair of noncommutative directions does not affect the late time complexification rate at all, but turning on the second pair does increase the rate. It means that we cannot use the argument as for $p = 2$ to explain the zero enhancement here because obviously the bound was not saturated yet.

D5 Brane

It's another case where we need to take into account the self-duality issue. Again we can have $m = 2$, and the R-R field contents are

$$F_3 = dC_{p-3}^{(1,2)} + *^{-1}\left[dC_{p+1} - \sum_i \left(C_{p-1}^{(i)} \wedge H^{(i)}\right)\right], \tag{2.43}$$

$$\tilde{F}_5 = \sum_i \left[dC_{p-1}^{(i)} - \frac{1}{2}C_{p-3}^{(1,2)} \wedge H^{(i+1)} + \frac{1}{2}dC_{p-3}^{(1,2)} \wedge B^{(i+1)}\right] + \text{self dual}. \tag{2.44}$$

The complexity growth rate including all contributions has late time limit

$$\dot{S}_{5,2} = c_5 \times \left(\frac{11}{2} + \frac{a_1^2 a_2^2 r_H^4 - 2}{2(1 + a_1^2 r_H^2)(1 + a_2^2 r_H^2)} + \frac{a_2^2 \log(1 + a_1^2 r_H^2)}{2a_1^2(a_1^2 - a_2^2)} + \frac{a_1^2 \log(1 + a_2^2 r_H^2)}{2a_2^2(a_2^2 - a_1^2)}\right). \tag{2.45}$$

We can also examine the $m = 1$ case by taking $a_2 = 0$ and $a_1 = a$:

$$\dot{S}_{5,1} = \left(5 - \frac{1}{1 + a^2 r_H^2}\right) c_p, \qquad \dot{S}_{5,0} = 4c_p \tag{2.46}$$

In contrast with $p = 4$, turning on the first pair of noncommutative directions already changes the complexity, and turning on the second enhances more.

D6 Brane

Finally we may investigate a case where we can turn on 3 pairs of noncommutative directions, hence D6 brane. For $m = 3$, the R-R field contents are

$$F_2 = dC_{p-5}^{(1,2,3)} + *^{-1}\left[dC_{p+1} - \sum_i \left(C_{p-1}^{(i)} \wedge H^{(i)}\right)\right], \tag{2.47}$$

$$F_4 = \sum_i \left[dC_{p-3}^{(i+1,i+2)} - C_{p-5}^{(1,2,3)} \wedge H^{(i)}\right] + *^{-1}\left[dC_{p-1}^{(i)} - \sum_{j\neq i} C_{p-3}^{(i,j)} \wedge H^{(j)}\right]. \tag{2.48}$$

The complexity growth rate including all contributions has late time limit

$$\dot{S}_{6,3} = c_6 \times \left(4 + \frac{a_1 a_2 \log(1 + a_3 r_H)}{(a_2 - a_3)a_3(a_3 - a_1)r_H} + \frac{a_2 a_3 \log(1 + a_1 r_H)}{(a_3 - a_1)a_1(a_1 - a_2)r_H} + \frac{a_3 a_1 \log(1 + a_2 r_H)}{(a_1 - a_2)a_2(a_2 - a_3)r_H}\right) \tag{2.49}$$

The three a-dependent terms have the property that no matter how many a's you turn off, their sum is a constant as -1. Thus again, it is a situation where only turning on maximum number of non-commutativity can we increase the non-commutativity, similar to the $p = 4$ case.

$$\dot{S}_{6,0} = \dot{S}_{6,1} = \dot{S}_{6,2} = 3c_6 \tag{2.50}$$

However, this complexity growth rate seems to have no physical meaning, because there is not a world volume theory that is decoupled from gravity.

p	$m=0$	$m=1$	$m=2$	$m=3$	πB_L
2	12	12	-	-	7
3	8	10	-	-	6
4	5	5	8	-	5
5	4	5	6	-	4
6	3	3	3	4	3

Table 2.1: This table lists all the action growth rate at late time for general p and m. They are in unit of the constant c_p defined in eq(2.34). The last column is showing the Lloyd bound B_L also in unit of c_p.

The holographic principle is subtle in this case. We present the result here because the bulk computation can be done in a similar manner without noting the difference. Whether the quantity so computed has any physical meaning is an open question.

2.5.3 Summary of Results

From the above computation, we find that when we turn on non-commutativity on Dp branes, the complexity growth rate either stays the same, or increases. The fact that it does not decrease is encouraging for our argument given in section 2.3. However, the values of the enhancement ratio are not understood.

In the table 2.1, we list all the density of late time action growth rate in unit of c_p, in the limit that all m non-commutativity parameters a_i, $i = 1, .., m$, goes to infinity.

There are no obvious laws that govern these rates in general, but we do observe some interesting features. For both D3 and D5 branes, we have

enhancement from each pair of non-commuting directions. In particular, the ratio for the enhancement from the first pair are the same in both cases, and the enhanced amount from the first and second pair are also the same in D5 brane. These two cases seem to provide reasonable behaviors one may naively expect. On the other hand, the type IIA supergravity with even-ps does not always have complexification rate enhancement from non-commutativity. The reason for it may depend on the details of the boundary theory.

In the table 2.1, we also list the Lloyd bound computed from the ADM mass of the geometry (see Appendix 2.8). One may set the coefficient k in eq(2.8) to let any of the complexification rate to saturate the Lloyd bound. For instance, if we want to set the commutative $\mathcal{N} = 4$ SYM ($p = 3$, $m = 0$) to saturate the bound, we can take $\pi k_{p=3} = 3/4$. However, the consequence is that we can always turn on the non-commutativity and violate this bound. In order that the Lloyd bound is not violated, we need to guarantee that the maximum complexification rate for each p is bounded by B_L, thus

$$k_2 \leq \frac{7}{12\pi}, \quad k_3 \leq \frac{3}{4\pi}, \quad k_4 \leq \frac{5}{8\pi}, \quad k_5 \leq \frac{2}{3\pi}, \quad k_6 \leq \frac{3}{4\pi}. \tag{2.51}$$

If one follows the argument at the end of section 2.3, and get an enhanced bound for non-commutative field theory, the bound on k_p will be weaker. On the other hand, the Lloyd bound is defined under the assumption that all gates take a generic state to an orthogonal state, which is usually not true. It is argued that we simply should not take this bound seriously [35]. This objection will make it hard to determine what k should be, but for our

purpose, k does not affect our main results.

2.6 Conclusion

In this work, we have considered the effects of non-commutativity on the holographic complexity of SYM according to the complexity = action conjecture. We have done this in the hope that this would produce further evidence about the validity of this conjecture, and of the concept of holographic complexity more generally. Our main result is that the late time complexification rate increases with the non-commutativity in a class of theories.

We computed the holographic complexity for 4D $\mathcal{N} = 4$ non-commutative super Yang-Mills, by evaluating the WDW action in the bulk geometry described by type IIB supergravity with D3 branes. We saw a $5/4$ enhancement for late time complexification rate in the non-commutative result over the commutative result. This was striking because it is well known that the thermodynamics of this theory are independent of the non-commutative parameter a. The observed changes to complexity support the idea that complexity is more than thermodynamics, and indicates that the CA prescription is reproducing this feature of complexity. Comparing to the Lloyd bound derived from the total energy, we discovered that using the coefficient of proportionality $k = 1/\pi$ as in [30] will make the commutative late time complexification rate violate the bound. One could in principle avoid this by arguing that k should not be universal for all kinds of theories, but the commutative black hole still can not saturate the bound because there should be space for enhancement from the

non-commutativity.

We presented a quantum argument to explain this enhancement and to argue that we should have expected it. We assume that the time evolution operator is approximated by sequential copies of the same quantum circuit, and the optimization of the total circuit when you combine them will be less efficient in non-commutative theories. We also argue that this expectation matches the k-locality model prediction if we relate the size of Moyal scale to the size of locality k. Then we investigate the finite time behavior of this complexification rate and see that the problematic finite time maximum gets suppressed by non-commutativity.

Finally, we generalized the solution for D3 branes to general Dp branes to get a broader class of noncommutative gauge theories. We presented similar calculations as for $p = 3$ and obtained the late time complexification rates for $2 \leq p \leq 6$ and all allowed ranks of the B field. The results for $p = 5$ are similar to those for $p = 3$ but can have another enhancement of the same magnitude from a second B field component. This is consistent with our heuristic argument. The results for the even p cases are less well understood. We found that there is no enhancement for $p = 2$ and that for $p = 4$ one must introduce a second B field component to get an enhancement. This result would seem to be in mild tension with the argument of section 2.3. The correct explanation for this behavior is left for future work. Despite not seeing an enhancement in some cases, it is at least encouraging that no decrease was observed, which would have been a much clearer contradiction to the

arguments of section 2.3.

Regarding the statement that non-commutativity enhances the complexification rate in general, there are several interesting aspects one can investigate. First, this result is in tension with the often expressed idea that the commutative AdS-Schwarzschild black hole is the fastest possible computer [30]. If non-commutativity can somehow increase the computational speed even further, it would be very interesting to see if it also increases the scrambling process of the black hole. Second, it also would be interesting to compute the complexity of a weakly coupled field theory on a non-commutative manifold in order to test the conclusion of our heuristic argument in a non-holographic context. Such a computation would, in light of this work, provide for a more robust check on the complexity = action conjecture. The work of [20, 44] might prove useful to such an endeavor.

Another interesting extension of this work would be to repeat the computations for the complexity = volume, and the complexity = spacetime volume conjectures, which will be both a test for our results and a test for the holographic complexity prescriptions. Finally, it was pointed out to us by Eoin Ó Colgáin that the geometry corresponding to the $D3$-brane case that we have considered here has been discovered to belong to a larger class of deformations of AdS_5, studied in e.g. [63–65]. It would perhaps be interesting to extend the results of this work to the more general case.

2.7 Appendix I: Calculation of $\dot{S}_{WDW}$

To minimize clutter in expressions, in this appendix we set $2\kappa^2 = (2\pi)^7\alpha^4 = 1$ and reinstate κ dependence only at the end. Following the systematic treatment of [59], the action on a bulk subregion is divided into contributions as follows:

$$\begin{aligned} S_{\mathcal{V}} = &\int_{\mathcal{V}} \big(\mathcal{R} + \mathcal{L}_m\big)\sqrt{-g}dV \\ &+ 2\Sigma_{T_i}\int_{\partial\mathcal{V}_{T_i}} K d\Sigma + 2\Sigma_{S_i}\text{sign}(S_i)\int_{\partial\mathcal{V}_{S_i}} K d\Sigma - 2\Sigma_{N_i}\text{sign}(N_i)\int_{\partial\mathcal{V}_{N_i}} \kappa d\sigma d\lambda \\ &+ 2\Sigma_{j_i}\text{sign}(j_i)\int_{B_{j_i}} \eta_{j_i} d\sigma + 2\Sigma_{m_i}\text{sign}(m_i)\int_{B_{m_i}} a_{m_i} d\sigma \end{aligned} \tag{2.52}$$

The first line we call the bulk contribution. The second line contains boundary contributions along timelike ($\mathcal{T}$), spacelike ($\mathcal{S}$), and null boundaries ($\mathcal{N}$), respectively. The final line contains joint contributions, divided into those which result from intersections of timelike and/or spacelike boundaries, and those which include one or more null boundaries. Sign conventions and notation for integrand quantities will be explained as needed in what follows.

While the action on a WDW patch is obviously of interest for its conjectured relation to Quantum Complexity, its time derivative is simpler to compute and interesting for diagnostic purposes. Due to the spacetime symmetries, this quantity reduces to the difference of two volume contributions ($\mathcal{V}_1$ and $\mathcal{V}_2$ in figure 2.1), one boundary surface contribution ($\mathcal{S}_\epsilon$ in figure 2.1), and two joint contributions (B_1 and B_2 in figure 2.1).

$$
\begin{aligned}
\delta S_{\text{WDW}} &= \delta S_{\text{bulk}} + \delta S_{\text{boundary}} + \delta S_{\text{joints}} \\
\delta S_{\text{bulk}} &= S_{\mathcal{V}_1} - S_{\mathcal{V}_2} \\
\delta S_{\text{boundary}} &= -2 \int_{\mathcal{S}_\epsilon} K d\Sigma \\
\delta S_{\text{joints}} &= 2 \int_{B_1} a_1 d\sigma - 2 \int_{B_2} a_2 d\sigma
\end{aligned}
\tag{2.53}
$$

2.7.1 Bulk Contribution

The bulk integral contributions are of the form:

$$
S_{\text{bulk}} = \int_{\mathcal{V}} \sqrt{-g_E} \big(\mathcal{R} + \mathcal{L}_m \big) d\mathcal{V}, \tag{2.54}
$$

where Einstein frame metric is used. For the action eq(2.7) and field content eq(2.3) we have

$$
\mathcal{R} = \frac{-2\sqrt{\hat{g}_s} \big(2a^4 r_H^4 + a^8 r^4 (r^4 + r_H^4) \big)}{\alpha' R^2 (1 + a^4 r^4)^{9/4}}, \tag{2.55}
$$

$$
\mathcal{L}_m = \frac{2\sqrt{\hat{g}_s} \big(4a^4 r_H^4 + a^8 r^4 (3r^4 + r_H^4) \big)}{\alpha' R^2 (1 + a^4 r^4)^{9/4}}. \tag{2.56}
$$

We let the integral over x_1, x_2, and x_3 give V_3 and the five-sphere Ω_5. Also abbreviate $C = \dfrac{\alpha'^4 \Omega_5 V_3}{\hat{g}_s^2}$. Further let $\rho(u, v)$ and $\bar{\rho}(u, v)$ denote the radial value r as implicit functions of advanced/retarded coordinates u and v from the appropriate quadrant (here the left and bottom quadrants, respectively). The form of these functions is not important here.

The bulk contribution for $\mathcal{V}_1$ can be written in (u, r) coordinates with radial limits expressed implicitly.

$$S_{\mathcal{V}_1} = C\int_{u_L}^{u_L+\delta t} du \int_{r=\epsilon}^{r=\rho_L(u-v_L)} dr \frac{4r^3(a^8r^8+a^4r_H^4)}{(1+a^4r^4)^2}, \tag{2.57}$$

Here $r=\epsilon$ is a surface close to the singularity which will be sent to zero. A similar expression can be written for $\mathcal{V}_2$ in (v,r) coordinates, and after the radial integration we have:

$$\begin{aligned}\frac{1}{C}(S_{\mathcal{V}_1}-S_{\mathcal{V}_2}) = &\int_{u_L}^{u_L+\delta t} du\big(G(\rho_L(u-(v_L+\delta t)))-G(\epsilon)\big)\\ &-\int_{v_L}^{v_L+\delta t} dv\big(G(\rho_L(u_L-v)))-G(\bar{\rho}(u_R,v))\big)\end{aligned} \tag{2.58}$$

Changing variables $u \to u_L+v_L-v+\delta t$ leads to a cancellation of terms such that for small δt we are left with

$$\begin{aligned}S_{\mathcal{V}_1}-S_{\mathcal{V}_2} &\approx C\bigg(G\big(\bar{\rho}(u_R,v_L)=r_B\big)-G\big(\epsilon\big)\bigg)\delta t,\\ G(r) &= \frac{a^4(2r^4+a^4L^8-r_H^4)-2(1+a^4r^4)\log(1+a^4r^4)}{(a^4+a^8r^4)}.\end{aligned} \tag{2.59}$$

This cancellation is expected from the boost symmetry of the left wedge of the spacetime, and also indicates the cutoff independence of our calculation. We denote the radial value at the bottom corner of the WDW patch $\bar{\rho}(u_R,v_L)\equiv r_B$. As $\epsilon\to 0$ we find a bulk contribution of

$$\dot{S}_{\text{bulk}} = \lim_{\delta t\to 0}\frac{S_{\mathcal{V}_1}-S_{\mathcal{V}_2}}{\delta t} = \frac{\alpha^4\Omega_5 V_3}{\hat{g}_s^2}\bigg(\frac{a^4r_B^4}{1+a^4r_B^4}(r_H^4-r_B^4)+2r_B^4-\frac{2\log(1+a^4r_B^4)}{a^4}\bigg) \tag{2.60}$$

Note that r_B is related to t_L in the manner that as $t_L\to\infty$, $r_B\to r_H$. Therefore, the late time limit can be obtained by taking $r_B\to r_H$ limit.

2.7.2 Boundary Contributions

We adopt the convention that the null boundary geodesics are affinely parameterized: $k^\mu \nabla_\mu k^\nu = \kappa k^\nu$ with $\kappa = 0$, which simplifies the action computation considerably because all but one boundary surface ($\mathcal{S}_\epsilon$) make no contribution. The boundary $\mathcal{S}_\epsilon$ is the spacelike surface $r = \epsilon \to 0$. The contribution is of the form

$$\delta S_{\text{boundary}} = -2 \int_{\mathcal{S}_\epsilon} K d\Sigma \tag{2.61}$$

where $d\Sigma$ is the induced volume element on the boundary hypersurface and K is the extrinsic curvature: $K = g^{\mu\nu} \nabla_\mu s_\nu$ with the unit normal s^ν chosen to be future directed, away from the WDW patch. This convention for choosing the direction of the surface normal is responsible for the minus sign on this term [59].

For our metric eq(2.6) we have

$$K = \left(\frac{\hat{g}_s}{\alpha^2}\right)^{1/4} \frac{4rh(r)f'(r) + f(r)\left(32h(r) - rh'(r)\right)}{8Rh(r)^{7/8}\sqrt{-f(r)}}, \tag{2.62}$$

which as $\epsilon \to 0$ leads to

$$\dot{S}_{\text{boundary}} = 4r_H^4 \frac{\alpha^4 \Omega_5 V_3}{\hat{g}_s^2} \tag{2.63}$$

2.7.3 Joint Contributions

There are two joints (B and B') which contribute to the complexification rate. Each of these is comprised of the intersection of two null surfaces,

so their contributions are of the form

$$S_J = 2\Sigma_{m_i}\text{sign}(m_i)\int_{B_{m_i}} a_{m_i} d\sigma \tag{2.64}$$

$$a_{m_i} = \log\left|-\frac{1}{2}k_L \cdot k_R\right|$$

where dS is the volume element on the joint. Here k_L and k_R are future-pointing null generators along the left-moving and right-moving boundaries, respectively. Both of the joints in question lie at the past of the corresponding null segments, which together form the past boundary of a WDW patch. Together these facts determine that the sign of each joint's contribution to the WDW patch action is positive [59], and so taking a difference of two patches leads to the signs given in equation 2.53.

In addition to the affine parameterization of boundary generators, a convention must be chosen to fix their normalization. It may be possible to associate the freedom allowed by this choice with corresponding conventions which must be established in the definition of quantum complexity (e.g., choice of reference state and gate set). Indeed, progress has been made in this direction [20]. For our purposes, establishing a normalization convention is necessary to make meaningful comparisons between different WDW patch actions (such as that implicit in our "time derivative") as parameters of the theory are adjusted.

We normalize according to $k_L \cdot t_L = -c$ and $k_R \cdot t_R = -\bar{c}$, where $\hat{t}_R$ and

$\hat{t}_L$ are normalized generators of time-translation on each boundary. With this in mind we choose

$$\begin{aligned}(k_L)_\mu &= -c(\delta^t_\mu - \sqrt{\frac{-g_{rr}}{g_{tt}}}\delta^r_\mu) \\ (k_R)_\mu &= \bar{c}(\delta^t_\mu + \sqrt{\frac{-g_{rr}}{g_{tt}}}\delta^r_\mu).\end{aligned} \tag{2.65}$$

For small δt, the joints B_2 and B_1 are at fixed radii $r = r_B$ and $r = r_B + \frac{1}{2}\sqrt{\frac{-g_{tt}}{g_{rr}}}\delta t$, respectively. The quantities a_m in equation 2.64 are easily evaluated at each joint and the combined contribution is found to be:

$$\begin{aligned}S_{B_1} - S_{B_2} =& 2\frac{\alpha^4 V_3 \Omega_5}{\hat{g}_s^2}\left(r^3 \log\big[-\bar{c}c\frac{R^2(\hat{g}_s^2 h(r))^{1/4}}{\alpha r^2 f(r)}\big]\Big|_{r=r_{B_2}}^{r=r_{B_1}}\right) \\ \approx& \delta t\frac{\alpha^4 V_3 \Omega_5}{\hat{g}_s^2}\left(\frac{2r_H^4 + r_B^4(2 + a^4(3r_B^4 + r_H^4))}{1 + a^4 r_B^4}\right. \\ &\left. + 3(r_H^4 - r_B^4)\log\left|\frac{c\bar{c}\sqrt{\hat{g}_s}R^2 r_B^2}{\alpha(1 + a^4 r_B^4)^{1/4}(r_H^4 - r_B^4)}\right|\right)\end{aligned} \tag{2.66}$$

2.7.4 Combined Contributions

We can combine contributions 2.60, 2.63, and 2.66 to arrive at the full time rate change of the WDW patch action (reinstating explicit κ dependence and immediately using $2\kappa^2 = (2\pi)^7\alpha^4$):

$$\begin{aligned}\dot{S}_{WDW} =& \frac{\Omega_5 V_3}{(2\pi)^7 \hat{g}_s^2}\left(\frac{-2\log(1 + a^4 r_B^4)}{a^4} + 4r_B^4 + 6r_H^4\right. \\ &\left. + 3(r_H^4 - r_B^4)\log\big|\frac{c\bar{c}\sqrt{\hat{g}_s}R^2 r_B^2}{\alpha(1 + a^4 r_B^4)^{1/4}(r_H^4 - r_B^4)}\big|\right)\end{aligned} \tag{2.67}$$

2.8 Appendix II: Thermodynamics and the Lloyd Bound

It is interesting that the thermodynamic quantities for these systems exhibit no dependence on the noncommutativity parameter a (see [50] for discussion). We find that for general p[7]

$$\begin{aligned} E &= \frac{(9-p)r_H^{(7-p)}}{2(2\pi)^7\hat{g}_s^2}V_p\Omega_{(8-p)} \\ T &= \frac{(7-p)r_H^{(5-p)/2}}{4\pi R^{(7-p)/2}} \\ S &= \frac{4\pi R^{(7-p)/2}r_H^{(9-p)/2}}{(2\pi)^7\hat{g}_s^2}V_p\Omega_{(8-p)} \end{aligned} \tag{2.68}$$

with E being the ADM mass. The first law $dE = TdS$ is easily confirmed.

In the original CA duality conjecture [12, 30] the proportionality constant in Complexity $= k \times$ Action was fixed by an expectation that black holes are the fastest computers in nature, and that at late times they would saturate a bound from Lloyd [33, 48]. Matching $\dot{C} = \frac{2M}{\pi}$ at late times for Schwarzschild AdS black holes sets the constant at $k = \frac{1}{\pi}$. The relevance of the Lloyd bound to these considerations is questionable [35], but in the interest of comparison we note that the systems studied in this work would require different constants to meet the same criterion: for the commutative black holes to saturate the bound at late times, $k = \lim_{t\to\infty} \frac{2M}{\pi\dot{S}}$ would be given by

	$p=2$	$p=3$	$p=4$	$p=5$	$p=6$
k	$\frac{7}{12\pi}$	$\frac{3}{4\pi}$	$\frac{1}{\pi}$	$\frac{1}{\pi}$	$\frac{1}{\pi}$

[7]Note that for $p = 5$ equations 2.68 would indicate zero specific heat. We take this as further evidence that results for $p \geq 5$ should be viewed skeptically.

Furthermore, if the proportionality k were fixed with reference to commutative black holes, the bound would still be violated by highly noncommutative black holes. Rather than proposing novel bounds or searching over all systems for a minimum necessary $k = \lim_{t\to\infty} \frac{2M}{\pi \dot{S}}$ (giving the weakest bound on $\dot{S}$) to be the true proportionality in $\mathcal{C} = kS$, we suspect that the precise proportionality cannot be universally generalized between systems, at least under the established conventions for computing the WDW action.

Chapter 3

Complexity as Volume

[1] We now turn to the CV proposal, and probe that duality in several directions. We show that the apparent lack of universality for large and small black holes is removed if the volume is measured in units of the maximal time from the horizon to the "final slice" (times Planck area). We define and employ a conserved "volume current" associated with a foliation of the bulk spacetime by maximal volume slices. The flux of this current measures the volume, and so provides an alternative perspective of the CV proposal by uniquely relating this vector field to the boundary complexity and its evolution. This flux picture suggests that there is a transfer of the complexity from the UV to the IR in holographic CFTs, which is reminiscent of thermalization behavior deduced using holography. It also naturally gives a second law for the complexity when applied at a black hole horizon. We further establish a result supporting the conjecture that a boundary foliation determines a bulk maximal

[1] This chapter is based on [2], with Josiah Couch, Ted Jacobson, and Phuc Nguyen. Ted Jacobson provided substantial conceptual insight throughout the paper. The computations of section 3.5 were first done by Phuc Nguyen, and the original sketch of the proof in appendix 3.7 was also due to him. Josiah Couch was a primary contributor to section 3.4. My role was to perform numerical and analytic computations, and assist in developing arguments pertaining to the general behavior of maximal volume slices in black hole spacetimes throughout the paper.

foliation without gaps, establish a global inequality on maximal volumes that can be used to deduce the monotonicity of the complexification rate on a boost-invariant background.

3.1 Introduction

Since its original proposal [8, 9], an apparent shortcoming of the complexity equals volume (CV) conjecture is that it requires a lengthscale be chosen to set the proportionality between quantum complexity and bulk volume. No constant choice seems to universally entail the expected growth rate of complexity in black hole systems, $\dot{C} \sim TS$. In order to match this rate, the complexity for black holes that are large compared to the AdS radius ℓ should be given in terms of the volume of the maximal slice by [9]

$$\mathcal{C} \sim \frac{V}{\hbar G \ell}. \tag{3.1}$$

In equilibrium, the maximal slice approaches a final maximal cylinder inside the horizon, with fixed cross-sectional area and a proper length that grows in proportion to Killing time. The above formula equates the complexity to this area, measured in Planck units, times the proper length of the cylinder, measured in AdS length units. For black holes small compared ℓ, the complexity should instead be given by

$$\mathcal{C} \sim \frac{V}{\hbar G r_+}, \tag{3.2}$$

so that the proper length of the cylinder is measured in horizon radius units r_+ [9]. Unlike the case for large black holes, this depends upon the black hole

size. This discrepancy is a principal reason for preferring CA over CV. The fact that the volume divisor in CV is ℓ for large black holes, but r_+ for small black holes, indicates an apparent lack of universality.

However, in both cases this divisor actually corresponds to an intrinsic property of the black hole: the maximum time τ_f to fall from the horizon to the final maximal cylinder is $\sim r_+/c$ for spherical black holes with $r_+ \leq \ell$ in $D \geq 4$ dimensions, and $\sim \ell/c$ for black holes with $r_+ \geq \ell$.[2] Hence the complexity formulae (3.1) and (3.2) actually coincide, up to an order unity numerical factor, if the length in the denominator is understood as $d_f := c\tau_f$. That is, in computing the complexity, the length of a section of the final cylinder ΔL_f should be measured in units of the maximal time to fall from the horizon to the cylinder. The universal expression for the late time complexity is thus

$$\mathcal{C} \sim \frac{V}{\hbar G \tau_f} = \frac{A_f}{\hbar G} \frac{\Delta L_f}{\tau_f}, \tag{3.3}$$

where A_f is the cross-sectional area of the final slice. It turns out that A_f equal to the horizon area A_H up to an order unity factor, so that $A_f/\hbar G \sim S_{\rm BH}$ can be identified with the black hole entropy, which is dual to the CFT entropy. The remaining factor in (3.3) is then $\Delta L_f/\tau_f$. In Sec. 3.3.4 we will show that, quite generally,

$$\frac{\Delta L_f}{\tau_f} \sim \kappa \Delta t \sim \frac{T_H}{\hbar} \Delta t, \tag{3.4}$$

[2] An alternative but related divisor would be the proper time from horizon to final slice along along the volume flow. This scales the same way with respect to the black hole parameters as the longest time, but the numerical factor differs.

where κ is the surface gravity, Δt is the elapsed Killing time, and T_H is the Hawking temperature of the black hole, which is dual to the CFT temperature. With these results, the expression (3.3) for complexity thus becomes

$$\mathcal{C} \sim \frac{T_{\rm H} S_{\rm BH}}{\hbar} \Delta t, \tag{3.5}$$

yielding the black hole dual of the expected complexification rate.

While the universality of the divisor τ_f is more satisfying than the previous ad hoc prescription, it should be admitted that we have no rationale for measuring the length of the final slice in units of τ_f, other than that gives the desired result. Another potential drawback is that this prescription only applies to defining the complexity when the state at late times is thermal equilibrium, so that a 'final' maximal slice exists. In a general dynamical setting, this prescription is inapplicable (although as discussed in Sec. 3.5.4 it *can* be applied in empty AdS, using the boost Killing field to define the notion of equilibrium). That said, as discussed in the next section, the notion of complexity itself is more ambiguous outside of a thermal setting, so it is not clear whether we should expect it to admit a universal holographic definition.

The CV proposal thus remains interesting, as it passes the same checks as does the CA proposal, in some cases (regarding monotonicity on a stationary background) even better as discussed in Sec. 3.4.0.1. The purpose of this work is to take a closer look at various aspects of the CV proposal, attempting to sharpen it and offer some interpretation of its definition and properties, as well as to extend the tests of it.

For both conceptual and computational reasons, we shall make use of a *volume current*, whose flux through the bulk maximal slices anchored at a boundary foliation is equal to the volume of those slices. This volume current is a unit, timelike, divergence-free vector field orthogonal to the bulk maximal foliation. Our interest in the role of this current was inspired by recent work of Headrick and Hubeny (HH) [66], which established a "min-flow/max-cut" theorem relating volumes of maximal slices to minimal fluxes of timelike, divergence-free, vector fields with norm bounded below by unity ("HH flows"). In Ref. [66], it was remarked that it is natural to relate minimization of the number of gates in defining the complexity of a state, in a dual field theory, to minimization of the flux of an HH flow in the bulk spacetime, suggesting a "gate-line" picture of holographic complexity. In this picture, our volume current would correspond to a "gate current".

Let us briefly describe here the HH theorem and its relation to our volume current. The theorem states roughly that, given boundary sub-region A, the maximal spatial volume of any slice homologous to A is equal to the minimal flux of an HH flow through the slice or (equivalently) through A. A given minimizing HH flow has unit norm on the corresponding maximal volume slice, and is orthogonal to that slice, but it is not otherwise uniquely determined. By contrast, the volume current we employ is a particular realization of an HH flow, determined by a boundary foliation, and its flux gives the volume of each slice of the corresponding maximal bulk foliation. That volume is not conserved, because there is flux through the cutoff boundary of

the bulk region.

Although the HH theorem assumes the spacetime is orientable and time-orientable, and assumes a maximal volume slice exists, its proof does not directly invoke any causality assumption or energy condition on the spacetime. By contrast, the volume current requires the existence of a foliation by maximal slices. We argue in Appendix 3.7 that such a foliation exists if i) maximal slices exist, ii) the spacetime satisfies a causality condition, and iii) the strong energy condition and Einstein equation hold. If the foliation is known to exist, then the HH theorem is a simple consequence: the flux of any HH flow is lower-bounded by the maximal volume (for a given boundary Cauchy slice), and the theorem asserts that this bound is actually saturated. The volume current, when it exists, saturates this bound, so our results can be viewed as providing a *constructive* proof of the HH theorem under certain additional assumptions.

The remainder of this chapter is structured as follows. Section 3.2 confronts the ambiguity in defining complexity. The notion seems most robust when applied to time evolution of thermal states, and we summarize several reasons for thinking the volume inside a black hole horizon captures the relevant quantity. Section 3.3 introduces the volume current, a useful tool for quantifying properties of maximal volumes and their evolution, and obtains several results using it. One of these is evidence for the flow of complexity from UV to IR in holographic CFTs. Section 3.4 deduces a global inequality on maximal volumes, and uses this to establish the monotonic increase of the rate of volume growth on a boost invariant background. Section 3.5 probes CV

duality in three settings: black hole formation with one or two shells of matter, spinning black holes, and empty AdS viewed as a pair of thermal Rindler wedges. Section 3.6 is a brief conclusion and outlook. In Appendix A it is argued, assuming the existence of maximal slices, a causality condition and the strong energy condition, that a boundary foliation determines a maximal volume bulk foliation. The unit vector field normal to this foliation is the volume current. The remaining three appendices derive useful technical results. For the balance of this work we use Planck units, with $\hbar = c = G = 1$.

3.2 Volume inside and outside the horizon

The complexity of a pure quantum state is a measure of how many simple unitary operations, or "gates," it takes to produce it, starting with some reference state [15, 67, 68]. Hence, in general, complexity is defined only relative to the choice of reference state and the choice of gates. The original motivation for the proposal of CV duality pertained to time development of complexity at the thermal scale in a finite temperature pure state. In this context, the reference state could presumably be taken to be the thermal microstate at any fixed time, and the gates could be taken to be a fixed collection of gates that act at the thermal energy and length scales, so the rate of change of complexity is intrinsically defined without significant arbitrariness.

However, the CV proposal encounters a divergence in asymptotically AdS spacetime, where the volume of a maximal slice diverges at spatial infinity. This divergence occurs for any state and, according to the usual UV-IR

relation in AdS/CFT duality, it would presumably correspond, according to CV duality, to a divergent UV complexity of the CFT vacuum. While the vacuum is simply the ground state of the theory, it is complex if considered as a state to be prepared, starting with a spatially unentangled state, by the application of local quantum gates. Some analysis has suggested that this interpretation of the UV limit of CV duality might be sensible [20], although the volume-complexity relation could be infinitely sensitive to the somewhat arbitrary definition of the reference state and gates, and to sub-leading modifications of the short distance structure of the state [69, 70].

The volume divergence has generally been dealt with in the literature by imposing a cutoff at some large radius, and focusing on the time dependence of the volume, which does not depend on the location of the cutoff. This corresponds, in effect, to taking the reference state to be the vacuum above the cutoff energy scale, and some "unentangled" state below that scale. The rate of change of the volume in a stationary, thermal state at late times is independent of the location of the cutoff, because the volume growth all happens inside the horizon of the black hole. For this reason, and several others, it makes a lot of sense to count only the volume behind the horizon:[3]

- It is only the complexity at the thermal scale that appears to have a robust significance, independent of the arbitrary choices of reference state and gates.

[3]It was also noted in Ref. [11] that the volume divergence can be regulated by counting only the volume behind the horizon.

- The complexity divisor of the volume, as explained in the introduction, is universal when recognized as a free-fall time from the horizon to the final maximal slice.

- The stationary state volume growth at late time occurs behind the horizon. This was explained in a picturesque way in [9], where it was referred to as "unspooling complexity" from the horizon.

- If the reference state is the vacuum, then only black hole states have complexity that scales as $O(N^2)$ in the CFT. This suggests that holographic complexity (with a vacuum reference state) should, at leading order in N, be associated only with black holes, and that the relevant volume in CV duality should be only that located behind a horizon.

- For a two-sided black hole, a natural reference state is the thermofield double, which is a "Euclidean vacuum" for this topology. The maximal bulk slice corresponding to this state is a global time slice invariant under time reflection (like the $t = 0$ slice in Schwarzschild coordinates), which does not enter the (future or past) horizon, and therefore has zero volume behind the horizon. The volume behind the horizon thus gives the "right" result: the complexity vanishes, since the reference state by definition has zero complexity, but it grows if the time on one boundary is boosted relative to that on the other.

- A "second law of complexity" [60, 61] follows directly when the horizon is a causal barrier, as discussed in the next section.

- The volume inside a white hole horizon can also contribute to the complexity, as in the shockwave scenario discussed below. This allows for *decreasing* complexity, when such behavior is expected.

- In the extremal limit of rotating or charged black holes, the exterior of the horizon develops an infinitely long throat. Regularizing the volume near the boundary (or, for that matter, anywhere outside the horizon) would predict that the complexity of the thermofield double state diverges in the IR as extremality is approached. This questionable feature is avoided by regularizing at horizon.

When applied in a general, time dependent setting, the proposal that complexity corresponds only to the volume behind the horizon suffers from a major drawback, however, if we use the *event horizon*, because the volume inside can grow *before* anything changes in the CFT, at the boundary of the maximal slice. This is illustrated by an example in Sec. 3.5.1 We therefore propose to use an "apparent horizon" as the cutoff surface when there is time dependence. We follow the prescription, used previously in the literature, of measuring the volume on leaves of a foliation of the spacetime by spacelike hypersurfaces that maximize the volume inside an outer cutoff boundary. The apparent horizon is then defined as the boundary of the region containing trapped surfaces on each leaf of this foliation. In (quasi)stationary black hole spacetimes, this apparent horizon will (nearly) coincide with the event horizon. A component of the apparent horizon that asymptotes to the event horizon consists of points lying on marginally outer trapped surfaces [71].

When focusing on the volume inside the horizon, we are limited to discussing the growth of complexity in states dual to a spacetime with a horizon. This is not as restrictive as it might seem, since even empty AdS is a thermal state, when viewed as a pair of Rindler wedges. Indeed, the much studied account of complexity increase for the two-sided black hole can be adapted in a straightforward manner to the Rindler case, where the relevant volume is that inside the Rindler horizon. The interpretation in this case appears to be fully consistent with that for black holes, as we explain in Sec. 3.5.

So far we have been referring to the volume inside the black hole horizon, which is relevant for late time equilibrium states. However an important test for any proposed holographic dual of complexity is that it exhibit the switchback effect [10], which brings the white hole horizon into play. The switchback effect refers to a small time-deficit in the growth of complexity, of order twice the "scrambling time", when a state is evolved backwards in time, perturbed relative to the reference state, and then evolved forwards in time. The calculations in [10] demonstrated that the volume of maximal slices does holographically capture the switchback effect for the thermofield double state, and in particular the maximal volume slices can traverse the black hole region on one side of the shock, and the white hole region on the other side. In the late time approximation used in [10], the portion of the maximal slice outside the horizons does not contribute to the total volume, because it is null, as illustrated in Fig. 3.1. Hence the volume inside the black and white hole horizons suffices to capture the switchback effect. In general, therefore, our

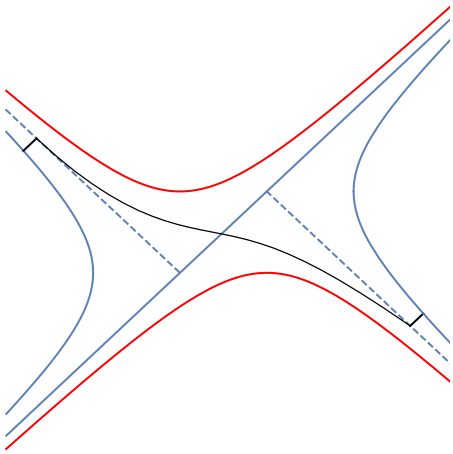

Figure 3.1: Shockwave geometry dual to a perturbed thermofield double state, with a maximal volume hypersurface anchored at late time on the left and early time on the right.

proposal must be taken to include the volume inside the white hole horizon. This appears somewhat natural, considering the fact that the derivation of the switchback effect involves reversed time evolution, and the time reverse of a black hole is a white hole.

Finally, although it appears difficult to relate the volume outside the horizon to a definition of complexity of the state in a universal manner, the assumption that such a relation exists leads to the interesting picture of complexity flowing from UV to IR, as explained in the following section.

3.3 Volume current

While the volume of maximal slices is a nonlocal construct, there is an associated local object, the “volume current," which can be used to infer the

volume growth behind the horizon and the second law of complexity, and which is suggestive the UV to IR flow of complexity. In this section we introduce the volume current, and use it to establish several important properties of the proposed CV duality.

A volume current will be defined given a foliation of spacetime by spacelike hypersurfaces with maximal volume. In the present application, we are interested in asymptotically AdS spacetimes, in which a maximal foliation is determined by a Cauchy foliation of the boundary by slices orthogonal to an asymptotic Killing flow defining time translation. Provided that there is a unique bulk maximal slice that terminates on any fixed boundary Cauchy slice, and provided these bulk slices do not skip over a "gap" in the bulk, the boundary foliation induces a bulk foliation by maximal slices Σ_t, labeled by a parameter t.

We establish the existence of such a bulk foliation by a reasonably convincing—if not mathematically rigorous—series of arguments in Appendix 3.7. To rule out the possibility of gaps we will need to assume that the timelike convergence condition (which is equivalent to the strong energy condition modulo the Einstein equation) holds. Whether or not a global foliation exists, our construction can be applied to the portion of spacetime prior to the final slice that is foliated without a gap. The divergence of the unit timelike vector field v orthogonal to the bulk foliation is the trace of the extrinsic curvature K of Σ_t, which vanishes since the slices are assumed to be maximal. This vector field is thus a conserved current, which we dub the *volume current* associated

with the maximal foliation. The volume of Σ_t is the flux of this current through Σ_t,

$$V_t = \int_{\Sigma_t} v \cdot \epsilon. \tag{3.6}$$

(Here ϵ is the spacetime volume element, and the dot indicates contraction on the first index of ϵ.) The construction of the volume flow v, starting from a boundary foliation, is illustrated in Figure 3.2.

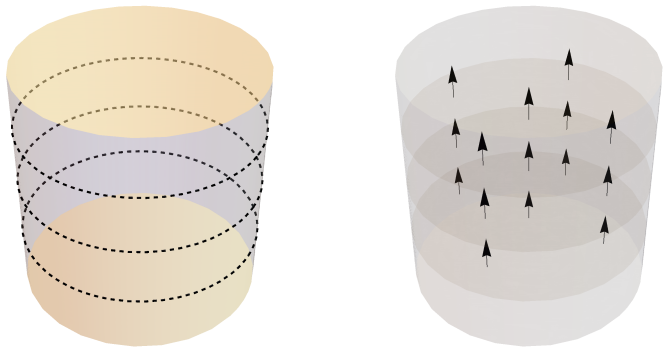

Figure 3.2: Left: Illustration of the boundary foliation $\Sigma(\tau)$ with 3 slices in the foliation. Right: Illustration of the corresponding bulk foliation by maximal slices, and the volume flow.

As discussed in Sec. 3.2, to obtain a finite volume, and hence a finite putative complexity, the integral must be cut off at some outer boundary $\partial\Sigma_t$. We will continue to use the letter "V" for this truncated volume.

3.3.1 Second law of complexity

Since the divergence of v vanishes, the change ΔV from one time slice to another is entirely accounted for by the flux of v through the boundary, or

boundaries, of that slice. If we restrict to the volume inside the horizon, then the change is accounted for by the flux of v through the horizon. Since v is a future pointing timelike vector, the flux through the future event horizon is positive, and it follows that the interior volume can only increase. When considering a spacelike portion of the apparent horizon forming a past boundary of the trapped region, again the flux is positive. CV duality then implies that in these situations, the complexity must increase, in accordance with the second law of complexity [60, 61]. Note that this argument applies in arbitrary dynamical black hole spacetimes, such as a black hole formed by collapse. If, however, the apparent horizon has a timelike section, which can happen when a black hole evaporates, and even when positive energy conditions hold [71], then we cannot rule out a decrease in the volume enclosed. This seems natural: when this horizon is not a causal barrier, there is no reason to expect the associated complexity to irreversibly increase.

Note that when the region behind the horizon includes the white hole, as with the two-sided black hole with a shockwave of Figure 3.1, the complexity can *decrease* as time increases on the side opposite to the shock [10]. Correspondingly, the volume of the maximal slice inside the white hole decreases, since the volume current can only exit the white hole horizon.

3.3.2 Complexity flow from UV to IR

The flux of the volume current inward across the horizon suggests a picture of complexity flowing from UV to IR, which is further corroborated

by examination of the flux through other surfaces. Consider the section of a maximal slice Σ_t stretching between the horizon of a black hole and the outer cutoff boundary in asymptotically AdS spacetime. The rate of complexification of the thermal degrees of freedom should not depend upon where the cutoff surface is placed, because that just changes the constant complexity assigned to the degrees of freedom that are in their ground state. Holographically, this works because at sufficiently large radius, as explained below, v is invariant under the asymptotic Killing flow. The volume between two large radii is thus independent of time, which implies that the flux of v through the boundary is independent of its (large) radius. Moreover, at sufficiently late times, as also explained below, v is invariant under the Killing flow *everywhere*, including on and inside the horizon. The flux of volume through the horizon is therefore equal to the flux through the outer boundary at the UV cutoff. According to CV duality, *the complexity thus flows from the UV to the IR, and accumulates at the thermal scale.*

This conclusion may be related to the fact that, in a holographic CFT, thermalization proceeds from UV to IR [72, 73]. On the other hand, it seems to be somewhat in tension with the fact that in a thermal state the UV degrees of freedom remain unexcited. If unexcited, how could they participate in the generation of complexity? Perhaps since their excitation is not strictly zero, but only exponentially suppressed, their dynamics could provide the source from which the complexity unfolds. Or is complexity generated purely from the thermal scale fluctuations? And if the latter is the case, then how can we

understand the dual flow of the volume current from large to small radii? We leave these questions to be addressed in the future.

3.3.3 Asymptotic late time flows on stationary spacetimes

At sufficiently large radius v is invariant under the asymptotic Killing flow, because the maximal slices must asymptote to the boundary slices defining the maximal foliation, which are taken into each other by the Killing flow. Nevertheless, in the two-sided eternal black hole spacetime, the Killing flow does not push both boundary slices to the future together, so in general the slices of the corresponding maximal foliation are not related by the Killing flow. However, at sufficiently late times the foliation becomes invariant under the Killing flow. This can be seen from the fact that the maximal slices approach the final maximal slice inside the horizon, and the final slice is taken into itself under the Killing flow. In Appendix 3.9, we demonstrate these claims by explicit computation with the AdS-Schwarzschild black hole. Figure 3.3 shows a plot of the volume current for the BTZ black hole, based on the analytical expression derived in 3.8.1. This figure illustrates the asymptotic invariance under the Killing flow at the boundary and as the final slice is approached.

The late time limit of this flow can be easily found in closed form in spherical symmetry, where it is given by $v = v^t\partial_t + v^r\partial_r$ in Schwarzschild coordinates. The normalization condition $v^2 = -1$ determines v^t in terms of v^r. At late times the components are independent of t, and the divergence free condition implies $v^r = -K/r$ where K is some constant. K can be determined

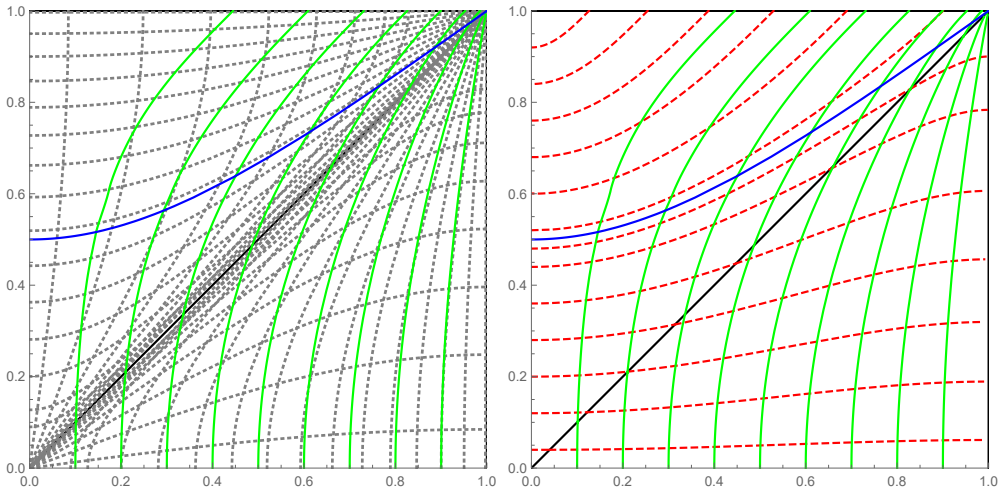

Figure 3.3: Plot of the flow lines of the BTZ volume current (in solid green) on a quarter of a Penrose diagram. Left: the flow lines are shown together with the Schwarzschild coordinate grid lines (dotted black), and the final slice (solid blue). Right: the flow lines are shown together with the maximal slices (dashed red).

by the normalization condition $g_{rr}(v^r)^2 = -1$ on the $t = 0$ line in the middle of the black hole interior region since, by symmetry, v^t vanishes there. Because we have assumed the late time limit, this must be done at the "final slice" [9, 10], which is the maximal slice at constant r in the black hole interior. For example, in the non-rotating case of the BTZ black hole treated in Sec. 3.5 we have

$$K = r_f \alpha_f = r_+^2/2\ell. \tag{3.7}$$

where α_f is the norm of the Killing vector ∂_t at r_f.

The constant K gives the rate of volume flow, with respect to Killing time, per unit angle, through any surface of constant r coordinate, e.g. the

horizon. To see this, note that the volume flux is given by the integral of $v \cdot \epsilon$ pulled back to the constant r surface. In t, r, ϕ coordinates, $\epsilon = r\, dt \wedge dr \wedge d\phi$, so this pullback is $-rv^r\, dt \wedge d\phi = K\, dt \wedge d\phi$. This conclusion generalizes to spherical black holes in any spacetime dimension.

3.3.4 Asymptotic volume growth and complexity

For the BTZ black hole [74], the K written above can be expressed in terms of the surface gravity $\kappa = r_+/\ell^2$ and the horizon area $A = 2\pi r_+$ as

$$K = \ell \kappa A/4\pi = 2\ell T_{\mathrm{H}} S_{BH}, \tag{3.8}$$

where T_{H} and S_{BH} are the black hole temperature and entropy, respectively. In this way, we can see that the late-time rate of growth is 2ℓ times $T_{\mathrm{H}} S_{BH}$. The factor ℓ is the "divisor," discussed in the introduction, that gives the ratio of volume to complexity.

The fact that $K \propto \ell T_{\mathrm{H}} S_{BH}$ is not an accident. It could be anticipated from the first equality in (3.7). In fact, that equality generalizes to a D dimensional spherically symmetric spacetime, where

$$K = r_f^{D-2} \alpha_f, \tag{3.9}$$

and to black holes of any size. This can be used to understand why, as mentioned in the Introduction, the ratio of volume to complexity should be the maximal proper time from the horizon to the final slice for black holes of any size. The factor r_f^{D-2} is the area per solid angle of a cross section of the final

slice. It turns out that $r^{D-2}\alpha(r)$ reaches its maximum not far from the horizon, so we have $r_f \sim r_+$. The first factor in (3.9) therefore scales as the horizon area per solid angle, times a numerical constant. The factor α_f is the norm of the Killing vector ∂_t at the final slice. The Taylor expansion for α around the horizon is $\alpha = \kappa\tau + \ldots$, where τ is the proper time from the horizon, in the direction orthogonal to the Killing flow.[4] Thus, for both large and small spherical black holes in any dimension, the volume grows at a rate

$$K \sim \tau_f \kappa A_+ \sim \tau_f T_{\rm H} S_{BH} \tag{3.10}$$

where the symbol $\sim$ denotes equality up to numerical constant that depends on spacetime dimension and is different for large and small black holes. Since complexity is expected to grow in the dual CFT at the rate $\sim TS$, we conclude that the ratio of volume to complexity should be τ_f (i.e. $\hbar G \tau_f$). In section 3.5.3 we show that this reasoning also applies to the Kerr metric (with vanishing cosmological constant).

3.3.5 Maximal time from horizon to final slice

In this subsection we first compute the maximal time τ_f from the horizon to the final slice for hyperbolic, planar, and spherical Schwarzschild-AdS black holes. We next give a general argument, analogous to that used in Hawking's cosmological singularity theorem, showing that for any black hole in a

[4] Quite generally, $\kappa = |d\alpha|_{\rm horizon}$, where α is the norm of the horizon generating Killing vector. Usually one sees this relation applied to the gradient in the spacelike direction from the bifurcation surface, but it can equally well be applied in the timelike direction as done here.

spacetime with negative cosmological constant Λ, and satisfying the strong energy condition for matter other than the cosmological constant, $|\Lambda|^{-1/2}$ sets an upper bound for the value of τ_f.

3.3.5.1 Schwarzschild-AdS black holes

The value of τ_f for Schwarzschild-AdS black holes is given by the proper time from r_+ to r_f along the line $t = 0$:

$$\tau_f = \int_{r_f}^{r_+} \frac{dr}{\alpha(r)}. \tag{3.11}$$

To estimate the value of this integral, we may use the Taylor expansion about the horizon. The line element has the form $ds^2 = -\alpha^2\, dt^2 + \alpha^{-2}\, dr^2 + r^2 h_{ij} dx^i dx^j$, and $(d\alpha^2/dr)_+ = (-2d\alpha/d\tau)_+ = -2\kappa$, so

$$\tau_f \approx \frac{1}{\sqrt{2\kappa}} \int_{r_f}^{r_+} \frac{dr}{\sqrt{r_+ - r}} = \frac{\sqrt{2(r_+ - r_f)}}{\kappa} \sim \frac{\ell r_+}{\sqrt{(D-1)r_+^2 + (D-3)k\ell^2}}, \tag{3.12}$$

where $k = -1, 0, 1$ for hyperbolic, planar, and spherical black holes, respectively. Thus for the BTZ black hole ($D = 3$) or planar black holes, or hyperbolic or spherical black holes with $r_+ \gg \ell$, we have $\tau_f \sim \ell$. If instead $r_+ \ll \ell$ and $D \neq 3$ and $k \neq -1$, then $\tau_f \sim r_+$.

The case of small hyperbolic black holes should be treated separately: this case has an extremal limit, i.e. a lower bound for r_+ of the order of ℓ [75]. The estimate for τ_f above assumes that $r_+ - r_f \sim r_+$ upto some order unity factor, but $r_+ - r_f = 0$ at extremality. A computation expanding around

extremality (similar to that for the Kerr case treated below in section 3.5.3) shows that $\tau_f \sim \ell$ for the extremal hyperbolic black hole.

3.3.5.2 Upper bound to τ_f set by the AdS scale

It is interesting to note that an upper bound of the form $\tau_f \lesssim \ell$ follows from a more general result. Consider the future domain of dependence $D^+(S)$ of any achronal spacelike surface S (not necessarily a Cauchy slice for the whole spacetime). $D^+(S)$ is itself a globally hyperbolic spacetime, so Theorem 9.4.5 in [76] tells us that any point p in $D^+(S)$ lies on a curve that maximizes the time to S, and Theorem 9.4.3 implies that this curve is a geodesic that meets S orthogonally, without a conjugate point between p and S. Integration of the Raychaudhuri equation for the congruence of geodesics orthogonal to S then shows that, regardless of the value of the trace of the extrinsic curvature of S (which is the expansion of this congruence evaluated at S), each geodesic must have a conjugate point within a time $\int_{-\infty}^{\infty} d\theta/(\theta^2/2+R_{ab}u^a u^b)$. To obtain this we neglect the squared shear term in the Raychaudhuri equation, since it would only make the time shorter. If there is a negative cosmological constant $\Lambda = -(D-1)(D-2)/2\ell^2$, and if the matter stress energy tensor satisfies the strong energy condition and the Einstein equation holds, then by neglecting the matter contribution we obtain the upper bound $\pi\sqrt{D-2}/\sqrt{-\Lambda} = \sqrt{\frac{2}{D-1}}\pi\ell$ to the time. No point inside $D^+(S)$ can lie at a time greater than this from S. For example, this result applies to the domain of dependence of a Cauchy slice for an asymptotically AdS spacetime, also known as the "Wheeler deWitt

patch".

To derive an upper bound for τ_f, we can apply this result to the case where the achronal surface S is a spacelike slice just inside the future horizon H of the black hole. As long as the final slice lies inside $D^+(H)$,[5] we obtain the upper bound

$$\tau_f \leq \sqrt{\frac{2}{D-1}}\pi\ell. \tag{3.13}$$

For $D = 3$ this becomes $\tau_f \leq \pi\ell$, which is consistent with the exact result $\tau_f = \pi\ell/4$ obtained in section 3.5.2 for the rotating BTZ black hole.

3.4 Global volume inequality and complexification rate monotonicity

In this section we discuss a global inequality relating the volume on different slices, which leads to an inequality on mixed partial derivatives with respect to boundary time. On a boost symmetric background, this allows us to obtain an inequality for the second time derivative of the volume, which implies that the complexification rate grows monotonically on boost invariant black hole backgrounds. We thus recover from a general viewpoint this fact found previously using explicit computations with eternal black holes in AdS. To derive the global volume inequality, we need only use the definition of maximal slices; no energy condition or other additional ingredient is needed.

[5] If $D^+(H)$ does not contain everything inside the event horizon, there is a Cauchy horizon, which is presumably unstable to formation of a singularity, eliminating the Cauchy horizon.

Consider for concreteness a compact box in an eternal black hole spacetime (Figure 3.4), with the vertical sides of the box taken to be some near-boundary cutoff. Let t_1, t_2 be two times on the left cutoff (with $t_1 < t_2$), and t_3, t_4 be two times on the right cutoff (with $t_3 < t_4$). The inequality then says that

$$\mathrm{Vol}(t_1, t_3) + \mathrm{Vol}(t_2, t_4) - \mathrm{Vol}(t_1, t_4) - \mathrm{Vol}(t_2, t_3) \geq 0, \tag{3.14}$$

where $\mathrm{Vol}(t_1, t_3)$ is the maximal volume between time t_1 on the left and time t_3 on the right, etc. Note that, even though each of the four maximal slice volumes diverges as the cutoff is sent to the boundary, the linear combination in (3.14) is UV-finite.

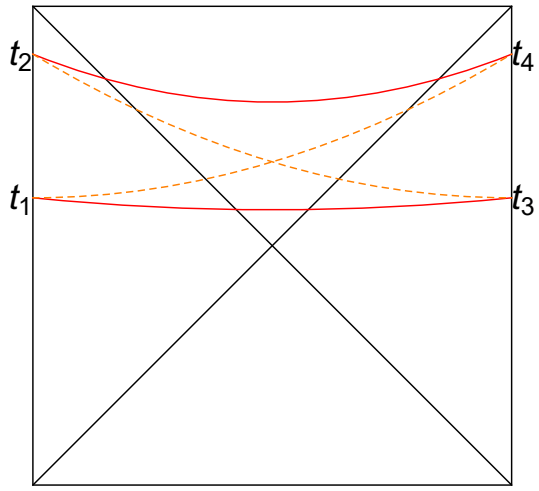

Figure 3.4: An SSA-like inequality is obeyed between the four maximal slices shown (solid red and dashed orange).

To establish the inequality, observe that the two dashed orange slices in Fig. 3.4 intersect each other, and we can divide them into four segments,

each connecting the intersection with one of the four boundary times. By maximality, we know that $\mathrm{Vol}(t_1, t_3)$ is greater than the sum of the volumes of the two lower orange segments. Similarly, we know that $\mathrm{Vol}(t_2, t_4)$ is greater than the sum of the volumes of the two upper orange segments. The sum of these two inequalities yields (3.14).

This example of a global volume inequality can be generalized to a general bulk spacetime, with one or more boundary components. We illustrate this in Figure 3.5 for a spacetime with one boundary. Let σ_1 and σ_2 be two Cauchy slices of the boundary, and let Σ_1 and Σ_2 be the corresponding maximal slices. (As before, we regulate the volume by placing a cutoff surface in the asymptotic region.) Assuming the bulk is time orientable, it admits a foliation by timelike curves, which also extends to the boundary. Each of these curves intersects each of the Cauchy slices once. On the boundary define two new piecewise smooth Cauchy slices σ_- and σ_+, consisting of the first and second intersection points respectively, and similarly define two new bulk slices (which are also only piecewise smooth), Σ_- and Σ_+. Then the boundary of $\Sigma_\pm$ is $\sigma_\pm$, and $\Sigma_\pm$ is generally not the maximal volume slice with this boundary. Generalizing the previous notation, let $\mathrm{Vol}(\sigma)$ denote the maximal volume for a slice bounded by σ, and now let $\mathrm{Vol}(\Sigma)$ be the volume of the bulk slice Σ. Then we have $\mathrm{Vol}(\sigma_\pm) \geq \mathrm{Vol}(\Sigma_\pm)$, and addition of these inequalities yields $\mathrm{Vol}(\sigma_+) + \mathrm{Vol}(\sigma_-) \geq \mathrm{Vol}(\Sigma_+) + \mathrm{Vol}(\Sigma_-)$. Moreover, $\mathrm{Vol}(\Sigma_+) + \mathrm{Vol}(\Sigma_-) = \mathrm{Vol}(\Sigma_1) + \mathrm{Vol}(\Sigma_2)$, simply because $\Sigma_+ \cup \Sigma_- = \Sigma_1 \cup \Sigma_2$, so it follows that

$$\mathrm{Vol}(\sigma_+) + \mathrm{Vol}(\sigma_-) - \mathrm{Vol}(\sigma_1) + \mathrm{Vol}(\sigma_2) \geq 0. \tag{3.15}$$

To recover the previous case from this generalization, take σ_1 to be the two-boundary slice consisting of the union of the t_1 and t_4 slices, and take σ_2 to be that consisting of the union of the t_2 and t_3 slices.

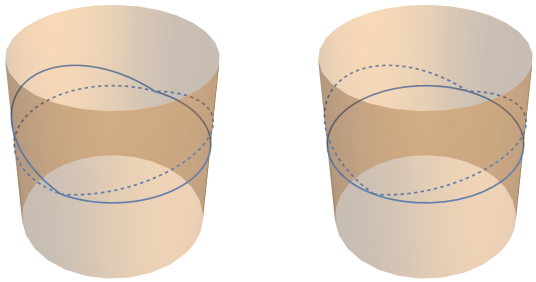

Figure 3.5: On the left are two Cauchy slices, σ_1 (in continuous blue) and σ_2 (in dashed blue), on the boundary of the Poincaré patch of an asymptotically AdS spacetime. On the right the corresponding σ_+ and σ_- are in dashed blue and continuous blue, respectively.

3.4.0.1 Monotonicity on a boost-symmetric background

We next explain how inequality (3.14) implies monotonic growth in time of the complexification rate.[6] Before showing this, let us discuss the physical significance of this monotonicity property. Black holes are expected to excel at scrambling quantum information and, in particular, should complexify the fastest. Thus, one can expect that their late-time rate of complexification (once transient effects have died out) saturates quantum-information bounds, and in particular should be greater than the complexification rates at earlier times. The monotonicity property coming out of CV-duality is in agreement with

[6] We thank Adam R. Brown for suggesting the following argument.

this general expectation. By contrast, CA-duality was recently discovered to violate this monotonicity property [1, 36], perhaps putting into question that particular proposal.

We now take the the infinitesimal limit of inequality (3.14), setting $t_1 = t_L$, $t_2 = t_L + \delta t_L$, $t_3 = t_R$, $t_4 = t_R + \delta t_R$. To leading order in small quantities, we find:

$$\begin{aligned} &\mathrm{Vol}(t_L, t_R) + \mathrm{Vol}(t_L + \delta t_L, t_R + \delta t_R) - \mathrm{Vol}(t_L, t_R + \delta t_R) - \mathrm{Vol}(t_L + \delta t_L, t_R) \\ &= \frac{\partial^2 \mathrm{Vol}}{\partial t_L \partial t_R} \delta t_L \delta t_R. \end{aligned} \tag{3.16}$$

Therefore the global inequality (3.14) implies positivity of the mixed partial derivative:

$$\frac{\partial^2 \mathrm{Vol}}{\partial t_L \partial t_R} \geq 0. \tag{3.17}$$

In terms of the new variables $t_\pm = t_L \pm t_R$, this inequality becomes

$$\frac{\partial^2 \mathrm{Vol}}{\partial t_+^2} - \frac{\partial^2 \mathrm{Vol}}{\partial t_-^2} \geq 0. \tag{3.18}$$

For an eternal black hole, the boost symmetry implies that the maximal volume cannot be a function of t_- [10]. We thus end up with the simple statement:

$$\frac{\partial^2 \mathrm{Vol}}{\partial t_+^2} \geq 0. \tag{3.19}$$

which implies that the first derivative of Vol with respect to t_+ (or equivalently, with respect to either t_L ot t_R with the other one kept fixed) is monotonic. Replacing the volume by the complexity $\mathcal{C}$, this implies the monotonic increase of the complexification rate discussed above.

Note that inequality (3.14) does not imply monotonicity of the complexification rate for a general bulk spacetime, since we used the boost symmetry of a 2-sided black hole to deduce it. Nevertheless, we can take the infinitesimal version of the inequality (3.15) for a generic spacetime, and derive a condition similar to the positivity of the mixed partial derivative (3.17). To this end, consider the case where the two boundary Cauchy slices σ_1 and σ_2 coincide except on two small disjoint bumps to the future, one on σ_1 and one on σ_2. Expanding to leading order in the size of the bumps, we find that the "off-diagonal" part (since the bumps are disjoint) of the second functional derivative of the maximal volume $\mathrm{Vol}(\sigma)$ with respect to σ variations is nonnegative.

3.5 Quenches, rotation and AdS-Rindler: further probes of CV duality

CV duality has been primarily probed in the setting of the eternal black hole, where interesting time dependence is introduced either by examining foliations that are not Killing time slices, or by introducing shockwave perturbations. In this section we extend the set of examples, by considering multiple quenches, where the black hole temperature changes, spinning black holes, where the angular momentum provides an extra parameter on which the dependence can be checked, and AdS-Rindler spacetime, where the time dependence of the vacuum complexity in the Rindler wedge is seen to be equivalent to that in a black hole spacetime.

3.5.1 AdS-Vaidya: event horizon vs apparent horizon

The time dependence of holographic complexity has been studied for quenched systems, i.e. systems into which a finite energy density is injected, using the AdS-Vaidya solution [11, 69, 77, 78]. In this subsection, we compare the growth of the volume inside the horizon for an AdS-Vaidya spacetime in the thin shell limit, using different definitions of the volume cutoff, and we extend existing studies to the case of two infalling shells.

In Section 3.2 we discussed several reasons supporting the notion that volume inside the black hole horizon is perhaps a more robust measure of complexity of the thermal state than is the volume of a global maximal slice with a cutoff at large distances from the black hole. When the black hole forms from collapse, the degeneracy between different definitions of the horizon is lifted, hence we should examine which (if any) is more appropriate for CV duality. In particular, while the absolute event horizon remains a null hypersurface defined teleologically as the boundary of the past of future null infinity, we shall also consider the apparent horizon, defined here as the boundary of the region containing outer trapped surfaces on the leaves of the maximal foliation An apparent horizon defined this way is an example of a holographic screen [79, 80], i.e. a hypersurface foliated by marginally trapped surfaces. Recent work [81, 82] has shown that the area of a leaf of such a foliation is related to a certain coarse grained holographic entropy, which lends support to the idea that the volume inside such surfaces might be directly related to complexity [83].

When the spacetime is time dependent, the maximal time from the horizon to the final slice (the "complexity divisor" of the volume) in general becomes time dependent, and in that context it might well make more sense to measure the time from the apparent horizon rather than from the event horizon. We shall make no attempt here to determine which precise extension of the concept is more appropriate. Instead, we will just address the case where the black hole is either the BTZ black hole in $D = 3$ dimensions, or in higher dimensions is large enough so that the time $\sim \ell$ is the always the relevant one.

3.5.1.1 Single quench

Consider, then, a black hole formed by an infalling shell in AdS. If the event horizon forms "at the same time" as the time on the boundary when the shell starts to fall in, i.e. the time at which an external agent injects some energy into the CFT ground state, then the maximal slice volume inside the horizon remains zero until the injection time, and starts growing after that. This would be consistent with the general expectation that the CFT state starts to complexify after the energy injection. However, the horizon forms before the injection time if the final horizon radius is greater than the AdS length scale, and after the injection time if it is less [84].

To illustrate this, let us work for simplicity in the in the thin-shell limit, and in three spacetime dimensions. The BTZ-Vaidya metric in (r, v)

coordinates reads:

$$ds^2 = -f(r,v)dv^2 + 2dvdr + r^2 d\phi^2 \tag{3.20}$$

$$f(r,v) = 1 + r^2 - \Theta(v)(1 + r_+^2) \tag{3.21}$$

where Θ is the unit step function. This metric describes a spherical shell at $v = 0$ collapsing to form a black hole. To draw the conformal diagram, we need to pass to conformally compactified coordinates (R, T) (see [84] for the coordinate transformation). The metric becomes:

$$ds^2 = \frac{-dT^2 + dR^2}{\cos^2 R} + r(T,R)^2 d\phi^2 \tag{3.22}$$

$$r(T,R) = \begin{cases} \frac{(1-r_+^2)\sin R - (1+r_+^2)\sin T}{2\cos R} & \text{if } R+T > 0 \\ \tan R & \text{if } R+T < 0 \end{cases} \tag{3.23}$$

Fig. 3.6 shows the conformal diagrams for three choices of horizon radius (larger than L, equal to L and smaller than L). The center of AdS is at $R = 0$, the boundary is at $R = \frac{\pi}{2}$, and the singularity is at $(1 - r_+^2)\sin R = (1 + r_+^2)\sin T$. As illustrated in Fig. 3.6, the horizon forms at the same time T as the injection time on the boundary only in the special case when the horizon radius of the final black hole is exactly equal to the AdS length.

Now consider the large black hole case, and consider a constant T slice to the past of the infalling shell, where the geometry is locally AdS. This slice is invariant under the T reflection isometry, so it has vanishing extrinsic curvature, hence is maximal. We depict such a maximal slice in blue on the left panel of Fig. 3.6. Clearly the portion inside the horizon starts growing even before the energy injection occurs on the boundary.

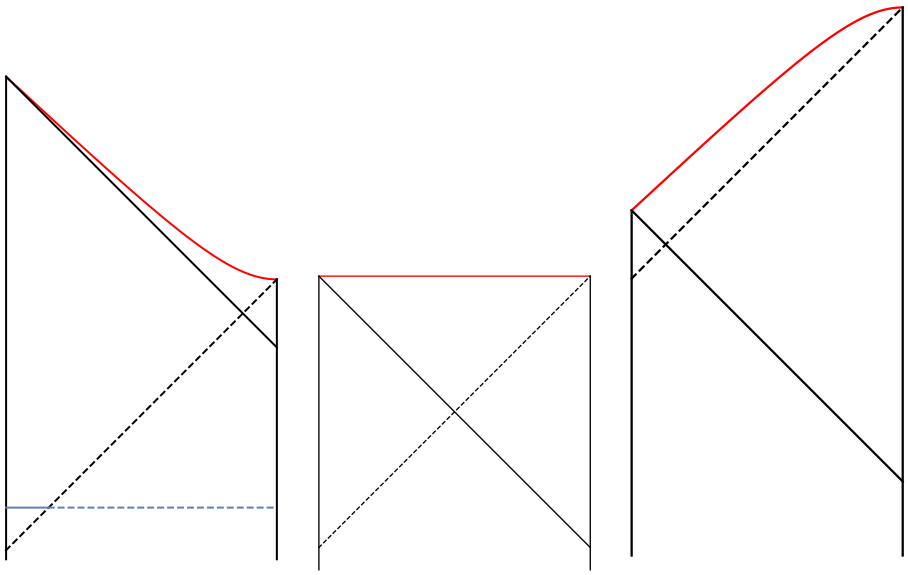

Figure 3.6: Conformal diagram for the BTZ-Vaidya spacetime in the thin-shell limit for three representative choices of the horizon radius r_+ (left: $r_+ = 5L$, center: $r_+ = L$, right: $r_+ = L/5$). For all three panels, the center of AdS, the infalling shell and the boundary are in continuous black, the horizon is in dashed black and the singularity is in red. Moreover, on the left panel, we depict a maximal slice anchored at a boundary time to the past of the infalling shell in blue. The portion inside the event horizon is in continuous blue, and the portion outside the horizon is in dashed blue.

The apparent horizon for Vaidya-BTZ consists of two segments in the conformal diagram (illustrated in 3.7). One segment is the event horizon $r = r_+$ in the BTZ portion of the spacetime, and the other segment is the infalling shell itself. The interior of the apparent horizon (i.e. the trapped region) is shaded in light blue in Fig. 3.7. It is clear that the volume inside the apparent horizon can grow only after the injection occurs, with a delay because the maximal slice does not have any portion inside the light blue region of Figure

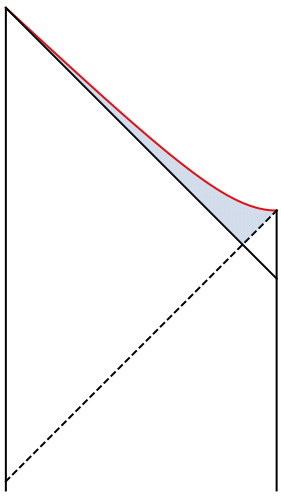

Figure 3.7: The region inside the apparent horizon is shaded in blue.

3.7 immediately after injection.

In Fig. 3.8 we plot the volume inside the horizon as a function of the boundary time, and compare with the volume inside some large cutoff near the boundary, as well as with the volume inside the apparent horizon (see below). The plots on the left are for a large black hole with $r_+ = 5\ell$, while those on the right are for a small black holes with $r_+ = \ell/5$. (To produce this plot, we solved numerically for the maximal slices; the details are explained in Appendix 3.10.) Several features of this figure are worth remarking upon:

- The volume inside a near-boundary cutoff is shown as the blue curve. It starts to grow at the injection time. For a large black hole, the volume inside horizon, shown by the red curve, starts growing before the injection time.

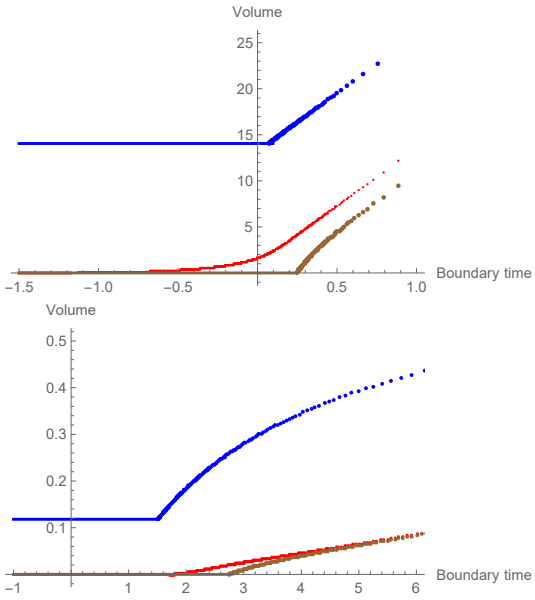

Figure 3.8: Plot of volume versus boundary time, for a large black hole (left) with $r_+ = 5\ell$ and a small black hole (right) with $r_+ = \ell/5$. In both panels, the blue curve is the volume inside some large cutoff, the red curve is the volume inside the event horizon and the brown curve is the volume inside the apparent horizon. The boundary time is measured in units of ℓ.

- For a large black hole, the volume inside a near-boundary cutoff (blue curve) grows at essentially the late-time rate as soon as the energy is injected. For a small black hole, the growth rate starts out higher, then decreases to to late time rate.

- The growth rates all converge at late time both for large and small black holes. This verifies the expectation that all late time growth of volume occurs inside the horizon for a one-sided black hole, as it does for a two-sided one.

- From a geometrical viewpoint, there are two distinct regimes for the volume inside the event horizon: it may be contained entirely inside the pure AdS part of the spacetime, or it may include a part in the AdS portion and a part in the BTZ portion. There is a critical boundary time at which the former regime transitions to the latter one, on the maximal slice, A priori it seems that the volume curve might have a kink at this transition, however inspection of the red curves suggests that the derivative is actually continuous at the transition.

- The brown curves show the volume inside the apparent horizon, which is always the last to start growing. In particular, no growth occurs before injection, and in fact there is a delay between injection and the onset of growth of the volume inside the apparent horizon. This delay is perhaps related to a thermalization timescale. As shown in [72, 73] thermalization takes a time on the order of the AdS length scale, with specific behavior depending on the scale at which thermalization is probed.

- The rate of change of the volume inside the apparent horizon starts out higher than the late-time rate, and then approaches the late-time value from above. This is contrary to the monotonic increase expectation. This decreasing behavior was also observed in [77]. Moreover, the longest time to the final slice is the same from all points on the outer portion of the apparent horizon (which coincides with the event horizon), and is longer than any other time from inside the horizon, so there is presumably no

additional time dependence coming from the divisor τ_f in the complexity formula.

3.5.1.2 Two quenches

In this subsection we consider BTZ-Vaidya with two infalling shells. The field theory picture is that energy is injected twice into the CFT. After the first injection thermalizes, we expect a linear growth of complexity at a rate proportional to the energy injected, since $TS \propto E$. After the second injection, the system now has more energy, so we expect the complexification rate to increase.

If the second injection occurs sufficiently far to the future of the first one, so that the complexity has enough time to reach the linear growth regime before the second injection, CV duality would imply that the plot of maximal volume versus time will consist of three linear regimes (zero slope, a finite slope, and a bigger finite slope).

The metric is still given by eq. (3.20), except that the function $\Theta(v)$ is no longer a unit step function, but a "double step function":

$$\Theta(v) = a\theta(v) + (1-a)\theta(v-b) \tag{3.24}$$

where a is a real number between 0 and 1, b is a positive real number, and θ is the unit step function. The function $f(r,v)$ becomes:

$$f(r,v) = \begin{cases} 1+r^2 & v<0 \\ r^2-R^2 & 0<v<b \\ r^2-r_+^2 & b<v \end{cases} \tag{3.25}$$

with $R^2 \equiv a(1+r_+^2) - 1$. Thus, we have AdS for time $v < 0$, and the usual BTZ with horizon radius r_+ for $b < v$. In the intermediate regime, $0 < v < b$, we have two qualitatively different cases depending on the sign of R^2 (it need not be positive): If $R^2 > 0$ we have a BTZ black hole with horizon radius R, while if $-1 < R^2 < 0$ we have a "conical defect" geometry.[7]

We have solved numerically for the maximal slices and their volume with the parameter choice $a = 1/2$, $b = 1$ and $r_+ = 2$ (see appendix 3.10 for the technical details). The shape of a maximal slice anchored at late time on the boundary is depicted using an Eddington-Finkelstein diagram in Fig. 3.9. The effect of the outer shell is to push the slice further from the singularity, which can be explained intuitively as follows: the final slice for the BTZ-Vaidya should approach the final slice of the eternal BTZ black hole (with the same total mass) at late time, which is a constant radius slice with $r \propto r_+$. Since the effect of the outer shell is to increase the horizon radius, it also pushes the final slice further from the singularity.

In Fig. 3.10, we plot the volume of the portion of the maximal slice lying inside the apparent horizon as a function of the boundary time t_b at which the slice is anchored, with the same parameter choice used for Fig. 3.9. Note that for a brief period of time after the maximal slice crosses the point where the second shell meets the apparent horizon, the slice has two disconnected

[7] This conical defect geometry is also a possibility in the single-shell case. This can be seen as follows: the stress-energy tensor of the single-shell AdS-Vaidya in three dimensions is $T_{vv} = \frac{1+r_+^2}{2r}\Theta'(v)$. If $-1 < r_+^2 < 0$, we do not have a black hole final state, yet the null energy condition is still obeyed. This is the conical defect regime.

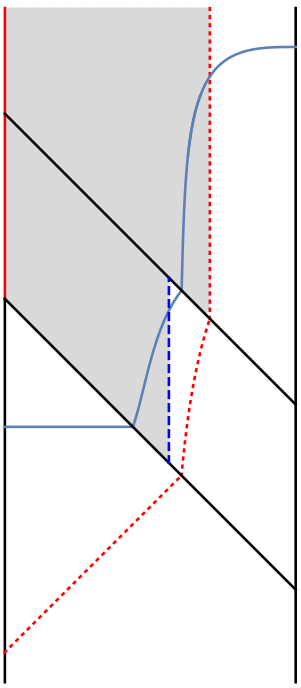

Figure 3.9: Eddington-Finkelstein diagram of the BTZ-Vaidya solution with two infalling shells. The abscissa and ordinate for the plot are $\rho = \arctan(r)$ and $t = v - \rho$, respectively. The two infalling shells, the center of AdS, and the boundary are in thick black, the singularity is in solid red, the constant radius portion of the apparent horizon between the shells is in dashed blue, the event horizon is in short-dashed red, and the maximal slice anchored at late boundary time is shown in continuous blue. The apparent horizon is the boundary of the grey shaded region.

parts lying inside the apparent horizon, separated by an annular region falling outside the apparent horizon.

It would be interesting to consider similar double quenches but in $D \geq 4$ dimensions, with spherical black holes of different sizes, so that the time dependence of the time to final slice divisor τ_f might come into play.

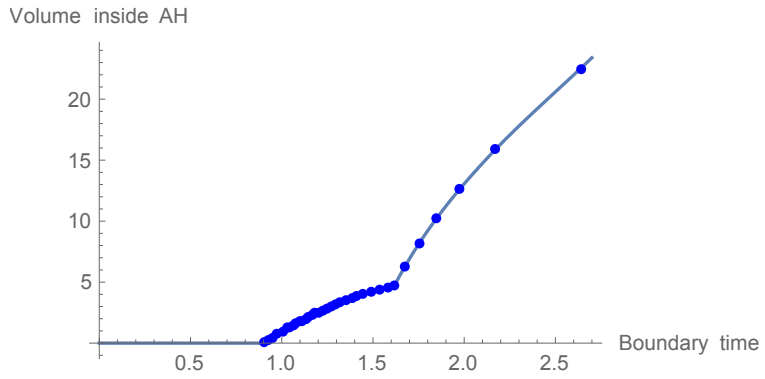

Figure 3.10: Plot of the maximal slice volume inside the apparent horizon in a Vaidya spacetime with two shells. The kinks occur when the maximal slice crosses the points where the first and second shells meet the apparent horizon.

3.5.2 Rotating BTZ black hole

A further probe of CV duality is provided by considering rotating black holes. A rotating black hole is dual to a rotating thermal CFT state. The complexity in such a state should presumably grow, with respect to time in the rotating frame, as the entropy of the state times the temperature $T_{\rm rot}$ in that frame, since that is the frame in which thermal equilibrium is established. That is, one would expect that $d\mathcal{C}/dt_{\rm rot} \sim T_{\rm rot} S$. While the CFT entropy is frame independent, and is thus equal to the dual black hole entropy, $T_{\rm rot}$ is not equal to the dual black hole temperature $T_{\rm BH}$. Considering that the thermal frequency defines a clock in the rotating frame, there is a time dilation shift of the temperature, and we have $T_{\rm rot}\, dt_{\rm rot} = T_{\rm BH}\, dt_{\rm BH}$, where $dt_{\rm BH}$ is the Killing time increment in the asymptotic rest frame of the black hole. It follows that the rate of complexity growth can equally be expressed as $d\mathcal{C}/dt_{\rm BH} \sim T_{\rm BH} S_{\rm BH}$. We will now show, for the case of a rotating BTZ black hole, that CV duality

indeed predicts this complexity growth rate at late times.

The metric for the rotating BTZ black hole can be written as

$$ds^2 = -\alpha^2 dt^2 + \alpha^{-2} dr^2 + r^2(d\phi - \Omega dt)^2, \tag{3.26}$$

with

$$\alpha^2 = \frac{(r^2 - r_+^2)(r^2 - r_-^2)}{r^2 \ell^2}, \qquad \Omega = \frac{r_- r_+}{r^2 \ell}, \tag{3.27}$$

and the surface gravity is $\kappa = (r_+^2 - r_-^2)/\ell^2 r_+$. The "final slice," i.e. the Killing-invariant maximal slice inside the horizon lies where $(r\alpha)' = 0$, which is at r_f given by $r_f^2 = (r_+^2 + r_-^2)/2$. This is a cylindrical surface, with induced metric $ds^2 = -\alpha_f^2 dt^2 + r^2(d\phi - \Omega_f dt)^2$, and volume (area) form $r_f \alpha_f \, dt \wedge d\phi$, where $\alpha_f := \sqrt{-\alpha(r_f)^2}$. The volume of a dt section of the slice is thus $dV = 2\pi r_f \alpha_f \, dt$, so the rate of change of the total volume inside the horizon, growing at both ends, is $dV/dt = 4\pi r_f \alpha_f$. The longest time path from the outer horizon to the final slice has length

$$\tau_f = \int_{r_f}^{r_+} \alpha^{-1} dr = \pi \ell / 4, \tag{3.28}$$

which is the divisor we use in relating the complexity to the volume. (Note that, unlike in higher dimensions, this time is independent of the horizon radius, even for small black holes. In the next section we consider the Kerr black hole in four dimensions, and find that one still obtains TS even for small black holes, when the time to the final slice is used as the divisor.)

The rate of change of the complexity with respect to t is thus

$$\frac{d\mathcal{C}}{dt} = \frac{4}{\pi \ell} \frac{dV}{dt} = \frac{16 r_f \alpha_f}{\ell} = \frac{8(r_+^2 - r_-^2)}{\ell^2} = 8\kappa r_+ = 32 T_{\rm BH} S_{\rm BH}. \tag{3.29}$$

As explained above, $T_{\rm BH}S_{\rm BH}$ is equivalent to the rate $T_{\rm rot}S_{\rm rot}$, which is what one would expect from a thermal state [8]. This is a nontrivial check, since the rotating black hole possesses another dimensionless parameter, r_-/r_+, on which the result might have depended.

We note also that, in the case of the rotating BTZ black hole, the this complexification rate from "complexity = volume" is interestingly the same as the one found for "complexity = action" [12]: the late-time rate of growth is proportional to $r_+^2 - r_-^2$ in both cases. Here we emphasize the proportionality of this result with $T_{\rm H}S_{\rm BH}$, whereas Ref. [12] emphasizes the proportionality with $M - \Omega J$, noting that the late-time rate of growth is slowed down compared to M, due to the presence of the conserved charge J.

3.5.3 Kerr black hole

Next, we discuss rotating black holes in higher dimensions. This case is substantially more complicated to study than the rotating BTZ one due to the lack of spherical symmetry, and this may be why it has not been studied at all in the literature in the context of CV-duality.[8] We will consider the case of the Kerr solution in four spacetime dimensions, since the asymptotically flat case is somewhat simpler, and since its maximal slices have already been studied to some extent in [86]. Our aim is to check whether the complexification rate (with the time to the final slice divisor taken into account) continues to be of

[8] The volume of constant radius slices inside the Kerr horizon has been studied previously in [85].

the order of $T_{\rm H} S_{\rm BH}$.

The Kerr metric for a black hole of mass M and angular momentum aM is given in Boyer-Lindquist coordinates by

$$ds^2 = -\frac{\Sigma\Delta}{B}dt^2 + \frac{B}{\Sigma}\sin^2\theta\,(d\phi - \Omega dt)^2 + \frac{\Sigma}{\Delta}dr^2 + \Sigma d\theta^2, \tag{3.30}$$

where

$$\Sigma = r^2 + a^2\cos^2\theta, \quad \Delta = r^2 - 2Mr + a^2,$$
$$B = (r^2+a^2)^2 - a^2\Delta\sin^2\theta, \quad \Omega = 2aMr/B.$$

The inner/outer horizons $r_\pm$ are the roots of $\Delta = (r - r_+)(r - r_-)$, $r_\pm = M \pm \sqrt{M^2 - a^2}$.

A general axially symmetric maximal slice is described by some function $r(t, \theta)$. The final slice is a late time limit, so is t-independent due to t-translation symmetry of the background, and is therefore described by a function $r(\theta)$ which extremizes the volume. The volume element on such a slice between the inner and outer horizons (where $\Delta < 0$) is

$$\sqrt{\Sigma(|\Delta| - r_{,\theta}^2)}\sin\theta\, dt \wedge d \wedge d\theta \wedge d\phi \tag{3.31}$$

As argued in [86], $r(\theta)$ must lie between two values, $r_{\rm min}$ and $r_{\rm max}$, which are the extrema of $\Sigma\Delta$ with respect to r at $\theta = 0$ and $\pi/2$, respectively, and which are very close to each other for all values of the spin parameter a/M. The final slice therefore comes very close to being a slice of constant r.

We will adopt $r_f \equiv r_{\max}$ for that approximate constant value of r, which is given by

$$r_f = \frac{3}{4} M \left[1 + \sqrt{1 - 8a^2/9M^2}\right]. \tag{3.32}$$

This radius is never parametrically different from the horizon radius r_+: for $a = 0$ it is $3r_+/4$, while for extremal spin it is r_+. The volume element on this cylinder is given by

$$\epsilon_f = \alpha_f \, dt \wedge \mathcal{A}_f, \quad \alpha_f = \sqrt{\frac{\Sigma_f |\Delta_f|}{B_f}}, \quad \mathcal{A}_f = \sqrt{B_f} \sin\theta \, d\theta \wedge d\phi. \tag{3.33}$$

The volume of a dt section on the final slice is thus $dV = dt \int \alpha_f \mathcal{A}_f$, where the integral is over a constant t slice of the cylinder.

Next let us evaluate the maximal time to fall from the horizon to the final slice, τ_f. Since the coefficient of dr^2 in the line element (3.30) is negative, while those of the other three terms are positive, the longest time is clearly attained with $dt = d\theta = d\phi = 0$. Moreover, the maximum of these is attained at $\theta = 0$, so

$$\tau_f = \int_{r_f}^{r_+} dr \sqrt{\frac{r^2 + a^2}{|\Delta|}} \tag{3.34}$$

Our proposal for the t derivative of the holographic complexity due to growth on one side of the final cylinder is thus

$$\frac{d\mathcal{C}}{dt} = \frac{\int \alpha_f \mathcal{A}_f}{\tau_f}. \tag{3.35}$$

Since $r_f \sim r_+$, the rate (3.35) will agree with $\sim T_{\rm H} S_{\rm BH}$ provided $\alpha_f \sim \kappa \tau_f$, where κ is the surface gravity. If α_f were the norm of the horizon generating

Killing vector $\partial_t + \Omega_+ \partial_\phi$ as before, then this last relation would again follow as the first order Taylor expansion, as explained in the introduction. However, in fact, α_f is the norm of $\partial_t + \Omega_f \partial_\phi$. Nevertheless, again, because $r_f \sim r_+$, these two vector fields are not so different, and so it is plausible that indeed $\alpha_f/\tau_f \sim \kappa$.

To test this relation at the extreme, we define the parameter $\epsilon = \sqrt{1 - a^2/M^2}$, and expand around extremality, $\epsilon = 0$. Expanding to lowest order in ϵ, using units with $M = 1$, we have $r_\pm = 1 \pm \epsilon$, $r_f = 1 + \epsilon^2$, and $\Delta = (r-1)^2 - \epsilon^2$, hence $\Delta_f = -\epsilon^2$. Thus, in computing the volume to lowest order, we may set $r = 1$ in all expressions other than Δ. In particular, $\alpha_f \mathcal{A}_f \to \epsilon\sqrt{1 + \cos^2\theta}\sin\theta\, d\theta \wedge d\phi$. At this lowest order in ϵ we therefore have

$$dV/dt = 2\pi[\sqrt{2} + \sinh^{-1}(1)]\epsilon, \tag{3.36}$$

and

$$\tau_f = \sqrt{2}\int_1^{1+\epsilon} \frac{dr}{\sqrt{\epsilon^2 - (r-1)^2}} = \frac{\pi}{\sqrt{2}}, \tag{3.37}$$

so our proposal for the complexification rate yields

$$\frac{d\mathcal{C}}{dt} = 2\sqrt{2}[\sqrt{2} + \sinh^{-1}(1)]\epsilon \approx 6.49\epsilon. \tag{3.38}$$

On the other hand, the temperature and entropy of the Kerr black hole are

$$T_{BH} = \frac{1}{2\pi}\frac{\sqrt{M^2 - a^2}}{r_+^2 + a^2}, \qquad S_{BH} = \pi(r_+^2 + a^2), \tag{3.39}$$

so it follows that

$$T_{\rm H} S_{\rm BH} = \frac{1}{2}\sqrt{M^2 - a^2} \to \tfrac{1}{2}\epsilon. \tag{3.40}$$

The important thing is that (3.38) and (3.40) are both $O(\epsilon)$, so that their ratio approaches a nonzero pure number in the extremal limit. While the ratio depends on the spin parameter a/M, it is does not go to zero or infinity as this parameter goes to zero. Finally to exhibit the ratio over the full parameter range, we evaluated it numerically. As expected, the plot in Fig. 3.11 of the ratio of these quantities does not vary substantially over the whole range of a/M. It would be interesting to generalize this analysis to Kerr-AdS, in any spacetime dimension.

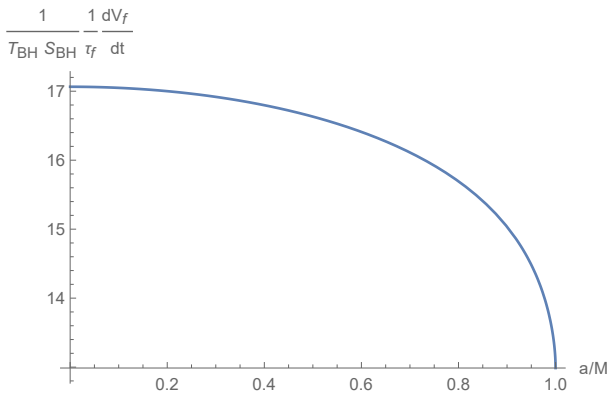

Figure 3.11: Plot of (rate of change of final slice volume $\div$ longest time from the horizon to the final slice) :$(T_{\rm H}S_{\rm BH})$, versus the spin parameter for a Kerr black hole in four spacetime dimensions. The ratio is roughly constant over the entire range from nonspinning to maximal spin.

3.5.4 Rindler wedge complexity growth

It has previously been observed that many aspects of black hole thermodynamics and horizon entanglement apply to acceleration horizons, and specifically to Rindler horizons in flat or AdS spacetimes. In particular, in the

AdS/CFT setting, the CFT can be partitioned in to two equal halves, and in the ground state the corresponding bulk entanglement wedges are Rindler wedges, separated by a horizon and future and past “interior" regions analogous to the two-sided black hole interior. Each half of the CFT vacuum is a thermal state with respect to the Hamiltonian generating the conformal boost symmetry of its diamond-shaped domain of dependence [87, 88]. The analogy with the two-sided black hole is close enough that we may expect the complexity of the thermal state to grow in time when boosting toward the future on both halves of the partition (as opposed to boosting one side to the future and the other to the past). Moreover, the expected growth rate would be TS, where T is the conformal boost temperature and S is the (entanglement) entropy. We now demonstrate that this is indeed the case for $\mathrm{AdS}_3/\mathrm{CFT}_2$.

The metric of AdS in Rindler coordinates is actually just the BTZ metric (3.26), with $r_- = 0$ and $r_+ = \ell$ [75]. The maximal foliation of interest is defined by constant Rindler time slices of the boundary, and the final slice of this foliation therefore meets the boundary at the Rindler horizon. Fig. 3.12 displays a plot of this slice in global coordinates, which lies at $r_f = r_+/\sqrt{2}$ as seen in the previous subsection (3.5.2). The results of that section also show that the rate of complexification at late times, measured with respect to the conformal boost time, is $\propto TS$, where $T = 1/2\pi$ is the Unruh temperature, and S is the (infinite) Bekenstein-Hawking entropy of the Rindler horizon. The dual quantities in the CFT are the conformal boost temperature, and the entanglement entropy of the semicircle, as implied by the Ryu-Takayanagi for-

mula. The state on the semicircles is also conformally equivalent to a thermal state on two-dimensional Minkowski space. In higher dimensions it would be conformally equivalent to a thermal state on a static hyperbolic space [89].

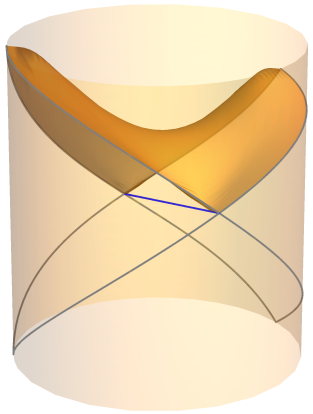

Figure 3.12: A plot of the final slice of AdS-Rindler embedded into global AdS. Here we use global coordinates for AdS, in which the metric reads $ds^2 = L^2(-\cosh^2\rho d\tau^2 + d\rho^2 + \sinh^2\rho d\phi^2)$, except that we have compactified the radial coordinate by applying the *arctan* function (in other words, the boundary of the cylinder is at radius $\pi/2$). The line running across the cylinder is the bifurcation line of the Rindler horizon.

3.6 Conclusion

In this work, we proposed that the apparent lack of universality in the CV duality for large and small black holes is removed if one identifies the complexity with the volume measured in units of the maximal (free-fall) time τ_f from the horizon to the final slice times Planck area. The distance $c\tau_f$ is $\sim$ the AdS radius for spherical black holes large compared to the AdS radius, and it is $\sim$ the horizon radius for small black holes, thus accounting in both cases for the divisor that had been previously introduced by hand in order for

the complexification rate to match the temperature-times-entropy expectation. We also checked that this prescription matches TS for the rotating BTZ black hole, and the Kerr black hole in four dimensions, for all spin parameters. While this does seem an improvement over the previous ad hoc assignment, it should be admitted that we have no reason from first principles for thinking the time τ_f should be relevant, other than that it can be related to the surface gravity and redshift factor at the final slice, as explained in the Introduction and in Sec. 3.3.4. Moreover, τ_f is of course only defined when a horizon and final slice are present, so is of no use otherwise. In this respect, CA duality appears much more universal. However, it is not so clear whether the notion of complexity and its growth should be expected to have a universal meaning, outside of thermal states, because then the dependence on the arbitrary choice of reference state and gates with which to define the complexity may be more severe.

We proposed that to capture complexity at the thermal scale one should count only the volume inside the horizon, and introduced the "volume current," orthogonal to a foliation of spacetime by maximal slices. This current is a divergence-free vector field, whose flux through the slices of the foliation measures their volume. This flux picture suggests that there is a transfer of the complexity from the UV to the IR in holographic CFTs, which is reminiscent of thermalization behavior decuced using holography. It also naturally gives a second law for the complexity when applied at a black hole horizon. We further showed how the volume current is a useful tool for establishing various

properties of the volumes of a maximal foliation, established a global inequality on maximal volumes that can be used to deduce the monotonicity of the complexification rate on a boost-invariant background, and probed CV duality in the settings of multiple quenches, spinning black holes, and Rindler-AdS. Finally, we established the existence of a maximal foliation without gaps (on which the existence of the volume current depends) provided that there exists a maximal slice anchored at each boundary slice, and assuming a causality condition, the strong energy condition, and the Einstein equation.

Taken together, these results demonstrate the mathematical and physical utility of the notion of volume current associated to a maximal foliation. In the setting of CV duality it is tempting to think of the current as a "gate current" [66]. Perhaps this could be given a more concrete meaning in the context of tensor network models of bulk spacetime.

3.7 Appendix I: Boundary foliation induces maximal bulk foliation

We advertised in Section 3.3 that a foliation of the boundary of AdS induces a foliation by globally maximal volume slices in the bulk (assuming there exists such a slice terminating on each boundary slice). To establish this, we first show that, if two boundary slices do not intersect, then the corresponding bulk maximal slices[9] do not intersect. Next we argue that the (nonintersecting) bulk slices fail to be a foliation only if there are two distinct

[9]In this appendix, "maximal" will always by default mean "globally maximal".

maximal slices anchored at the same boundary slice, and we prove, assuming the strong energy condition and the Einstein equation, that this cannot happen. In order to deal with finite volumes, we take the boundary to lie at a finite cutoff surface, which can be taken to infinity at the end.

The argument works by contradiction. Suppose the maximal slice anchored at the upper boundary slice dips down sufficiently low in the bulk that it intersects the maximal slice anchored at the lower boundary slice (see Figure 3.13). Then we can write one maximal slice as the union of components a and

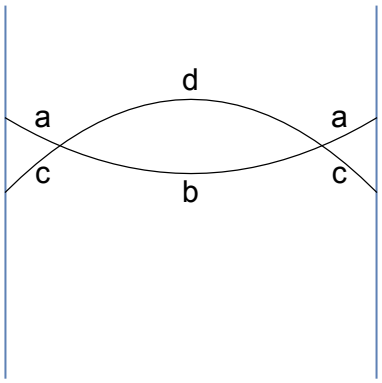

Figure 3.13: Hypothetical situation where two maximal slices anchored on different boundary Cauchy slice intersect.

b, and the other maximal slice as the union of components c and d as in the figure. If $\mathrm{Vol}(b) < \mathrm{Vol}(d)$, then $\mathrm{Vol}(ab) < \mathrm{Vol}(ad)$, contradicting the maximality of the (ab) slice. If $\mathrm{Vol}(d) < \mathrm{Vol}(b)$, then $\mathrm{Vol}(cd) < \mathrm{Vol}(bc)$, contradicting the maximality of the (cd) slice. The only possibility remaining is $\mathrm{Vol}(b) = \mathrm{Vol}(d)$. If that is the case, then (ad) and (bc) would also have to be maximal slices.

But they cannot be maximal, since they have corners, and by rounding off the corners their volume can be increased. If the slices are tangent, rather than intersecting transversally, this "rounding the corners" argument is not applicable, but by moving the boundary slices slightly closer together, one would expect that the tangency generically becomes a transversal intersection, which would be ruled out by the argument already given.[10] Although not quite a rigorous argument, this seems adequate for our present purposes.

Now if the bulk maximal slices do not intersect, then the boundary foliation will induce a bulk foliation unless there are gaps where the family of maximal volume slices jumps discontinuously across some spacetime region. Since the metric is assumed continuous, however, the maximal volume function itself cannot jump discontinuously as the boundary slice is pushed toward the future. Hence, if a gap does occur there must be two maximal slices with the same volume, anchored at the same boundary slice. We now argue that this cannot happen, given a causality assumption, the Einstein equation, and the strong energy condition. In fact, the argument will establish a stronger result: there cannot be two extremal bulk slices with the same boundary.

Suppose there are two such slices, Σ_1 and Σ_2, with Σ_2 to the future of Σ_1, with the same, co-dimension-2 boundary, and both with $\mathrm{Tr}K = 0$. While the domains of dependence $\mathcal{D}_1$ and $\mathcal{D}_2$ of Σ_1 and Σ_2 are each automatically

[10] This argument is essentially an adaptation to Lorentzian signature of a similar argument presented in [90, 91] for Euclidean signature in the context of holographic entanglement entropy, establishing the property of "entanglement wedge nesting" on a static slice.

globally hyperbolic, we need to assume that $\Sigma_2 \subset \mathcal{D}_1$ and $\Sigma_1 \subset \mathcal{D}_2$, which amounts to assuming that the domains of dependence coincide, $\mathcal{D}_1 = \mathcal{D}_2$. This condition "obviously" holds for "normal" causal structures. Under this causality assumption, we can invoke Theorems 9.4.3 and 9.4.5 and Lemma 8.3.8 of Ref.[76] to infer that every point p on Σ_2 lies on a geodesic that maximizes the proper time from p to Σ_1, meets Σ_1 orthogonally, and has no conjugate points between p and Σ_1. The congruence of these geodesics maps (possibly a subset of) Σ_1 onto all of Σ_2. The expansion θ of the congruence at Σ_1 is equal to $\mathrm{Tr}K$, which vanishes by assumption. The Raychaudhuri equation together with the timelike convergence condition or, assuming the Einstein equation, the strong energy condition, then implies that θ is decreasing everywhere along the congruence.[11] Moreover, θ cannot go through $-\infty$ before reaching Σ_2 since, as stated above, the time-maximizing curve has no conjugate points between p and Σ_1. It follows that θ is negative everywhere, which implies that the geodesic flow is volume-decreasing. That is, the volume of a small ball carried along by the flow will *decrease*, as measured in the local rest frame of the flow. Furthermore, since the geodesics do not generally meet Σ_2 orthogonally, the volume of a small patch of Σ_2 on which the flow lands will be *less* than the volume of the small ball carried by the flow. It follows that the volume of Σ_2 is less than the volume of the pre-image of Σ_2 in Σ_1 under this flow, and *a fortiori* the volume of Σ_2 is less than that of Σ_1. Similarly, we can argue the

[11] Strictly speaking, we need here to assume the generic condition, that $R_{ab}u^a u^b \neq 0$ somewhere along each geodesic, where u^a is the geodesic tangent. In the case with a (negative) cosmological constant, this is automatic.

opposite, and thus we reach a contradiction, since the volume of Σ_2 cannot be both less than and greater than that of Σ_1. The initial assumption is therefore false: there cannot be two extremal slices with the same boundary. Together with the previous results, this implies that a boundary foliation determines a maximal bulk foliation without gaps. Note that the latter need not completely cover the bulk, however. For example, as discussed in the text, the maximal slices for a two-sided black hole do not extend beyond a final slice, located inside the event horizon.

We established the uniqueness property of extremal slices with a given boundary using a global argument in which the existence of time maximizing curves without conjugate points played a key role. However, it was briefly mentioned by Witten, in a conference talk [92], that uniqueness can be proved in a different fashion, namely, by (i) showing that the volume of any extremal slice is a local maximum with respect to small deformations, and (ii) arguing that if there were two local maxima, there would necessarily also be a saddle point of the volume, contradicting the fact that all extremal slices are local maxima of the volume. The reasoning for point (i) is simple and local: the expansion of the congruence of timelike geodesics orthogonal to any extremal slice starts out zero at the slice, and the strong energy condition (together with the Einstein equation) implies that it is negative and decreasing off the slice. The transversal spatial volume therefore decreases along the congruence, and non-orthogonality of the congruence to the deformed slice implies that the latter has even smaller volume, so the extremal slice is a local maximum of

volume. The reasoning for (ii), the existence of the saddle point, was not as explicit in the talk, but it was pointed out in a picture that there would necessarily be a local minimum along some one-parameter family of slices joining them. This is of course a necessary condition for the existence of a saddle point, but it is not clear to us that a saddle point is guaranteed to exist.

We end this appendix with an example where the strong energy condition does *not* hold, and consequently there can be more than one extremal hypersurface with the same boundary, and the extremal slices are *not* local maxima of volume: de Sitter spacetime. The constant time slices of a static patch of de Sitter spacetime are all anchored at the same location on the boundary of the patch, all are extremal, and all have the same volume. To visualize this, consider the two dimensional de Sitter hyperboloid embedded in three dimensional Minkowski spacetime. The constant-time slices of the static patch are equatorial semicircles on the de Sitter hyperboloid, and are related to one another by Lorentz boosts in the embedding spacetime.

3.8 Appendix II: Techniques to evaluate the maximal volume

In this appendix, we demonstrate the use of the flux picture of complexification as a technical tool for explicit computation. The techniques presented here complement existing studies in the literature such as [36], where the maximal volume was computed by maximizing the volume functional directly. In

subsection (3.8.1), we evaluate the volume flux for the BTZ black hole. In subsection (3.8.2), we present a variation of this technique when the cutoff is null, in which case the flux density is given by the lapse function.

3.8.1 Direct evaluation of flux

In this appendix, we present the derivation of the volume current and the volume flux for the BTZ black hole. The boundary foliation is the symmetrical one $t_L = t_R$.

Let us start with the BTZ black hole. We work in (r, v) coordinates, which are regular across the horizon:

$$ds^2 = -f(r)dv^2 + 2dvdr + r^2 d\phi^2 \tag{3.41}$$

$$f(r) = \frac{r^2 - r_+^2}{L^2} \tag{3.42}$$

The function $v(r)$ describing the shape of the maximal slices was essentially worked out in [36]. Its derivative is given by:

$$\frac{dv}{dr} = \frac{\sqrt{f(r)r^2 + C^2} - C}{f(r)\sqrt{f(r)r^2 + C^2}} \tag{3.43}$$

where C is a positive constant.[12] The constant C labels the particular maximal slice in the foliation, and it ranges from 0 (for the slice anchored at $t_L = t_R = 0$) to $r_+^2/2L$ (for the final slice).[13] The unit normal 1-form to the slice labeled by

[12] C is the negative of the "energy" E in [36]. From the viewpoint of that paper, the constant C arises as a "conserved quantity" associated with the v-independence of the volume functional.

[13] To see this, note that $\frac{dv}{dr} = \frac{1}{f}$ on the slice $t_L = t_R = 0$ (since this slice is at $t = 0$). As for the final slice, symmetry dictates that it is a slice of constant r, and $\frac{dv}{dr}$ diverges. Both of these facts are verified by plugging in $C = 0$ and $C = \frac{r_+^2}{2L}$ respectively.

C is:

$$n_\mu dx^\mu = -\sqrt{f + \frac{C^2}{r^2}}dt - \frac{C}{rf}dr \tag{3.44}$$

To get the volume current v^μ, we glue together the unit normal to all the slices labeled by different values of C. This amounts to promoting C to the function of v and r implicitly given by integrating (3.43) from the midpoint (also called the "throat" in the numerical relativity literature) outward:

$$v = -\frac{1}{r_+}\text{arctanh}\left(\frac{r_C}{r_+}\right) + \int_{r_C}^{r} \frac{\sqrt{f(x)x^2 + C^2} - C}{f(x)\sqrt{f(x)x^2 + C^2}}dx \tag{3.45}$$

The first term on the right-hand side is the tortoise coordinate of the throat, and r_C is the radius of the throat given by:

$$r_C = \sqrt{\frac{1}{2}(r_+^2 + \sqrt{r_+^4 - 4C^2L^2})} \tag{3.46}$$

The two equations above define $C(r, v)$. We then find the volume current:

$$v^\mu\partial_\mu = \frac{1}{f(r)}\left(\sqrt{f(r) + \frac{C(r,v)^2}{r^2}} - \frac{C(r,v)}{r}\right)\partial_v - \frac{C(r,v)}{r}\partial_r \tag{3.47}$$

It can be checked that both components of v^μ are regular at the horizon. The volume element is $\epsilon = r dv \wedge dr \wedge d\phi$. Computing the interior product $v \cdot \epsilon$ and restricting to the cutoff at constant $r = r_c$ yields:

$$v \cdot \epsilon\Big|_{r_c} = C(r_c, v)dv \wedge d\phi \tag{3.48}$$

Note that r_c is allowed to be the horizon since our formalism can handle null surfaces. Evaluating the flux, we then find the change in the volume between v_1 and v_2 to be:

$$\Delta V = 2\pi \int_{v_1}^{v_2} C(r_c, v)dv \tag{3.49}$$

In the usual near-boundary cutoff $r_c \to \infty$, the v coordinates becomes the boundary time coordinate t and the function $C(r_c, v)$ is nothing but the flux density, or the complexification rate. The main lesson from this computation is that the flux density coincides with a certain time function C for the maximal slicing.

We also note that it is possible to work with Schwarzschild coordinates (r, t) instead of (r, v), despite the coordinate singularity at the horizon. In Schwarzschild coordinates, the shape of the maximal slice reads:

$$t = -\int_{r_C}^{r} \frac{C}{f(x)\sqrt{f(x)x^2 + C^2}} dx \tag{3.50}$$

To integrate across the horizon, we should understand the integral above in the sense of the Cauchy principal value [93]. In fact, the plot (3.3) of the volume flow was generated by working in Schwarzschild coordinates and using the Cauchy principal value to continue the maximal slice across the horizon.

Finally, it might appear surprising that the flux of the volume flow yields a finite answer when the cutoff is taken to the boundary, especially if we think about the flow direction near the boundary. The maximal slice should become tangential to the constant Killing time slices near the boundary, and since the volume current is orthogonal to the maximal slices, it may seem that the volume flux across a constant-r cutoff is zero as $r \to \infty$. That this is not the case can be understood as follows: at a finite but large cutoff in the bulk, the flow direction has a small component not orthogonal to the constant Killing time slice. As the cutoff is sent to the boundary, this small component

tends to zero, but the volume element on the cutoff also diverges in the same time. This divergence cancels the vanishing of the subleading component in a way to yield a finite answer.

3.8.2 Flux across a null surface

In this appendix, we elaborate on the particular case of the volume flux across a null surface, and relate this flux to the lapse function for a time function τ defining the maximal foliation. Recall that to a time function τ we can associate a *lapse function* N defined by:

$$n = N d\tau \tag{3.51}$$

where n is the unit normal 1-form to a constant τ slice, with sign chosen so that $N > 0$. Since the volume current vector v is the unit normal vector to the maximal slices, we have $v \cdot n = 1$. Now let k be the null normal 1-form to the horizon, normalized so that $v \cdot k = 1$, and let $\mathcal{A}$ be the area form of the intersection of the maximal slice with the horizon, so that $\epsilon = k \wedge n \wedge \mathcal{A}$. The volume current is then $v \cdot \epsilon = n \wedge \mathcal{A} - k \wedge A$, whose pullback to the null surface is $n \wedge A = N d\tau \wedge \mathcal{A}$, since the pullback of k vanishes. The 2-form $N\mathcal{A}$ thus serves as the volume flux density.

This fact can be seen more geometrically as depicted in Figure (3.14). We pick two slices in the foliation labelled by τ and $\tau + \Delta\tau$, with $\Delta\tau$ small. Let A be the intersection between slice τ and the horizon, and let C be the intersection between slice $\tau + \Delta\tau$ and the horizon. Moreover, consider a volume flow worldline passing through A, and let B be the intersection of that

worldline with the slice $\tau + \Delta\tau$. Since $\Delta\tau$ is infinitesimal, the geometry of

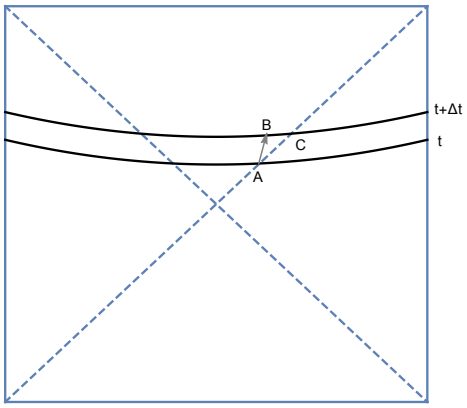

Figure 3.14: Illustration of the derivation of (3.53).

the triangle ABC is like in flat space. Since AB is orthogonal to BC, we conclude that $AB = BC$, where AB denotes the proper time elapsed along the worldline between A and B, and BC denotes the proper length of the segment of the slice $\tau + \Delta\tau$ between B and C.

Now consider the increment in the volume ΔVol between τ to $\tau + \Delta\tau$. We have $\Delta\text{Vol} = 4\pi r_+^2 BC = 4\pi r_+^2 AB$, where we work in 3+1 dimensions for concreteness, and in the second equality we used the relation derived in the previous paragraph. (There is also an identical contribution from the left-side of the Penrose diagram, which we ignored.) On the other hand, we have $AB = N(A)\Delta\tau$. Thus, we can relate the volume increment to the lapse as

follows:

$$\Delta \text{Vol} = 4\pi r_+^2 N(A) \Delta\tau. \tag{3.52}$$

For a finite time difference, we integrate the lapse:

$$\Delta \text{Vol} = 4\pi r_+^2 \int_{\mathcal{H}} N d\tau. \tag{3.53}$$

This is the formula we are after: the volume flux across the horizon is also the integral of the lapse along the horizon. In other words, the lapse on the horizon serves as the volume flux density.

3.9 Appendix III: Stationarity of maximal foliation and volume flow in the late-time regime

In this appendix, we focus on the AdS-Schwarzschild in 3+1 dimensions, and explicitly check that the maximal foliation and volume flow are stationary at late times. To do this, we first write the Schwarzschild-AdS black hole in the "maximal slicing" gauge:

$$ds^2 = -\alpha^2 d\tau^2 + \gamma^2 (dr + \beta d\tau)^2 + r^2 d\Omega_2^2, \tag{3.54}$$

in which the slices of constant τ are the left-right symmetric maximal slices that asymptote to constant Schwarzschild time slices at the two boundaries. The radial coordinate r and the angles θ and ϕ on the sphere can be chosen to be the same as the usual Schwarzschild coordinates. The functions α, β and γ are functions of τ and r, given by:

$$\gamma^{-2} = 1 - \frac{2M}{r} + \frac{C(\tau)^2}{r^4} - \frac{\Lambda}{3} r^2 \tag{3.55}$$

$$\alpha = \gamma^{-1}\left[1 + C_{,\tau}\int_r^\infty \frac{\gamma^3(\tau, r')}{r'^2}dr'\right] \tag{3.56}$$

$$\beta = \frac{\alpha C(\tau)}{r^2} \tag{3.57}$$

for some function $C(\tau)$. To derive equations (3.55), (3.56) and (3.57), we can, for example, feed the metric (3.54) into Einstein's equation. Analogous calculations for black holes in flat space have been done in the numerical relativity literature (see for example [93]). In writing (3.56) we have imposed the boundary condition $\alpha\gamma \to 1$ as $r \to \infty$, so that τ will agree asymptotically with the standard AdS global time coordinate.

The function $C(\tau)$ is determined by regularity of the maximal slice at the "middle". According to (3.54), the metric induced on the maximal slice is $\gamma^2 dr^2 + r^2 d\Omega_2^2$, so in particular γdr is a unit 1-form on the slice. Since r reaches a minimum at the middle of each slice, the pullback of dr to the slice vanishes at the middle, so γ must diverge there. This implies

$$C^2 = 2Mr_m^3 - r_m^4 + \frac{\Lambda}{3}r_m^6, \tag{3.58}$$

where $r_m = r_m(\tau)$ is the r coordinate at the middle of each constant τ slice. In the late time limit, $r_m(\tau)$ approaches a constant, namely r_f, the radial coordinate of the "final slice". Therefore $C(\tau)$ too approaches a constant. It follows that the metric functions α, β, and γ all become constant in the late τ limit, which implies that the coordinate vector field ∂_τ approaches the Schwarzschild time Killing field. The unit normal 1-form $\alpha d\tau$ therefore becomes invariant under the Killing flow, as does the volume current

$$v = \alpha^{-1}(\partial_\tau - \beta\partial_r), \tag{3.59}$$

which is minus the contravariant form of $\alpha d\tau$.

3.10 Appendix IV: Maximal slices in Vaidya: a closer look

Consider a maximal slice anchored at boundary time t_b in the double shell Vaidya/AdS spacetime in $2+1$ dimensions, (3.20), (3.25)). For $t_b < 0$, the slice stays entirely inside the AdS part of the geometry and is given by a constant t slice (where t denotes the global time in AdS). When $0 < t_b < b$, the slice crosses the first shell and has two portions, one in the AdS region (still a constant t slice) and one outside the shell. The volume functional for the part outside the shell reads:

$$\text{Vol} = 2\pi \int r\sqrt{2r' - f}dv \tag{3.60}$$

where we write the slice as a function $r(v)$. Since the functional is independent of v, we have a conserved energy:

$$E = r'\frac{\partial L}{\partial r'} - L = \frac{r(f - r')}{\sqrt{2r' - f}} \tag{3.61}$$

Similarly, there is a conserved energy in the AdS region, which can be shown to vanish by smoothness at the center ($r = 0$). The maximal slices consist of locally maximal slices apart from on the shells, where they satisfy a Weierstrass-Erdmann corner condition [94]. Since the shells are located at a constant value of v, the corner condition simplifies to the requirement that the "conjugate momentum"

$$p_r = \frac{\partial L}{\partial r'} = \frac{r}{\sqrt{2r' - f}} \tag{3.62}$$

be continuous across the junction, which amounts to requiring that the jump in r' is $1/2$ the jump in f. Together with the fact that the portion of the maximal slice in the AdS region must be constant global time slice, this determines the derivative of $r(v)$ at the junction on the BTZ side:

$$\left.\frac{dr}{dv}\right|_{r_{1,+}} = 1 + r_1^2 - \frac{a}{2}(1 + r_+^2) \tag{3.63}$$

where r_1 is the r-coordinate of this junction, and $r_{1,+}$ means an r value slightly larger. Similarly, for $t_b > b$, the maximal slice crosses both shells and the junction condition has to be imposed at each junction. At the outer junction, located at $r = r_2$, the discontinuity of the derivative of $r(v)$ is found to be:

$$\left.\frac{dr}{dv}\right|_{r_{2,-}} - \left.\frac{dr}{dv}\right|_{r_{2,+}} = \frac{1-a}{2}(1 + r_+^2). \tag{3.64}$$

Chapter 4

Holographic Purification Complexity

[1] In this final chapter we study holographic subregion complexity, and in particular its possible connection to purification complexity suggested by Agón et al [4]. We test the conjecture that subregion complexity is dual to purification complexity by considering holographic purifications of a holographic mixed state. We argue that these include states with any amount of coarse-graining consistent with being a purification of the mixed state in question, corresponding holographically to different choices of the cutoff surface. We find that within the complexity = volume and complexity = spacetime volume conjectures, the subregion complexity is equal to the holographic purification complexity. For complexity = action, the subregion complexity seems to provide an upper bound on the holographic purification complexity, though we show cases where this bound is not saturated. One such example is provided by black holes with a large genus behind the horizon, which were studied by Fu et al. As such, one must conclude that these offending geometries are not holographic, that CA must be modified, or else that holographic subregion

[1] This chapter is based on [3] with Elena Caceres, Josiah Couch, and Willy Fischler. The idea of testing the role of purification complexity to holography using "purifying geometries" was mostly due to Josiah Couch. Elena Caceres and Willy Fischler provided conceptual insight throughout. I contributed to all writing and computational aspects of the paper.

complexity in CA is not dual to the purification complexity of the corresponding reduced state.

4.1 Introduction

Quantum complexity entered into discussions of quantum gravity and holography in a novel way following the 'complexity equals volume' (CV) conjecture [8, 9], which speculated that the volume of a maximal spatial slice is dual to the circuit complexity of the dual quantum state living on the intersection of that spatial slice with the boundary. It was soon after suggested to replace CV with 'complexity = action' (CA) [12, 30], and while the bulk of the discussion on the topic is concerned with these two conjectures, at the boundaries at least two other speculations exist, namely 'complexity = spacetime volume' (CV2.0) [31] and 'CA-2' [32][2]. CA modifies CV by replacing the volume of a maximal spatial slice by the action evaluated on the WDW patch associated with the slice, i.e. the causal development of the (UV-regulated[3]) slice. CV2.0 modifies CA by replacing the action on the WDW patch with the spacetime volume of the WDW patch.

Of course all of these bulk quantities can be computed on any geometry, and even on some subregion of the bulk. We would not expect for these quanti-

[2]Though in general distinct, CA-2 reduces to CV 2.0 for Einstein-Hilbert gravity with no sources other than a cosmological constant, and as such we will not consider CA-2 separately in this work.

[3]For a slice not cut-off by some UV-regulator, the WDW patch only corresponds to the causal development of the slice if one forgets the reflecting boundary conditions at infinity.

ties computed for an arbitrary bulk subregion to have any particular meaning in the boundary theory. However, considering that the state on a subregion of the boundary is dual to the entanglement wedge, as argued in [38–40], it is tempting to say that these proposals applied to an entanglement wedge might be dual to the complexity of the reduced state on the corresponding boundary subregion. This has been suggested by a number of authors [41, 95], and the 'complexity' thus computed is termed 'subregion complexity.' This, however, raises the question: What is the complexity of a mixed state? There is not a unique way to extend the usual definition of circuit complexity from pure states to mixed states, so which extension are we talking about? To answer this question, the authors of [4] considered a number of possible definitions of mixed state complexity and compared them to what happens in holography. They came to the conclusion that the 'purification complexity,' which is roughly defined as the minimum state complexity among pure states which reduce to the appropriate density matrix on a subsystem, is a good candidate to be dual to subregion complexity in CA. On the other hand, none of the definitions they considered provides a likely dual to subregion complexity in CV. In this work we further investigate purification complexity, first as defined in [4] but also with minor variations, providing an independent discussion of its behavior for general quantum states and specifically motivating its connection to holographic subregion complexity.

The purification complexity of a holographic mixed state can be bounded from above by considering all its holographic purifications. Beginning with the

entanglement wedge dual to the mixed state in question, all holographic geometries which geodesically complete the wedge provide a family of purifications in their boundary dual states. In any such geometry, we argue (supported by an analogy to the entanglement of purification) that different choices of the cut-off surface in the region complement to the original entanglement wedge correspond to different coarse-grainings of the purifying state. By minimization over cut-offs we argue on general grounds that the purification complexity is bounded above by the subregion complexity in all of CV, CA, and CV2.0. We then prove that so long as we restrict our attention to holographic purifications, this inequality is saturated in CV and CV2.0, because complexity in these proposals is superadditive.

The situation for CA, by contrast, is more complicated. In the absence of a superadditivity property, we must worry that the subregion complexity is not truly minimal among all holographic purifications. To examine this possibility, we consider geodesic completions of the one-side BTZ geometry dual to a thermal state. We find that there are indeed cases where the true minimum is smaller than the subregion complexity, thereby contradicting the conjecture in question.

Our results thus differ here from [4]: we are led to the conclusion that in CV and CV2.0, subregion complexity = purification complexity, whereas in CA it seems either this is not the case, or else that certain asymptotically AdS geometries are not holographic.

The remainder of this chapter is organized as follows: In section 4.2

we define purification complexity and investigate its additivity properties on subsystems of general quantum states. We use this analysis to sharpen our expectations on the behavior of any bulk holographic dual to purification complexity. In section 4.3 we motivate the connection between purification complexity and holographic subregion complexity by analogy with the concept of "entanglement of purification", of which we give a brief overview. We note that for any geodesic completion of the entanglement wedge dual to our mixed state, there will be one purification which corresponds to a cutoff skirting just outside the entanglement wedge along the HRT surface. This purification will have a complexity equal (up to a possible boundary like the term discussed at the end of the section), to the subregion complexity. In section 4.4 we prove that complexity according to either CV (in its usual form, without a boundary term) or CV2.0 is superadditive. This, in turn, implies that the complexity of the state dual to any geodesic completion of our entanglement wedge, with any choice of cutoff, must be larger than the subregion complexity as ordinarily defined. We are thus led to the conclusion that in CV and CV2.0, the purification found in section 4.3 was indeed optimal among holographic purifications.

In section 4.5 we consider the case of CA, where the purification found in section 4.3 need not be optimal. We consider several families of geodesic completions of the one-sided BTZ geometry. One such family are the n sided genus g generalizations of the two-sided BTZ geometry, where we borrow computations done in [96]. These solutions lead to challenges to the purification

complexity interpretation of subregion action, namely that the complexity of certain purifications can be lower than the subregion complexity of the BTZ thermal state, and can even be computed to be negative in some cases, although the issue of the negativity of the action was already raised by [96]. We come to the conclusion that if one is not to abandon the proposal that subregion complexity is dual to purification complexity in CA, one must impose even stricter limits on the geometries considered. We further find that one must impose a limit on the cutoffs considered.

4.2 Purification Complexity: Quantum Expectations

In this section, we will explore some aspects of purification complexity as defined in [4]. We first define the quantity as well as discuss ambiguities and variations on the definition which could lead to qualitatively different behavior on subsystems. We then discuss the expected behavior of purification complexity on subsystems. It should be noted that Agón et al. give a compelling but inconclusive argument that purification complexity should be subadditive for the left and right factors of the thermofield double state, and plausibly more generally. We here give an independent discussion indicating that purification complexity is neither superadditive nor subadditive in general. We then place this discussion in the context of the decomposition into basis and spectrum complexities utilized by [4], and discuss how this breakdown is sometimes insufficient for discerning additivity properties. We then conclude this section with a discussion of how these expectations ought to manifest in holographic

states, listing some basic consistency checks which must be obeyed by any bulk quantity dual to purification complexity.

4.2.1 Definition and Refinements

Purification complexity $C^P(\rho)$ of a density matrix ρ is defined in [4] to be the minimum pure state complexity over all its purifications, subject to the constraint that every additional qubit of the purifying system ends up entangled with the original "physical" qubits. That is,

$$C^P(\rho) = \min_{|\psi\rangle \in \mathcal{P}} C(|\psi\rangle) \tag{4.1}$$

where $\mathcal{P}$ is the set of all purifications $|\psi\rangle$ of ρ which have no separable factors which are also purifications, i.e. there is no decomposition $|\psi\rangle = |\psi_1\rangle \otimes |\psi_2\rangle$ such that $|\psi_1\rangle$ also purifies ρ. This last condition is necessary so that purification complexity reduces to ordinary state complexity on pure states. If $|\phi\rangle$ is a pure state, then any 'purification' of it results in a separable state $|\psi\rangle = |\phi\rangle \otimes |\psi'\rangle$, but since $|\phi\rangle$ is pure and hence a purification of itself, no $|\psi\rangle$ with non-trivial $|\psi'\rangle$ is in our set $\mathcal{P}$, and hence $C^P(\rho_\phi) = C(|\phi\rangle)$ (where $\rho_\phi = |\phi\rangle\langle\phi|$). If we however included such purifications in our minimization, we can at best say that $C^P(\rho_\phi) \leq C(|\phi\rangle)$. In purifications satisfying this criterion, we say that the state on the ancillary Hilbert space is 'fully entangled' with the original state $|\psi\rangle$, and we'll refer to such purifications as 'valid' purifications.

It is easy to imagine alternatives to the above definition which share the same spirit as minimization over purifications, but restricting by more or

less the allowed class of purifications. At one extreme we could consider 'unrestricted' purification complexity, with the minimum taken over all possible purifications. Such a procedure will not reproduce the usual definition of complexity of pure states, but it does provide a different, competing definition, which in principle could be the one relevant for holography (though we are not making that claim here). On the other hand we could place more stringent conditions on the purifying states, or instead, constrain the ancillary Hilbert space used to purify. As an example of the latter type of constraint, we could dictate that only a Hilbert space of minimal dimension may be used, this being fixed by the rank of the density matrix in question. This last possibility is also compatible with the usual pure state definition, and in fact, discussions of section 4.3 indicate that such a restriction may be relevant for subregion complexity.

All of these definitions implicitly assume that a notion of pure state complexity has been defined, not only for the original Hilbert space but for every allowed dimension and form of the purifying Hilbert space. A reference state and gate set must be chosen which scale unambiguously with these Hilbert spaces. Mixed state complexity thus inherits all the same ambiguities as any pure state complexity, and in a sense even more. Though at first disconcerting, this feature is perhaps appropriate considering the holographic conjectures; these presumably employ some natural reference and gate set, each suitably adjustable to any cutoff scale[4].

[4]The need to define mixed state complexity has been most keenly appreciated with the

For developing intuition with N-qubit systems, one plausible procedure is to take the "all zeros" state as the reference, regardless of N. For the gate set, one could specify a universal gate set on two-qubit systems and then allow the same logical operations on any pair of qubits. This is referred to as a two-local gate set. With any k-local gate set (defined analogously), the same prescription scales unambiguously as the Hilbert space adds or eliminates degrees of freedom, though the rate at which new gates proliferate with additional degrees of freedom depends on the specifics of these choices. This leads only to the restriction that subsystems should not be considered below k qubits.

We hold such prescriptions loosely in mind, but with the exception of a few comments, we will henceforth remain agnostic about the choice of gate set and reference state. Instead, we seek to identify features of purification complexity which transcend these ambiguities and therefore inform our expectations about any holographic dual ever before such specifics are understood.

4.2.2 Additivity Properties

First, we focus on states which are fully entangled between two subsystems A and B. [5] For these states, purification complexity can easily be seen

intent to generalize the holographic prescriptions to subsystems, but even considering CFT states at finite cutoff, having traced out some UV degrees of freedom one might wonder if even the original holographic complexity conjectures already require a notion of mixed state complexity to be well-defined. However, at leading order in $1/N$, total states have no entanglement entropy even at finite cutoff and can be thought of as a pure state living on the reduced Hilbert space. In this work, we restrict ourselves to this limit, where 'total state' entails 'pure state'.

[5] Here again, by 'fully entangled' we mean that no subsystem of either A or B factorizes from the full system, i.e., A is fully entangled with B and B is fully entangled with A.

to obey

$$\mathcal{C}(\rho_A) \leq \mathcal{C}(\rho_{AB}) \qquad \text{(fully entangled subsystems)} \tag{4.2}$$

by noting that any valid purification of AB is also a valid purification of A (or B), and so the minimum complexity over valid purifications of A (or B) is upper bounded by that of AB. This inequality immediately leads to another which we dub 'weak superadditivity':

$$\mathcal{C}_A + \mathcal{C}_B \leq 2\mathcal{C}_{AB} \qquad \text{(fully entangled subsystems)} \tag{4.3}$$

where we introduce the notation of using a subscript to denote the subsystem, e.g. $C^P(\rho_A) = C^P_A$.

The proof given above for weak superadditivity breaks down when we consider states which factorize on any subsystem of A or B, owing to the constraint that in valid purifications the ancilla system must end up fully entangled with the system it purifies. For example, consider a separable pure state on AB. While such a state is undoubtedly a purification of the states on A and B respectively, it is not a valid purification.

In fact, for pure states which are factorizable on any number of subsystems, purification complexity is demonstrably subadditive over these separable factors. To see this, note that the complexity of each subsystem is an ordinary state complexity (because the state on each subsystem is pure), obtained using gates which act unitarily within that subsystem. The circuits which are individually optimal for these subsystems may also be used together to prepare the full product state, but for that purpose, it may not be optimal since

circuits over the whole system may additionally utilize gates which couple the subsystems. [6] This composite circuit's state complexity is the sum of the individual state complexities, and it puts an upper bound on the total state complexity. A nearly identical proof guarantees subadditivity for factorizable systems, regardless of whether or not they are pure:

$$\mathcal{C}_A + \mathcal{C}_B \geq \mathcal{C}_{AB} \qquad \text{(factorizable subsystems)} \tag{4.4}$$

Note that the inequalities (4.3) and (4.4) do not contradict each other. In fact it's conceivable that together they bound the span of purification complexity on general subsystems:

$$C_{AB} \leq C_A + C_B \leq 2C_{AB} \qquad \text{(not proven!!!)} \tag{4.5}$$

However neither of these inequalities is proven in general, rather each is proven for a different corner of state space (factorizable subsystems and completely non-factorizable subsystems, respectively). It is natural to ask whether either of these classes can violate the opposing inequality and whether intermediate classes of states obey either inequality. We return to these question

[6] It may first seem that if we start with an unentangled reference state, then gates which couple unentangled subsystems should play no role in the optimal circuit because these gates create entanglement. However, though such gates are necessary to create entanglement between the two subsystems, they do not always do so. It is easy to find factorizable states and gate sets where the optimal circuit utilizes these gates without ever creating entanglement between the subsystems, even at intermediate stages.

shortly, but pause here to relate these statements to the work of [4] and the decomposition of purification complexity into spectrum and basis components.

4.2.3 Basis and Spectrum decomposition

Given an arbitrary mixed state and a large enough ancillary Hilbert space (e.g., a duplicate Hilbert space is always sufficient), it's always possible to construct a purification through a two-part process: first prepare a state with the appropriate spectrum on the reduced system, then from this state rearrange the subsystem basis until the target density matrix is achieved. There is an optimal circuit which performs each of these tasks, and their complexities define the spectrum complexity C^S and the basis complexity C^B respectively [7]. In sequence these operations prepare the full mixed state; there may be more efficient routes to prepare a purification, but the sum of these circuit complexities upper bounds the purification complexity:

$$C^P \leq C^S + C^B \tag{4.6}$$

In [4], the authors consider the possibility that any one of these complexities (C^P, C^S, or C^B) might correspond to holographic subregion complexities as computed using the Complexity = Action (CA) or Complexity = Volume (CV) conjectures. The best tentative match aligned the CA subregion

[7] In [4] what we call basis complexity is denoted $\tilde{C}^B$, while C^B denotes the exact difference $C^P - C^S$. We avoid using this exact difference to ensure that C^S and C^B are the complexities of circuits which can be applied in succession to prepare the correct mixed state

prescription with the full purification complexity C^P. This correspondence was particularly encouraged by the expectation that C^P should be subadditive, and among holographic prescriptions only CA includes bulk contributions which are not positive-definite, allowing that at least in the case considered CA was also subadditive. We will revisit this particular holographic example in section 4.5, but we here give a schematic outline of the reason for these expectations.

Consider a two-sided eternal black hole with the subregions being the full left and right boundaries (we will use subscripts L and R for "left" and "right" on a Penrose diagram, and subscript T for "total" or "thermofield double state"). The individual subregions each decompose into a basis and spectrum part.

$$\begin{aligned} C_L^P &\leq C^S + C_L^B \\ C_R^P &\leq C^S + C_R^B \end{aligned} \tag{4.7}$$

Because the combined state is pure, the spectrum part is the same for left and right subsystems. To prepare the total state, we can presumably borrow the circuits utilized in the above decompositions, but importantly the spectrum part need only be prepared once at the beginning of this process:

$$C_T^P \leq C^S + C_L^B + C_R^B \tag{4.8}$$

Each of the preceding circuit decompositions only upper bounds the

true purification complexity, but if we blithely suppose that the bounds are approximately saturated, then comparing (4.7) and (4.8) leads to the expectation that

$$C_T^P \leq C_L^P + C_R^P \leq 2C_T^P \tag{4.9}$$

These inequalities match those of Eq. (4.5). In the case considered here, with the subsystems being left and right halves of an eternal black hole, the rightmost inequality of (4.9) follows rigorously from (4.3) for fully entangled subsystems. The leftmost inequality is less certain. Particularly, in equation (4.8), we assume the total state can be prepared by "borrowing the circuits" used to prepare the subsystem density matrices. However, it is only guaranteed that this combined circuit will prepare a state with the correct subsystem density matrices. There are many such states, and these can have vastly different complexities; preparing the correct total state may require complex operations which are effectively unnoticed by either subsystem and are not accounted for in any of the C^S, C_L^B, or C_R^B circuits of equation (4.7). To illustrate this point, recall the behavior of the thermofield double state evolved away from the $t_L = t_R = 0$ slice:

$$U(t_L, t_R)|TFD\rangle = e^{-iE_n(t_L+t_R)}e^{-\beta E_n/2}/\sqrt{Z}|n\rangle_L|n\rangle_R \tag{4.10}$$

where $U(t_L, t_R) = U_L(t_L) \otimes U_R(t_R) = e^{-iH_L t_L} \otimes e^{-iH_R t_R}$ implements time evolution independently on each boundary (with times set to increase 'upward' on both sides of a Penrose diagram). The effects of this operation, apparent

in the leading phase factor of (4.10), go unnoticed by either subsystem and of course, it is precisely these effects which lead to the famed late-time linear growth of the pure state complexity. Away from the time symmetric slice of the two-sided black hole, the growth of the total state complexity will inevitably break the left-hand side inequality in (4.9).

If we consider the $t_L = t_R = 0$ boundary state only, the total state complexity is minimal among the family of states in 4.10, and so expected to obey $C_T \leq C_L^P + C_R^P$. Indeed this is the chief expectation which found a match in the Complexity=Action subregion calculations of [4]. However, there is a subtlety related to the degeneracy of the energy spectrum which may muddle even this expectation. It was pointed out in [97] that when a subsystem density matrix has a degenerate spectrum, it has interesting implications for purification complexity. Unitaries which enact rotations or phase shifts within such a degenerate subspace act trivially on the subsystem density matrix (effectively limiting the basis complexity of the density matrix), so they never contribute to the purification complexity. However the same unitaries can affect the pure state on the combined system, sometimes increasing the complexity of the target state[8].

If we consider the most extreme case of a fully degenerate spectrum (or the $T \to \infty$ limit), we have maximally mixed subsystems. Preparing both

[8]The unitaries enacting time evolution on the thermofield double state are a special case among this class of unitaries. Even if the spectrum is entirely non-degenerate, there are phase rotations within each energy subspace which go unnoticed by either subsystem density matrix but contribute non-trivially to the total state complexity.

subsystems is equivalent to preparing N bell pairs. This can be thought of as minimizing complexity over a huge family of states which all prepare the appropriate subsystem density matrices:

$$|\psi\rangle = U_L \otimes U_R \left(\frac{1}{\sqrt{N}} \sum_{i=1}^{N} |i\rangle_L |i\rangle_R \right) \tag{4.11}$$

Any state among these is a valid purification, and the subsystem purification complexities are upper bounded by minimizing state complexity overall U_L and U_R. The total state, on the other hand, will be some particular state among (4.11) with particular U_L and U_R. If the total state happens to be the minimally complex state among these, then $C_L^P = C_R^P = C_T$ and weak superadditivity is saturated. On the other hand, by choosing U_R, U_L to make the total state maximally complex we can engineer the total state to violate subadditivity.

If we consider again the thermofield double state at finite temperature on a time-symmetric slice, the total state complexity is at least minimal among

$$|\psi\rangle_T = e^{-iH_L t_L} \otimes e^{-iH_R t_R} \left(\frac{1}{\sqrt{N}} \sum_{i=1}^{N} |i\rangle_L |i\rangle_R \right) \tag{4.12}$$

However, if there is some degeneracy in the energy spectrum, then in preparing the subsystem density matrices we can minimize over a larger class of unitaries (all those which do not intermix degenerate subspaces, but not all U_A and U_B). This class of unitaries is still potentially much larger than minimization over the time evolution unitaries which occurs at the $t_L = t_R = 0$ slice. It is not immediately clear how much the “extra minimization" over a larger class of

unitaries affects the subsystem complexity in comparison to the total state complexity in the case of the thermofield double state. It would seem to depend on the specifics of the energy eigenstates and the gate set involved.

Unfortunately, through these considerations, we are only able to cast doubt on the expectation that the $t_L = t_R = 0$ thermofield double state ought to have purification complexity which is subadditive on the left and right factors, and not provide a rigorous alternative. We will nevertheless consider this example (specifically the BTZ case) holographically in section 4.5 and subject it to other consistency checks.

4.2.4 Expectations for Holographic States

The additivity relationships discussed in subsection 4.2.2 hold for different types of quantum states. Under what circumstances are these relationships relevant to holographic quantum states? We here consider this question, and then give a short list of consistency checks which must be satisfied by any holographic dual to purification complexity.

A pure state which factorizes between subsystems has no entanglement between those subsystems. On the other hand, the smoothness and connectedness of a holographic spacetime indicate that the state on any boundary subregion is fully entangled with its complement. We, therefore, consider the smoothness and connectedness of the classical geometry as the necessary and sufficient condition preventing factorization of the boundary pure state. Holographic states dual to connected spacetimes are therefore of the 'fully

entangled' type in subsection 4.2.2.

Though connected geometries are dual to fully entangled states, we may still consider factorizable holographic pure states. To do so we merely treat multiple independent holographic geometries as product states, living in separate Hilbert spaces with boundary theories decoupled. This thought experiment provides at least one valuable lesson. Any of the geometric prescriptions for subregion complexity will be exactly additive on such factorizable subsystems. While utilizing gates which couple the combined Hilbert space could in principle allow for increased efficiency in preparing the combined state, evidently the notion of complexity dual to bulk action or volume does not take advantage of such gates. Either holographic states are always of the sort that they are never optimally constructed utilizing these gates, or such gates should be excluded from the outset. This latter possibility stands in tension with naive prescriptions for choosing the gate set to vary only with the size of the Hilbert space with no other concern for locality or the entanglement structure of the state (such as the k-local gate set prescription outlined in section 4.2.1). This also indicates that if we consider only holographic purifications, the validity constraint excluding unentangled factors is redundant, because evidently including such factors never results in a 'speed up.'

Turning again to connected holographic spacetimes, if we consider only such systems we can apply our expectations about fully entangled states (see subsection 4.2.2). Along with the basic requirement that purification complexity is positive definite, we have a primitive list of consistency checks to

perform on any proposed holographic dual to purification complexity. For any boundary subregion A and neighboring (connected, but not necessarily small) extension of that boundary subregion δA, we expect

$$\begin{aligned} \text{Positivity:} \qquad & C_A^P > 0 \\ \text{Monotonicity:} \qquad & C_{A+\delta A}^P > C_A^P \\ \text{Weak Superadditivity:} \qquad & C_A^P + C_{\delta A}^P < 2C_{A+\delta A}^P \end{aligned}$$

The monotonicity property, which is symmetric on A and δA, implies weak superadditivity. The same applies to the case already discussed in section 4.2.3, the two sides of an eternal black hole solution. In this case δA is replaced with A^c, the boundary region complement to A. This is not a 'neighboring' boundary subregion (they are only connected through the bulk), but they form a partitioning of the total boundary (T) and the subsystems are fully entangled.

$$\text{Weak Superadditivity:} \quad C_A^P + C_{A^c}^P < 2C_T$$

4.3 Holographic Purification Complexity

In this section, we consider in detail the conjecture(s) that volume or action on a subsystem entanglement wedge in holographic geometries might be dual to the purification complexity of the corresponding boundary mixed state. We first motivate the relationship to purification complexity, as opposed to some other notion of mixed state complexity, by considering what the total

state complexity conjecture may already imply about the meaning of subregion complexity. We do so through an analogy with the concept of 'entanglement of purification,' explained in subsection 4.3.1.

In 4.3.2 we make the case that the volume prescription for subregion complexity is computing a type of purification complexity. To be precise, if the class of purifications considered is all holographic purifications, then the prescription computes precisely the minimum complexity among these. Over any less restricted class of purifications, the subregion prescription merely bounds from above the purification complexity so defined. The same arguments applied to the action prescription do not lead so inexorably to the notion of purification complexity. They imply that the prescription computes the complexity of a particular purification, but it is not clear that it is the optimal one. We defer more explicit holographic tests of this idea for subregion action to section 4.5.

The considerations of this section imply that the volume prescription matches our general expectations for purification complexity more or less automatically, but in 4.3.3 we discuss a puzzle with this interpretation and use it to motivate a modification of the bulk volume prescription to include a boundary term on the HRT surface.

4.3.1 Motivation from Entanglement of Purification

.

We would like to test the conjecture that subregion complexity is dual

to purification complexity by finding a holographic estimate of the purification complexity (independent of the usual subregion complexity prescription). For guidance on how to construct such a holographic estimate, we turn to discussions *entanglement of purification* in holography. Entanglement of purification is defined as follows: Given a bipartite system consisting of subsystems A and B, and a state ρ_{AB} on that system, the entanglement of purification between A and B of ρ_{AB} is the minimum entanglement entropy $S(\rho_{A\bar{A}})$ of the reduced state $\rho_{A\bar{A}}$ minimized over all purifications $|\psi\rangle_{A\bar{A}B\bar{B}}$ of ρ_{AB} and all partitions of the purifying system into $\bar{A}$ and $\bar{B}$. If ρ_{AB} is pure, then the entanglement of purification is simply the entanglement entropy of the reduced state ρ_A and ρ_B. Recent work [98–100], has discussed a conjectured holographic dual to this quantity for holographic CFTs, which is given as follows: Consider subregions A and B on the boundary, and the joint entanglement wedge of AB. The holographic entanglement of purification is then given by the area of the minimal surface in the entanglement wedge which divides A from B (refer to figure 4.1). In the case where there is no mutual information between A and B, and so the entanglement wedge is disjoint, we have that A and B are already divided, and so the entanglement of purification is zero. In the case of two disjoint intervals with non-zero mutual information, the minimal surface goes between the two disconnected pieces of the RT surface, and we need only minimize over which points on the RT surface it will intersect.

The intuition behind this definition is as follows: There is an optimal purification, which lives on the subregion AB on the boundary, as well as the

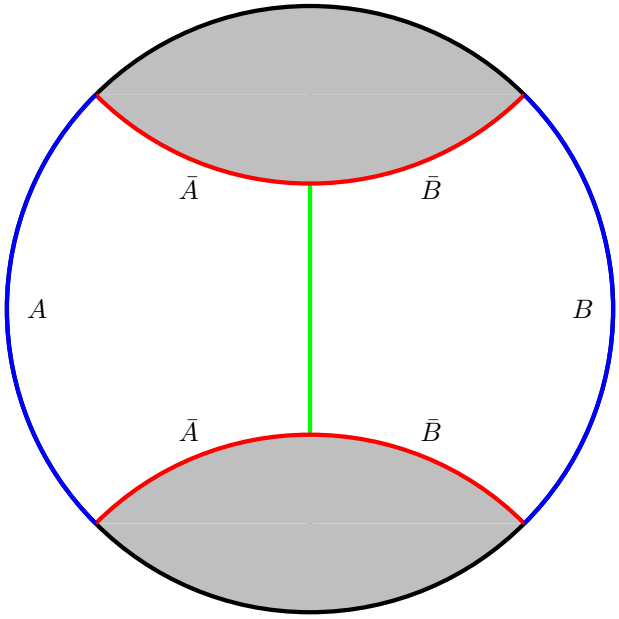

Figure 4.1: Entanglement of purification between two interval subregions with non-zero mutual information. The minimal surface whose area gives the entanglement of purification is shown in green.

on the RT surface of AB. The auxiliary states on the RT surface can be partitioned into an $\bar{A}$ system and $\bar{B}$ system in different ways, and for each partition, we may compute the entropy of $A\bar{A}$ using the RT prescription. By minimizing over such partitions, we arrive at the entanglement of purification, as given above. But how did we arrive at the fact that the purifying auxiliar system 'lives' on the RT surface? This is supported by intuition from tensor

networks, but we can justify it as follows:

In minimizing over purifications, we certainly know that the state on the full boundary is a purification of the state on AB. However, this state contains much more information than is needed to purify the reduced state ρ_{AB} on AB. As a consequence, for any partition, there more entropy than we needed. We can fix this by renormalizing the state, thereby getting rid of the extra information. These renormalized states correspond to putting different cutoffs in the bulk, which agree with our original cutoff in the entanglement wedge of AB, but which outside that wedge can be different. Each of these cutoffs corresponds to a different renormalization of the global state, and as such a different purification of ρ_{AB} (see figure 4.2). Clearly then, the cutoff which will give the smallest RT surface, and likewise the one that corresponds to course graining away all the information not needed to purify ρ_{AB}, is the one which hugs the RT surface of AB. We then get the prescription above.

Of course, there are potentially other holographic purifications of ρ_{AB}. Suppose there is an isometric embedding of the entanglement wedge of AB into a geodesically complete asymptotically AdS spacetime, such that the entanglement wedge of the image $\tilde{A}\tilde{B}$ of AB is the image of the entanglement wedge of AB. Then according to subregion duality, the reduced state on $\tilde{A}\tilde{B}$ simply is ρ_{AB}, since both states are dual to geometries which are identical up to isometry. We may then repeat the above procedure on the new geometry. For entanglement of purification, we will inevitably be led to the same purification, by the arguments above. We will nevertheless term such geometries

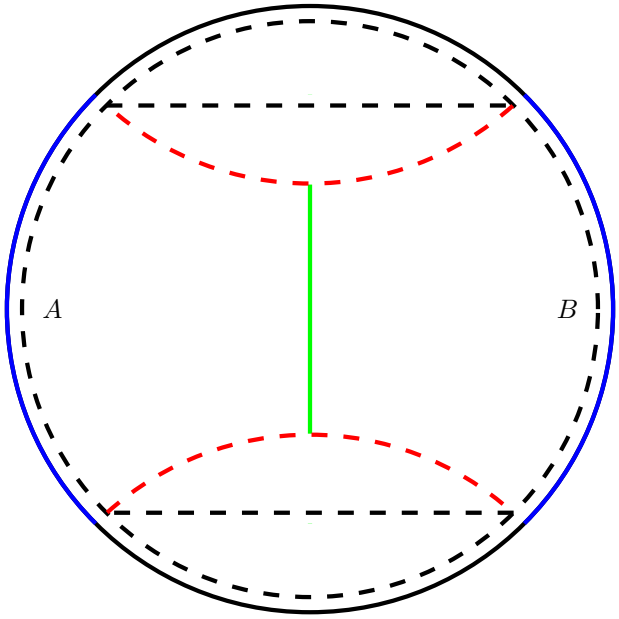

Figure 4.2: We may purify the state on AB to states with different course grainings, corresponding to different cutoffs, shown here as a dashed line. The optimal purification will correspond to cutoff which hugs the RT surface, shown here as a red dashed line.

'purifying geometries' for the holographic state ρ_{AB}.

We claim that this same procedure of minimizing over purifications by considering all purifying geometries, and all cutoffs on these purifying geometries compatible with our cutoff in the entanglement wedge, should be applied to find the purification complexity of a given reduced state holographically.

We flesh out this claim in the following subsection.

4.3.2 Purification Complexity

Suppose we take for granted the original complexity=volume conjecture, that the maximal volume slice asymptoting to a fixed boundary Cauchy slice is dual to some notion of complexity for the total state on that boundary slice [9]. Consider all possible holographic geometries which geodesically complete a fixed entanglement wedge. The states dual to these 'purifying geometries' provide a set of purifications of the density matrix on the original boundary subregion (any pure state is, of course, a purification of all its subsystems). Further consider all possible cutoff surfaces in the complementary portion of these spacetimes, subject to the restriction that they can at least sustain a Cauchy slice for the original entanglement wedge. The corresponding set of coarse-grained states provides an even larger class of purifications to consider.

Trusting the total state complexity conjecture, we can compute all the

[9] In the complexity = volume conjecture, a choice of lengthscale is necessary to turn a proportionality into a true equality. Traditionally this length scale has simply been taken to be the AdS scale, but recent work [2] has suggested that a variable scale determined by features of the total geometry may be more appropriate. It is not clear how such a variable lengthscale should be set for the arbitrary subregions considered in this work. For simplicity, we first consider the case where the length scale is the AdS scale. For our conclusions about additivity to hold for complexity and not just volume in a proposal with variable lengthscale, we at least require that the length scale is the same for the subregion, the total state, and the complement subregion. In a hypothetical scheme where the length scale changes even with the cutoff surface, the minimization procedures described in this section applies to complexity as well as volume only if variations in the cutoff surface which increase the max volume obey $\delta \log (V/V_0) \geq \delta \log (l/l_0)$, with l being the variable lengthscale, and V_0, l_0 being some reference values.

complexities of these purifications and find the minimum. With the complexity=volume prescription, we are inevitably led to the conclusion that the minimum pure state complexity among all holographic purifications corresponds to choosing a cutoff surface which traces just outside (see next section) the HRT surface for the subregion; deviation from this choice results in either an increase in volume and a higher complexity, or in the exclusion of some portion of the entanglement wedge, which invalidates the state as a purification of the original density matrix. The first statement follows intuitively from the positive-definiteness of volume, and more rigorously from the superadditivity relationship proven in the next section 4.4. The second statement relies on the specific duality between an entanglement wedge and the corresponding boundary mixed state. Any cutoff contour which cannot sustain a Cauchy slice for the original entanglement wedge will inevitably exclude some bulk operators which ought to be described by the original boundary subregion's mixed state. In so far as we consider only holographic purifications of a boundary mixed state, these considerations imply that the volume subregion prescription on an entanglement wedge is computing precisely the minimum complexity among purifications. The same claims follow analogously for the complexity=spacetime volume prescription.

Now consider the same series of statements for the complexity=action subregion prescription. We can consider purifying geometries of a fixed entanglement wedge, and we can vary over cutoff surfaces. The action on the entanglement wedge submanifold is just another pure state complexity, with

the complementary degrees of freedom course-grained to the limiting case of the HRT surface itself. However, lacking in these considerations is the idea that computing this particular purification's complexity amounts to a minimization over holographic purifications. The action is not a positive-definite quantity, and other choices of cutoff surfaces in some purifying geometry may provide a purification of lower complexity. Finding any such state amounts to a disproof that the action subregion prescription can be called a purification complexity, in the usual sense of a minimization over the complexity of purifications. We find such counterexamples in 4.5.

We now provide an example of the procedure just outlined by considering the two-sided black hole (see figure 4.3). If our aim is to estimate the purification complexity of the left boundary mixed state with a certain cutoff $r = \delta_L$, and we are allowed to minimize over the purifying right cutoff, δ_R, an interesting result emerges: When one sets $\delta_R = r_+$, and regularizes the WDW patch by settings its 'corners' on the cutoff surfaces, one recovers (in this limit) the usual subregion complexity of the left side! Analogous procedures result in similar conclusions for other two-sided geometries, or for subregions of AdS_3. In fact, for a general boundary subregion A, allowing a minimization over possible cutoffs in the complement region, subject to certain consistency conditions (e.g., the total cutoff must be continuous), will lead to the inequality

$$C^P(A) \leq C^{\text{subregion}}(A) \tag{4.13}$$

whenever the entanglement wedges of a region and of its compliment meet

on a single surface. By the HRT prescription, this should always happen for geodesically complete geometries.

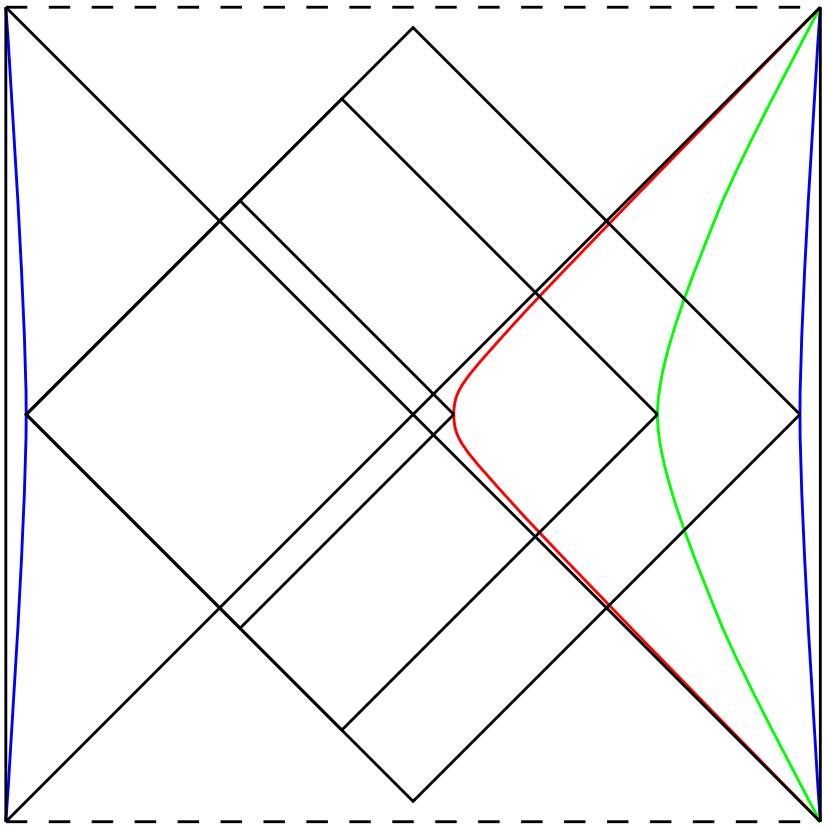

Figure 4.3: A two sided black hole, with different cutoff surfaces on the right side. For each cutoff surface, we have draw the corresponding regulated WDW patch.

Under either CV or CV2.0, superadditivity holds for any values of the left and right cutoff (we give a proof in section 4.4), and we thus have that

$$C(|\psi\rangle) \geq C^{\text{subregion}}(A) \tag{4.14}$$

for any holographic purification $|\psi\rangle$ of ρ_A. However, then this means that if we

define a purification complexity only with respect to holographic states (which is perhaps appropriate at leading order in $\frac{1}{N}$), then we have that subregion complexity = holographic purification complexity. This strongly suggests that the duality proposed in [4] for CA works for both CV and CV2.0. The situation with CA is actually less clear, as the action is not positive definite and equation (4.14) does not apply. The inequality (4.13) does still hold for CA though, provided this minimization over the right cutoff is valid.

4.3.3 Adding a boundary term

One issue with this proposal to minimize over all cutoffs is that, for the optimal purification, the subregion complexity of the reduced state on the purifying right system vanishes. However, this reduced state must have a fixed entanglement entropy, as the state on the whole system is pure. Either we must have a mixed reference state (which seems unusual), or something else must be going on. We can resolve this issue by not allowing the cutoff surface to be pushed all the way to the horizon surface, instead taking it only to the stretched horizon. This too has a number of interesting consequences, the first of which is that it makes the purification complexity in CV subadditive on a slice about which there is time reflection symmetry. This is because the left and right purification complexities both include the volume of the slice between the left and right stretched horizon, and so this part of the volume gets counted twice when one adds the two purification complexities, and only once when one computes the total complexity. This is reminiscent of the argument in section

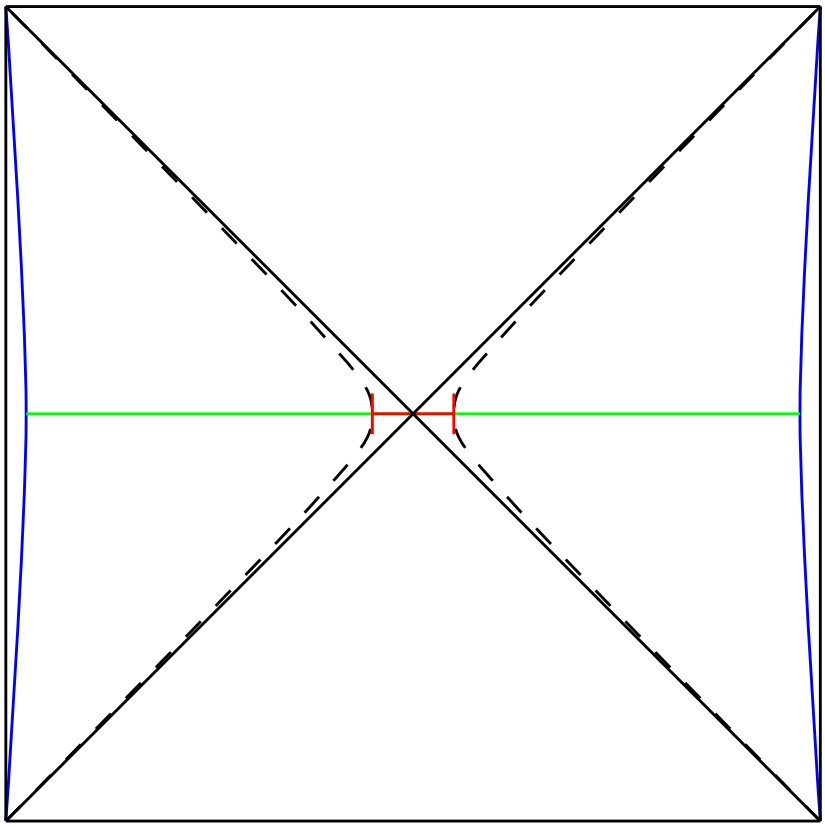

Figure 4.4: The dashed lines in this figure represent the stretched horizon. The purification complexity in CV of the left (right) reduced state is given by the volume of the left (right) green segment plus the red segment. The complexity of the total state is given by the volume of both green segments plus the volume of the red segment. We thus have that $C_L + C_R - C_T$ is given by the volume of the red segment, and as such is positive definite. We may identify the green segments with the basis complexity, and the red segment with the spectrum complexity, as per the discussion in section 3.3 of [4].

3.3 of [4] that the spectrum complexity gets double counted when adding the purification complexities, suggesting that perhaps this segment of the volume between the left and right stretched horizons should be identified with the

spectrum complexity of the mixed state. We would then identify the part of the volume between the left cutoff and the left stretched horizon as the basis complexity.

When considering the thermofield double state away from the $t_L = t_R = 0$ slice, the maximal slice will not pass through the HRT surface, and the simple "double counting" mentioned in the above case does not apply. However, for these total states, we argued (see section 4.2.3) that the spectrum/basis decomposition of the subsystems is insufficient to parse total state complexity. In these cases, the behind-the-horizon region probed by the maximal slices should roughly correspond to operators which mix degenerate subspaces and go unnoticed by either subsystem density matrix. See [101] for a recently proposed definition of a related quantity, the "binding complexity."

At this stage, one might be worried that we have ruined the upper bound of purification complexity by subregion complexity. However, our bound on purification complexity differs from subregion complexity by a term proportional to the area of the HRT surface (namely the volume between the true horizon and the stretched horizon), which could thus be thought of as an extra boundary term in the subregion complexity prescription. We will take the view that such a discrepancy likely should be corrected by altering the definition of subregion complexity in this way[10].

Such boundary terms could also be included for CV2.0, CA, and CA-2.

[10] We would like to thank Phuc Nguyen for suggesting including a boundary term in CV.

In these cases, however, one does not automatically get subadditivity. For CV2.0 in particular, there will generally be a significant contribution to the total state complexity from behind the entanglement horizon which cannot be identified with either the spectrum or basis complexity (see figure 4.5). As suggested above for CV off of the $t = 0$ slice, this can perhaps be identified with the complexity in the total state due to gates acting within a degenerate eigenspace of the left and right density matrices, or even rotating the relative phase for a non-degenerate eigenspace. Discussions of this sort have occurred in [83], with proposals for decomposing a holographic spacetime into subregions of particular significance for the quantity of "uncomplexity" (though those proposals did not strictly include a boundary term).

4.4 Superadditivity

It was noted in [4] that in CV, holographic subregion complexity obeys

$$C(\rho_{AB}) \geq C(\rho_A) + C(\rho_B). \tag{4.15}$$

when A and B partition a complete boundary Cauchy slice. Recently, a related property for "uncomplexity" was discussed in [97] for quantum systems. In this section we provide an independent discussion of this property, which we will call 'superadditivity.' We will give a proof that subregion complexity obeys this property for general subregions in CV, as well as in CV2.0, and discuss whether it may hold in CA.

Note that superadditivity implies that the subregion complexity of a

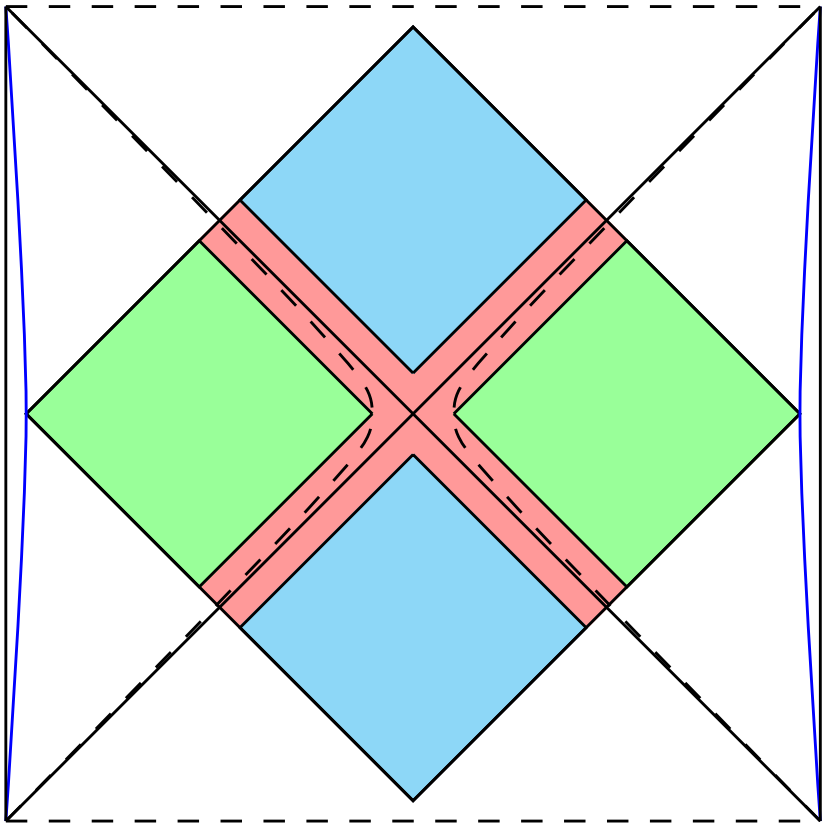

Figure 4.5: Similarly to CV, we may decompose the action in CA, CV2.0, or CA-2 by associating different parts of the WDW patch to the spectrum, basis, and degeneracy complexity. Roughly speaking, we suggest the green regions should correspond to the basis complexity, the blue regions to the degeneracy complexity, and the red to the spectrum complexity.

given subregion must be less than or equal to the complexity of any of its holographic purifications. This will hold regardless of the cutoff imposed, as it is merely a statement about maximal volumes on Lorentzian manifolds with boundary. If we suppose (as is reasonable at leading order in $\frac{1}{N}$) that one need only consider holographic purifications, this result along with the discussion

above is enough to guarantee the subregion complexity = purification complexity, provided one accepts complexity = volume or complexity = spacetime volume for geometries dual to pure states.

4.4.1 Maximal volumes of subregion wedges

Here we will give a proof of superadditivity of holographic subregion complexity in CV. Let w_X denote the entanglement wedge [102] of a given boundary subregion X of a boundary time slice, and let Σ_X denote the maximal volume slice of w_X. By the maximal slice of w_X, we follow the proposal in [95], according to which we maximize over the volumes of slices anchored at both X and the HRT surface of this boundary subregion. Given non-overlapping subregions A and B on a Cauchy slice of the boundary, we have the inequality

$$\mathrm{Vol}(\Sigma_{AB}) \geq \mathrm{Vol}(\Sigma_A) + \mathrm{Vol}(\Sigma_B) \tag{4.16}$$

That this inequality is obeyed can be easily seen as follows: First, let us note that because A and B are non-overlapping, it is also true that w_A does not overlap w_B (see [38]). Now either Σ_A and Σ_B meet to form a spatial slice of w_{AB}, or there is a gap between them. An example of the first case is a two-sided black hole, with A and B taken to be the entire left and right boundary respectively (see figure 4.6 for an illustration). An example of the second case is two entanglement wedges in pure AdS, the union of which is not the whole bulk (see figure 4.7 for an illustration). In the case without a gap the inequality is immediate: Σ_{AB} is the *maximal* spatial slice over w_{AB}, so the slice formed by

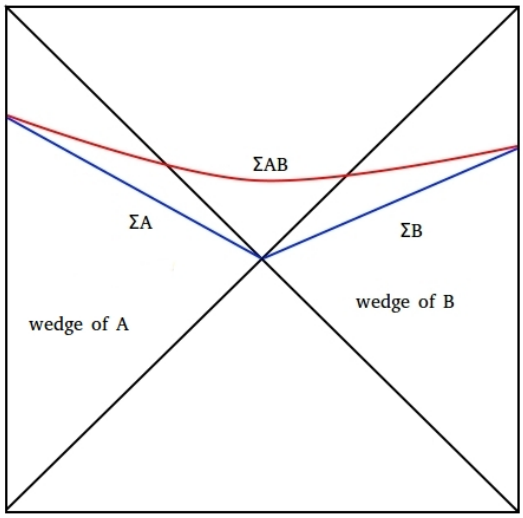

Figure 4.6: A slice through entanglement wedges who share an HRT surface, as in the case of a two-sided BH, or the wedges of two halves of the boundary of pure AdS.

the union of Σ_A and Σ_B (whose volume is the sum of the individual volumes) must have a volume which does not exceed that of Σ_{AB}. In the case where there is a gap between Σ_A and Σ_B in w_{AB}, we may bridge this gap with a slice Σ_{bridge} of $w_{AB} - w_A - w_B$ which meets Σ_A and Σ_B at their boundaries. We will moreover require that Σ_{bridge} contains the HRT surface for AB. Then it is clear that the union of Σ_A, Σ_B, and Σ_{bridge} forms a Cauchy surface for w_{AB}. But once again, since Σ_{AB} is maximal, we have that

$$\text{Vol}(\Sigma_{AB}) \geq \text{Vol}(\Sigma_A) + \text{Vol}(\Sigma_B) + \text{Vol}(\Sigma_{\text{bridge}}) \geq \text{Vol}(\Sigma_A) + \text{Vol}(\Sigma_B), \quad (4.17)$$

where the second inequality holds because volume is a non-negative quantity. This establishes the superadditivity property for maximal volumes of subregion wedges.

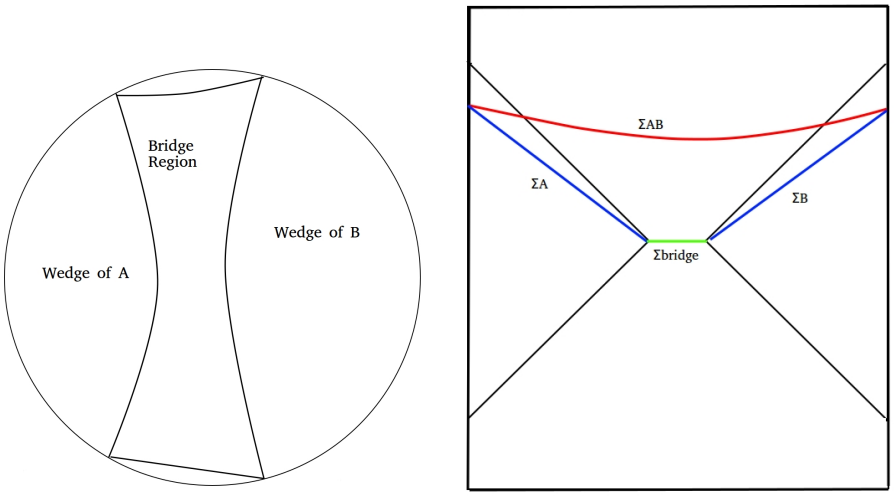

Figure 4.7: On the left is a spatial slice showing the wedge of a region A, the wedge of a region B, and a 'bridge region.' Here there is clearly a gap between a spatial slice on the A wedge and a spatial slice in the B wedge, as shown in the cross-section on the right. We can however always bridge this gap by an arbitrary spatial slice of the bridge region which meets the slices associated to A and B respectively at their boundaries

Notice that it is important to require that the bridge contains the HRT surface for AB. This is because the volume that computes the complexity is only maximal among Cauchy surfaces of the entanglement wedge, i.e. among surfaces anchored on this latter HRT surface (and also on AB). That Σ_{bridge} can be chosen in this way follows from the results in [90], according to which it is always possible to choose a spatial slice in the bulk containing simultaneous the HRT surfaces for A, for B and for AB (assuming Einstein gravity together with the null energy condition).

4.4.2 CV 2.0

Superadditivity also holds for the spacetime volumes of Wheeler-DeWitt (WDW) patches, which has also been proposed as the dual quantity to state complexity in [31].

The super-additivity of WDW patch volumes follows trivially from the fact that given boundary regions A and B, the entanglement wedges w_A and w_B of these regions are both subsets of the entanglement wedge w_{AB} of the combined system. Hence, it is also true that the intersections of the WDW patch with w_A and w_B respectively are contained in the intersection with w_{AB}. Because spacetime volume is additive, this means the subregion complexity on A , B, and AB respectively, which are given by the volumes of the intersections of the WDW patch with w_A, w_B, and w_{AB}, obey inequality 4.15. This is illustrated for a two-sided black hole in figure 4.8, where region A is taken to be the whole left boundary and region B is likewise taken to be the right boundary. Then the subregion complexity of A is given by the spacetime volume of the region shaded in green, that of B by the spacetime volume of the region shaded in blue, and the complexity on AB is given by the spacetime volume of the whole WDW. The difference $\mathcal{C}_{AB} - \mathcal{C}_A - \mathcal{C}_B$ is thus given by the spacetime volume of the region shaded in red, which is clearly a positive definite quantity.

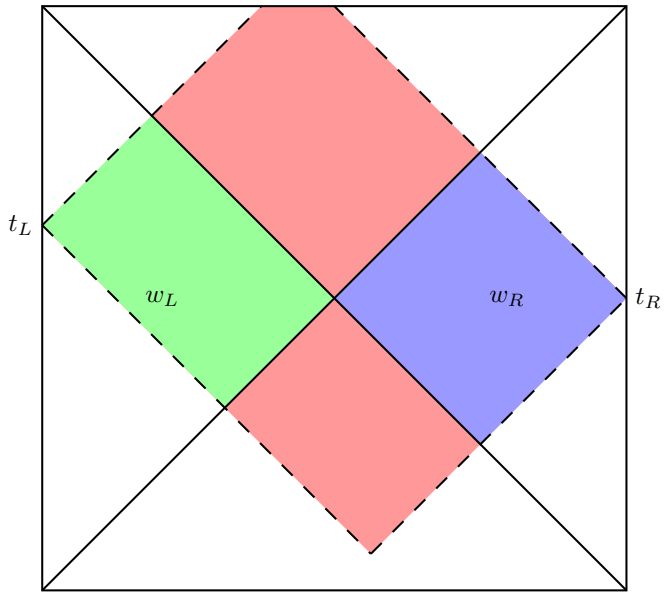

Figure 4.8: The WDW patch for a two-sided black hole, outlined with dashed lines. If we consider subregion A to be the left boundary and subregion B to be the right boundary, then the entire outside of the horizon on the left side, w_L, is the entanglement wedge of A, and likewise for the right side and B. The entanglement wedge of AB is the whole spacetime.

4.4.3 Additivity in CA?

Since we have not proved superadditivity in either CA or CA-2, it is natural to wonder under what conditions, if any, such a property holds for these conjectures. We do not pursue this question in depth here, but it is quick work to see that superadditivity is far from generic in either proposal. The spacetime regions considered under the complexity=spacetime volume proposal are identical to those considered in the action proposals, namely, the intersection of a region's entanglement wedge and the WDW patch of the boundary slice. The same nesting properties then hold here as in the previous section. However,

the fact that volume and spacetime volume are positive-definite quantities led to the superadditivity conditions above. On the other hand, the bulk integral of the action is often negative. For instance the Einstein Hilbert term in pure AdS spacetimes gives a negative integrand ($R - 2\Lambda = \frac{-2(d-1)}{L^2}$ in d spacetime dimensions). There are also contributions from subregion boundaries and boundary intersections which may be of either sign. Some of these contributions have ambiguities which require stating a convention before the overall sign could be determined [4, 59, 95]. In the next section, we will look at specific instances where both subadditivity and superadditivity occur for the action.

4.5 Additional Purifications

In subsection 4.3.2 we argued that assuming the complexity=volume or complexity=spacetime volume prescription for pure states, then the corresponding subregion prescription computes the purification complexity of the boundary mixed state, specifically minimizing complexity overall holographic purifications. The consistency conditions mentioned in 4.2.4 follow automatically for these proposals. Similar demonstrations for subregion action prescription are not forthcoming, so in this section, we put the action subregion prescription to the test holographically by considering what is perhaps the most canonical holographic mixed state, the thermal state dual to one size of a static eternal black hole.

4.5.1 Multisided Black Holes

In 2+1 spacetime dimensions, the entanglement wedge corresponding to the thermal mixed state under consideration amounts to one exterior region of a BTZ black hole. The most obvious purifying geometry is the two-sided eternal black hole solution, dual to the thermofield double state, and we will scrutinize this case more carefully in the next subsection. However, a much larger class of holographic purifying geometries exists, which we consider all together here: AdS_3 black holes with n sides and genus g. These geometries are an extension of the familiar BTZ black hole [74], obtained by quotienting pure AdS_3 by a discrete group of isometries, and they are studied in [103–105]. The states dual to these geometries were discussed in [106], and the entanglement structure was studied in [107]. The minimum complexity over all sides n and all genus g provides an upper bound on the purification complexity of the state on a single boundary.

The complexity of this family of black holes was computed for the $t_1 = t_2 = ... = t_n = 0$ spatial slice in [96] according to both the complexity = volume and complexity = action conjectures. The authors of that paper computed a quantity ΔC, which they defined as the difference in complexity between the solution of interest, and n copies of the one-sided $M = 0$ BTZ black hole. The results they found for an n sided black hole with a wormhole

of genus g are

$$\Delta C_A = \tfrac{1}{6} c\chi \tag{4.18}$$

$$\Delta C_V = -\tfrac{4}{3}\pi c\chi \tag{4.19}$$

where $c = \frac{3L}{2G}$ is the central charge of the boundary CFT and $\chi = 2 - 2g - n$ is the Euler characteristic of the $t_1 = t_2 = ... = t_n = 0$ spatial slice. One immediate consequence of this result noted in [96], is that at any fixed n, ΔC_A decreases with increasing g. This already casts doubt on the idea that purification complexity should be identified with subregion complexity in CA, as for any value of the subregion complexity (which certainly does not depend on the genus, a property of the purification), we may find a genus such that the corresponding 2-sided purification has a lower complexity. This would seem to be a problem for 'complexity = action' generally, in so far as it implies the purification complexity of our state in CA is $-\infty$. The authors of [96] suggest that perhaps this merely indicates an upper bound on the allowed genus of such black holes. In order to remain consistent with purification complexity = subregion complexity, however, one would need an even stricter bound than that implied by the positivity of complexity, or else our upper bound on the purification complexity will fall below the subregion complexity, the presumed true value.

By contrast, we see that for complexity = volume, increasing either the genus or the number of sides will only increase the complexity of the corresponding purification, and so our upper bound is provided by the ordinary

BTZ case where $n = 2$ and $g = 0$. We see that in that case that χ vanishes, and so the total complexity is twice that of the $M = 0$ black hole (this calculation, of course, did not include any boundary term as suggested in section 4.3.3). On the other hand, due to the mass independence of the subregion complexity of one side of BTZ, the subregion complexity is identical to that of one side of the $M = 0$ black hole, and so for CV we have that our upper bound on purification complexity is still larger than the subregion complexity, consistent with the conjecture that purification complexity = subregion complexity in CV.

This comes as no surprise, as this result was guaranteed by superadditivity. Given any subregion A of any asymptotically AdS geometry, we may partition the total boundary into A and its complement. Then superadditivity of CV, along with the positivity of volume, guarantees us that the holographic complexity of the total state (as computed in CV) is greater than the subregion complexity of A (or equal to, in the limiting case where A is the full boundary). Thus, given a state ρ on a subregion A of a CFT, and all classical geometries dual to purifications of ρ, i.e. all geodesic completions of the entanglement wedge W of A which preserve W as the entanglement wedge of A, we will always find that according to CV, our holographic estimation of the purification complexity of ρ is no greater than the subregion complexity of A.

Because the spacetime volume is also strictly positive, and because complexity according to CV2.0 is also superadditive, the same logic applies. Whether it applies to CA-2 in cases where it disagrees with CV2.0 is left to future work.

4.5.2 Two sided BTZ black hole: detailed treatment

Though the action results for the genus-g black hole solutions may cast doubt on the idea that subregion action is dual to purification complexity, they could alternatively be teaching us nontrivial information about limits on the genus which can be described holographically at a certain cutoff, or these solutions might be disallowed for some other unknown reason. With these possibilities in mind, we examine in more depth the standard case of a two-sided (genus zero) BTZ black hole. The metric is given by

$$ds^2 = \frac{L^2}{z^2}\left(-f(z)dt^2 + f(z)^{-1}dz^2 + L^2 d\theta\right)$$
$$f(z) = 1 - \left(\frac{z}{z_H}\right)^2$$

with $z \to 0$ representing the AdS boundary and z_H being the z coordinate of the horizon.

Subregion action calculations for this case were computed in [4], but we here report results which include an additional term[11] associated with null boundaries required to make the action reparameterization invariant [59]. Utilizing this term, the on-shell action of the Wheeler-DeWitt patch depends on an undetermined lengthscale, which we denote $\tilde{L}$. We additionally allow the cutoff surfaces (of constant $z < z_H$) on right and left to vary independently as $z_{\text{L,min}} = \delta_L$ and $z_{\text{R,min}} = \delta_R$. We report the action result for the $t_L = t_R = 0$ slice here, abbreviating $\bar{L} = \tilde{L}/L$ where $L = L_{AdS}, \bar{\delta}_L = \delta_L/z_H$, and $\bar{\delta}_R =$

[11] As this work was being prepared, we learned in private correspondence with the authors of [4] that they have also computed this term and will include it in work to appear soon.

δ_R/z_H:

$$\frac{\mathcal{A}^T(\bar{\delta}_L,\bar{\delta}_R)}{16\pi G} = \frac{2L^2}{z_H}\left(-\frac{2\left(s_L s_R-1\right)\log\left(\frac{4\bar{L}^2 s_L s_R}{\left(s_L s_R-1\right)^2}\right)}{s_L s_R+1}+\frac{\log\left(\left(1-\bar{\delta}_L^2\right)\bar{L}^2\right)}{\bar{\delta}_L}+\frac{\log\left(\left(1-\bar{\delta}_R^2\right)\bar{L}^2\right)}{\bar{\delta}_R}\right) \tag{4.20}$$

where $s_L = \sqrt{\frac{1+\bar{\delta}_L}{1-\bar{\delta}_L}}$ and $s_R = \sqrt{\frac{1+\bar{\delta}_R}{1-\bar{\delta}_R}}$. If the cutoffs are taken to be symmetric, this simplifies to

$$\frac{\mathcal{A}^T(\bar{\delta},\bar{\delta})}{16\pi G} = \frac{4L^2}{z_H}\left(-\bar{\delta}\log\left(\bar{L}^2\left(\frac{1}{\bar{\delta}^2}-1\right)\right)+\frac{1}{\bar{\delta}}\log\left(\bar{L}^2\left(1-\bar{\delta}^2\right)\right)\right) \tag{4.21}$$

The subregion action associated with either left or right side (restricted to the entanglement wedge[12]) is given by

$$\frac{\mathcal{A}^{L,R}(\bar{\delta})}{16\pi G} = \frac{2L^2}{z_H}\left(-\log\left(4\bar{L}^2\frac{(1-\bar{\delta})}{(1+\bar{\delta})}\right)+\frac{1}{\bar{\delta}}\log\left(\bar{L}^2\left(1-\bar{\delta}^2\right)\right)\right) \tag{4.22}$$

Comparing these results to expectations is complicated by the existence of the undetermined length scale $\tilde{L}$, which lacks a clear interpretation in relation to complexity in the boundary theory. Demanding that the complexity is a positive quantity in the strict UV limit ($\delta_L \to 0, \delta_R \to 0$) simply requires that we choose $\tilde{L} > L_{AdS} \implies \bar{L} > 1$. If the interpretations of section 4.3.2 are correct, however, and letting the cutoffs on both sides approach the horizon

[12] Joint contributions in the subregion action diverge if naively evaluated on the black hole horizon. We followed [4] by computing the action on an exterior region bounded by null surfaces just outside the future and past horizons and taking the limit that they coincide with the future and past horizons.

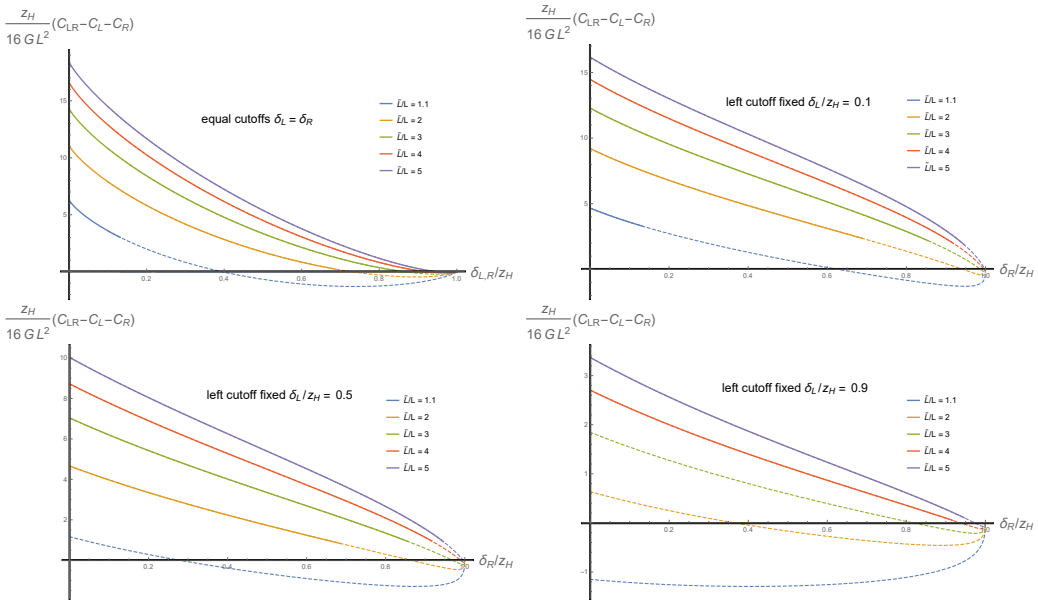

Figure 4.9: The above plots show the difference between the total state complexity $C_T = C_{LR}$ and the sum of left and right subregion complexities $C_L + C_R$ for the BTZ black hole at $t_L = t_R = 0$, computed using the complexity=action prescription. Positive values indicate that the left and right factors behave superadditively, and negative indicates subadditivity. The cutoffs are constant z surfaces $z_R = \delta_R$, $z_L = \delta_L$ and various choices of $\tilde{L}/L_{AdS}$ are displayed. Positivity in the strict UV limit ($\delta_L \to 0$ and $\delta_R \to 0$) requires that the lengthscale $\tilde{L}$ be chosen greater than L_{AdS}, so only such lines are displayed. The dashed portions of each line are excluded if we demand positivity of the total state complexity as well as both subregion complexities at the corresponding cutoffs. We find that in the remaining parameter space the system always behaves superadditively: $C_T > C_L + C_R$.

($\delta \to z_H$ or $\bar{\delta} \to 1$) amounts to coarse-graining the state on both boundaries, then positive complexity should be imposed over the whole range of allowed cutoffs. We find that $\bar{L}$ greater than but of order 1 easily results in negative complexity as the cutoffs are pushed inward (away from $z = 0$). For $\bar{L} \gg 1$, both cutoffs must approach the horizon itself before there is a problem with

negative complexity. For any choice of cutoffs, there is some $\bar{L}$ sufficiently large to avoid negative complexity. This is especially true if at least one cutoff remains in the deep UV (e.g., $\bar{\delta}_R \ll 1$).

If we ignore positivity requirements and allow any combination of fixed-z cutoffs, then we can find regions of subadditivity ($C_T < C_L + C_R$), as well as regions where the total state complexity is lower than one or the other of the subregion complexities ($C_T < C_L$ or $C_T < C_R$), which would violate the purification complexity interpretation of the corresponding subregion action. Neither of these properties occurs, however, if we restrict to regimes where the total state complexity as well as both subregion complexities are positive. See figure 4.9 for illustration of how requiring positivity excludes cases of subadditivity, for example.

To summarize the action results for this case, if we treat positivity as a strict condition for all complexities, then the choice of lengthscale $\tilde{L}/L_{AdS}$ can impose nontrivial restrictions on the allowable cutoff surfaces (especially for $\tilde{L}/L_{AdS}$ greater than but of order one). Over any combination of $\tilde{L}/L_{AdS}, \delta_L, \delta_R$ which gives positive complexities, we find that the total state complexity is always larger than either subsystem complexity, avoiding contradiction with the purification complexity = subregion action conjecture as could occur for the genus-g solutions of the previous section. In the parameter space consistent with positivity, the action behaves superadditively. As reviewed in section 4.2.3, this differs from the subadditivity expectation coming from the basis and spectrum decomposition utilized in [4]. The discussion of that section

cast some doubt on the subadditivity expectation, but we nevertheless found it plausible. The mixed results of this section do not give any strict violation of the purification complexity interpretation of subregion action, but without a reason to expect superadditivity as the generic behavior for these states it remains a puzzle facing that interpretation. The significance of $\tilde{L}$ is an important piece in that puzzle.

If we consider instead the subregion volume prescription for the same spacetime decomposition, including the boundary term on the HRT surface suggested in 4.3.3), then at least our most immediate expectations follow naturally. All complexities are manifestly positive, and subadditivity is always obeyed on the $t_L = t_R = 0$ slice. The sum of the subregion complexities "double counts" the boundary term, which the total state slice effectively counts only once. Because the boundary term is proportional to the area of the HRT surface (and therefore the entanglement entropy) and it does not vanish under any course graining, we loosely interpret it as the 'basis complexity' portion of the subregion complexity.

The volume prescription also incorporates the case we puzzled over after equation 4.11, where the total state happens to be exactly the minimal complexity purification of both subsystems, and we saturate the weak superadditivity limit $C_L + C_R = 2C_T$. This would not ordinarily occur for the thermofield double state unless it happened to be the minimally complex purification for both left and right factors. This can be realized as a limiting case, saturated by taking both cutoffs down to their limiting values around the HRT

surface (equivalently, sending the volume portion to zero and leaving only the HRT boundary term, refer to figure 4.4). This could perhaps be thought of as effectively course grains the 'basis complexity' on both sides to zero and leaves only the spectrum part, necessary to maintain the entanglement structure and give a pure state.

4.5.3 Subregions of pure AdS_3

Finally, we will consider the reduced state on interval subregion of pure AdS. Actually, the subregion complexity of general subregions of AdS_3 was computed according to CV in [108]. It remains, however, to repeat that computation for CA, and to compute the purification complexity of such subregions, by considering all (or at least a large family of) geodesic completions of the entanglement wedge. The state on any particular interval subregion in pure AdS_3 is related to the state on other interval subregions, whether of the global boundary or the Poincaré boundary, by boundary conformal transformations, and the entanglement wedge to which it is dual can be related to other entanglement wedges by bulk isometries. The entanglement wedge may also be isometrically mapped to an entanglement wedge of a subregion of the boundary of the BTZ black hole, or more generally to a subregion of a single side of the n sided genus g black hole. These transformations, however, will not, in general, preserve the cutoff, and so we must keep track of how the cutoff transforms under such transformations.

To begin with, we will consider an interval of length $2R$ along with a

cutoff defined by constant Poincaré bulk coordinate z, namely, we will put a hard cutoff at $z = \delta$. The metric in this scenario is the familiar

$$ds^2 = \frac{L^2}{z^2}\left(-dt^2 + dx^2 + dz^2\right). \tag{4.23}$$

One purifying geometry is of course the entire Poincaré patch, the complexity of which can be computed to be (according to CA)

$$C = \frac{V_x L}{4\pi^2 \hbar G \delta}\left[\log\left(\frac{\tilde{L}}{\delta}\right) - 3\right] \tag{4.24}$$

where L is the AdS length scale and $\tilde{L}$ is an arbitrary length scale. Periodically identified Poincaré space, where we identify x with $x + a$, also provides a purifying geometry for our interval, provided the periodic identification does not change the RT surface. This requires that the length of our interval must not be greater than half the length of the periodically identified boundary. One may see this as follows: Consider a region of length a on the Poincaré patch periodically identified as $x \sim x + R$. Clearly, for $\frac{a}{R}$ sufficiently small, the entanglement wedge of the region is the same as in the full Poincaré patch. How small though does $\frac{a}{R}$ need to be? In the periodically identified geometry, our interval from $x = 0$ to $x = a$ is homologous to the interval from $x = a$ to $x = R$. As a consequence, there are two surfaces competing to be the global minimum, one which lifts in the full Poincaré patch to the usual RT surface for the interval of interest, and one which lifts instead to the RT surface of the interval from $x = a$ to $x = R$. Clearly, the 'usual' RT surface wins out whenever $a < R - a$, i.e. when $\frac{a}{R} < \frac{1}{2}$. Because it is clear that the complexity

of such a purification grows monotonically with R, the lowest complexity in this family will be given by $R = 2a$, right at the point of transition between the two minima. The complexity of this periodically identified geometry will be the same as for the non-identified case, but with the infinite transverse volume simply replaced by $2R$, yielding

$$C^P(R) \leq \frac{LR}{2\pi^2 \hbar G \delta} \left[\log\left(\frac{\tilde{L}}{\delta}\right) - 3 \right] \tag{4.25}$$

Notice now that if we scale all the coordinates, as well as the size of our region and our cutoff, by a uniform constant α, that is an isometry, such that the image of our original cutoff entanglement wedge is the new cutoff entanglement wedge (with the new cutoff). If one does this while holding $\tilde{L}$ fixed, one may, in fact, cause the complexity of the regulated complexity to become negative. This may be avoided, however, if we scale $\tilde{L}$ along with the coordinates too, and the purification complexity bound found above is fixed under such rescalings.

We may also embed such regions as subregions of a single side of a BTZ black hole, or even to an entire side of a planar BTZ black hole (although the corresponding cutoff will not appear natural). To see this, first, consider that the entanglement wedge of an interval on the Poincaré patch may be mapped by a simple change of coordinates to one side of AdS-Rindler. By applying the map corresponding to our region of interest, we can get our entanglement wedge as one side of AdS-Rindler, and by considering a larger interval containing ours, we may get our interval as a subregion of the boundary

of one side of AdS-Rindler. Notice that the AdS-Rindler metric may be written as

$$ds^2 = \frac{L^2}{z^2}\left[-f(z)dz^2 + \frac{dz^2}{f(z)} + L^2 d\chi^2\right] \tag{4.26}$$

where $f(z) = 1 - \frac{z^2}{L^2}$. This is exactly the same metric as the planar BTZ black hole with $z_h = L$. Replacing $f(z)$ by $f(z) = 1 - \frac{z^2}{z_h^2}$ then, we have AdS-Rindler when $z_h = L$, but the metric is invariant under scaling all the coordinates along with z_h (but not the AdS length scale L) by any constant α. The rescaling gives us an isometry between AdS-Rindler and a BTZ black hole of any temperature. Composing the two isometries we have found, we may then embed our regulated entanglement wedge either as a full side of a BTZ black hole or as the entanglement wedge of a subregion of a single boundary. We may also see that the entanglement wedge of our interval may be embedded into BTZ by recalling that BTZ black holes (as a specific example of the n-sided genus g construction discussed above) may be obtained by a quotient of pure global AdS_3. Clearly then, any interval subregion of the boundary of AdS_3 may be mapped by a conformal transformation to an interval lying entirely inside a fundamental domain of our quotient space. Because such subregion lies entirely in a fundamental domain, that interval may be thought of as a subregion on the boundary of the quotient space. Either way, we may minimize the resulting embedding over a number of parameters, such as the size of the BTZ subregion or the BTZ temperature, but first, let us come back to the n sided genus g solutions discussed above. Clearly, for any embedding into a single side of a BTZ geometry, these also form a family of geodesic completions

of the entanglement wedge of our interval. However, the conclusion from considering this family is no different from those we already saw for the BTZ thermal state. For CV and CV2.0, the complexity increases both with the number of sides n and the genus g. For CA, the complexity increases in n (at least for a sufficiently small choice of the cutoff), but decreases without bound with increasing g. This leads to the same problems as before and doesn't tell us anything particularly new.

4.6 Conclusion

In this work, we have estimated the purification complexity of the reduced state on a boundary subregion holographically, by considering different geodesic completions of the dual entanglement wedge, and by considering different cut-offs, corresponding to different course grainings of the purifying state. We have shown that according to CV and CV2.0, the optimal holographic purification is given by a geodesic completion of the entanglement wedge with a cutoff which skirts the HRT surface of the compliment of our region. As such, the minimum complexity among holographic purifications reproduces the usual subregion complexity (possibly up to an extra boundary term, as discussed in section 4.3.3). As such, we may conclude that at least to leading order in the $\frac{1}{N}$ expansion, subregion complexity = purification complexity if either CV or CV2.0 is correct for geometries dual to pure states.

For CA, we still find that the subregion complexity corresponds to the complexity of a particular holographic purification, though we have no guar-

antee that there is not some other purification of smaller complexity. In fact, we have several explicit examples in which what naively appears to be a holographic purification is found to have a smaller complexity than the subregion complexity in question, and even that the complexity can become negative. From this we must choose from the following conclusions, namely that these combinations of geometry and cutoff are not genuinely holographic (i.e., they are not dual to some state in a boundary CFT), that the complexity = action conjecture is simply wrong, or that the complexity = action is a special case of a more general conjecture, so that in these cases CA does not apply and we must use the generalization. As an example of the last situation, one might imagine adding a term which depends explicitly on the Euler characteristic in order to 'fix' CA in case of arbitrary behind the horizon genus.

These results are in some tension with those found in [4]. In the case of CV, this tension is not so strong. While it is true that CV is superadditive (as the authors of that paper had pointed out), we argue that in most circumstances this is to be expected due to the existence of operations which can raise the complexity of a pure state while going unnoticed by the density matrices arising from a decomposition into subsystems. In the particular case that preparing the total state does not require any such operations (as may be the case for the $t_L = 0, t_R = 0$ thermofield double state decomposed on right and left factors), then subadditivity can be realized modifying the prescription for subregion complexity in CV by adding the boundary term discussed in 4.3.3. Once this modification is made, the arguments made in [4] that sub-

region complexity in CA matches purification complexity applies equally well to CV. For CA, the tension is perhaps stronger, though it mostly arises from cases not considered by those authors.

4.7 Appendix I: Calculation of two-sided BTZ Action

We here calculate the on shell action for the BTZ black hole with metric described by

$$ds^2 = \frac{L^2}{z^2}\left(-f(z)dt^2 + f(z)^{-1}dz^2 + L^2dx^2\right)$$
$$f(z) = 1 - \left(\frac{z}{z_H}\right)^2$$

We will allow the cutoffs on the left and right side to vary independently, though we still choose constant z surfaces, and we consider only the $t_L = t_R = 0$ slice. We denote these cutoffs as $z_L = \delta_L, z_R = \delta_R$, though they are not necessarily small.

We'll consider the total WdW patch action ($\mathcal{A}^T$), as well as that of the right subsystem ($\mathcal{A}^R$). The latter is obtained by restricting to the entanglement wedge of the subsystem, which is simply the right exterior of the black hole. The left subsystem action ($\mathcal{A}^L$) is the same as $\mathcal{A}_R$ with $\delta_R \to \delta_L$. Time reflection symmetry and additivity of the bulk action also allow for simple determination of the action on the behind-the-horizon regions to the future ($\mathcal{A}_F$) and past ($\mathcal{A}_P$) through $\mathcal{A}_F = \mathcal{A}_P = \frac{1}{2}(\mathcal{A}_T - \mathcal{A}_R - \mathcal{A}_L)$. These two bulk subregions are not expected to correspond to boundary state complexities in their own right so we do not compute them here.

We'll first use the prescription summarized in appendix C of [59] with the generators of null boundaries affinely parameterized. This leaves a dependence on the overall normalization of these generators (see equation 4.29). We'll also compute the boundary counterterms described in appendix B of [59], the inclusion of which makes the action result reparameterization invariant. In this appendix we report results with and without these terms.

4.7.1 Setup

Both the total state WdW patch and the left/right subregions we consider are "diamond shaped" on a conformal diagram, so we adopt a common labeling scheme for the boundaries and joints, shown in figure 4.10. In each case, the action $\mathcal{A}$ consists of a bulk contribution on the relevant volume $\mathcal{V}$, four contributions on null boundaries $\mathcal{N}_i$ ($i = 1, 2, 3, 4$), and four co-dimension two "joint" contributions[13]. We'll denote these joints as $\mathcal{J}_j$ ($j = 1, 2, 3, 4$). We'll also use sometimes use j_1 and j_2 to label the leftgoing/rightgoing null boundaries who's intersection forms the jth joint. For example for $j = 1$ the joint is the intersection of $\mathcal{N}_1$ and $\mathcal{N}_4$, so $(j_1, j_2) = (1, 4)$.

Before adding the term for reparameterization invariance, the action

[13]Note that a prescription using variable cutoff surfaces to define a family of purifications is more naturally suited to a joint (constant t) cutoff scheme as opposed to a timelike boundary cutoff, see fig. 4.11

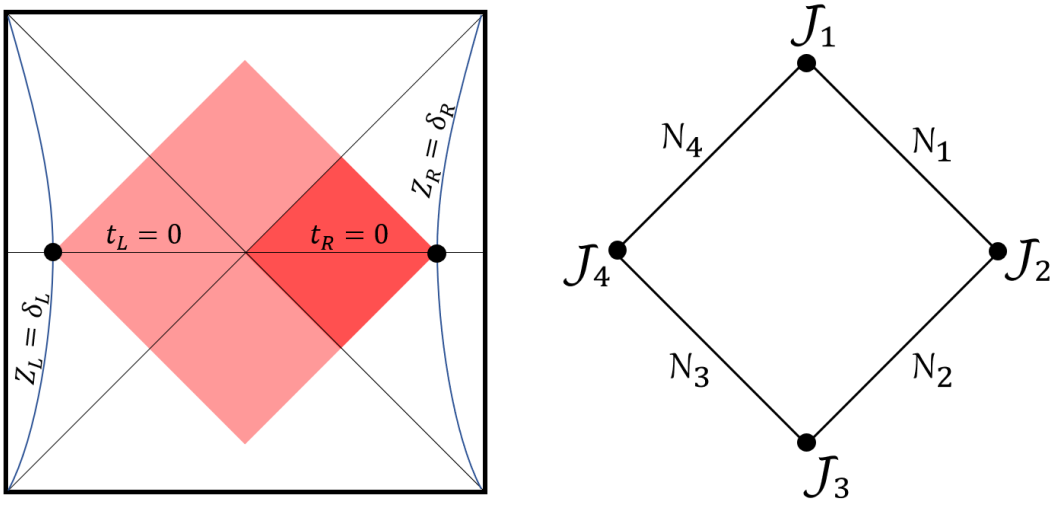

Figure 4.10: A conformal diagram for the two-sided BTZ spacetime is shown in the left panel. The Wheeler-DeWitt patch corresponding to the total state is shaded in light red, while dark red indicates the subregion of interest for the right subregion computation. Both regions are "diamond shaped" so we adopt a shared labeling scheme for the joints and null boundaries, as illustrated in the right panel.

on such a bulk regions is given by

$$16\pi G\,\mathcal{A} = \mathcal{S} = \int_{\mathcal{V}} (\mathcal{R} - 2\Lambda)\sqrt{-g}\,dV$$
$$- 2\sum_i \text{sign}(\mathcal{N}_i) \int_{\mathcal{N}_i} \kappa dS d\lambda_i + 2\sum_j \text{sign}(\mathcal{J}_j) \int_{\mathcal{J}_j} \ln|k_{j_1} \cdot k_{j_2}/2| dS$$

Here λ_i parameterizes the ith null boundary through $k_i^\alpha = dx^\alpha/d\lambda_i$ with κ defined by $k_i^\beta \nabla_\beta k_i^\alpha = \kappa\, k_i^\alpha$. We first choose this parameter to be affine, and express results in terms of arbitrary normalization constants for the k_i: $k_i \cdot \hat{t} = c_i$ with $\hat{t}$ being the static time coordinate vector $\hat{t} = \partial_t$. This leaves only the

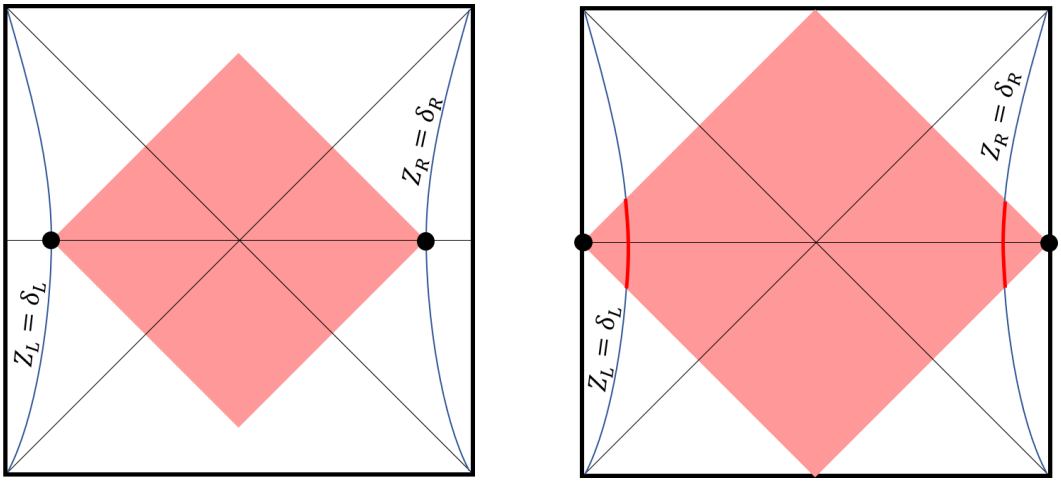

Figure 4.11: The cutoff prescription utilized in this work is that of the left diagram.

bulk and joint contributions, which we'll label $S_{\mathcal{V}}$ and $S_{\mathcal{J}}$.

$$S_{\mathcal{V}} = \int_{\mathcal{V}} (\mathcal{R} - 2\Lambda)\sqrt{-g}\, dV$$
$$S_{\mathcal{J}} = 2\sum_j \text{sign}(\mathcal{J}_j) \int_{\mathcal{J}_j} \ln|k_{j_1} \cdot k_{j_2}/2| dS$$

After computing these contributions we'll add counterterms associated with the null boundaries which make the action reparameterization invariant. These terms ultimately render the choices of the previous paragraph irrelevant (the affine parameterization and normalization of k_i^α), but they require the introduction of arbitrary lengthscale(s) which we'll denote $\tilde{L}_i$.

For the ith null boundary, the counterterm $\Delta S_{\mathcal{N}_i}$ is given by

$$\Delta S_{\mathcal{N}_i} = 2\,\text{sign}(\mathcal{N}_i) \int_{\mathcal{N}_i} \Theta_i \left(\ln|\tilde{L}\Theta_i|\right) dS d\lambda_i$$

where $\Theta_i = \frac{1}{\sqrt{\gamma}} \frac{d\sqrt{\gamma}}{d\lambda_i}$, the expansion parameter associated with λ_i. Here $\sqrt{\gamma}$ is

the volume element induced on the space transverse to fixed λ_i.

The normalization constants c_i, and the lengthscales $\tilde{L}_i$ should be the same on future-directed left-going and right-going null boundaries (this ensures, for instance, that the action goes to zero when the "diamond" is squashed along either null direction). At the end we'll impose this but we'll first denote them independently to illustrate more explicitly the replacement of c_i dependence by $\tilde{L}_i$ dependence. The signs for both null boundary and joint contributions will be listed in their respective subsections below.

4.7.2 Bulk contribution

The bulk contributions on each subregion simply integrate over the constant value of $R - 2\Lambda = -4/L^2$. The spacetime volume of each wedge (Right/Left/Future/Past) can be written $\mathcal{V} = \Delta x L^4 \left| \frac{1}{z_c} - \frac{1}{z_H} \right|$, where z_c is the position of the joint furthest from the bifurcation surface in each quadrant. In the right and left quadrants, z_c is simply the cutoff $z_c = \delta_{L,R}$. In the future and past quadrants we denote these joints as z_F and z_P, though symmetry dictates that these are at the same coordinate z-value, determined by the two cutoffs as

$$z_F = z_P = z_H \frac{1 + \sqrt{\frac{(z_H+\delta_R)(z_H+\delta_L)}{(z_H-\delta_R)(z_H-\delta_L)}}}{-1 + \sqrt{\frac{(z_H+\delta_R)(z_H+\delta_L)}{(z_H-\delta_R)(z_H-\delta_L)}}} \tag{4.27}$$

The bulk contribution in each quadrant can therefore be written in the unified form

$$S_{\mathcal{V}}^{\mathrm{R,L,F,P}} = -4\Delta x L^2 \left| \frac{1}{z_{R,L,F,P}} - \frac{1}{z_H} \right| \tag{4.28}$$

4.7.3 Joint contribution

Turning to the joint contributions, we utilize affinely parameterized future-directed boundary generators, normalized according to $k_i \cdot \hat{t} = -c_i$ where $\hat{t} = \partial_t$. For example in the right quadrant we choose future-directed ingoing and outgoing generators on $\mathcal{N}_1$ and $\mathcal{N}_2$ to be given by

$$\begin{aligned}(k_1)_\mu &= c_1\, \partial_\mu(-t + z^*(z)) \\ (k_2)_\mu &= c_2\, \partial_\mu(-t - z^*(z))\end{aligned} \tag{4.29}$$

where $z^*(z)$ is a BTZ 'tortoise' coordintate:

$$z^*(z) = \frac{z_H}{2} \log\left|\frac{z + z_H}{z - z_H}\right| \tag{4.30}$$

Analogous expressions apply for all k_i. For every joint we will consider, we have $\log|k_{j_1} \cdot k_{j_2}/2| = \log\left(\frac{c_{j_1} c_{j_2}\, z^2}{L^2 |f(z)|}\right)$ and $dS = L^2/z\, dx$, so the total joint contributions can be written

$$S_{\mathcal{J}} = 2\Delta x \sum_j \left(\text{sign}(\mathcal{J}_j) \frac{L^2}{z_j} \ln\left(\frac{c_{j_1} c_{j_2}\, z_j^2 z_H^2}{L^2 |z_j^2 - z_H^2|}\right)\right) \tag{4.31}$$

The signs of the joint contributions given by (see [59], appendix C) $\text{sign}(\mathcal{J}_1) = 1$, $\text{sign}(\mathcal{J}_2) = -1$, $\text{sign}(\mathcal{J}_3) = 1$, $\text{sign}(\mathcal{J}_4) = -1$.

4.7.4 Counterterm

Lastly, we compute the counterterms required for reparameterization invariance. This requires the introduction of a lengthscale which we'll denote $\tilde{L}_i$ on the null boundary $\mathcal{N}_i$. Once again these lengthscales should match for

left-going and right-going boundaries, but we first denote them independently to keep track of contributions and cancellations with joints. For each null surface we have a contribution depending on Θ_i, the expansion parameter associated with λ_i:

$$\Delta S_{\mathcal{N}_i} = 2\,\mathrm{sign}(\mathcal{N}_i)\int_{\mathcal{N}_i}\Theta_i\left(\ln|\Theta_i\tilde{L}|\right)dSd\lambda_i$$

For each of the four null surfaces in question, $\sqrt{\gamma} = (L^2/z)$ and so $\Theta_i = -\frac{1}{z}\frac{dz}{d\lambda_i}$. For the generators parameterized as in equation (4.29), we have $dz/d\lambda_i = \pm c_i\, z^2/L^2$. This allows us to write each contribution in the form:

$$\begin{aligned}\Delta S_{\mathcal{N}_i} =& -2\,\mathrm{sign}(\mathcal{N}_i)\Delta x\int_{z_i(\lambda_{\min})}^{z_i(\lambda_{\max})}\frac{L^2}{z^2}\log\left(\frac{c_i\tilde{L}_i z}{L^2}\right)dz\\ =&2\,\mathrm{sign}(\mathcal{N}_i)\Delta x\frac{L^2}{z}\left(1+\log\left(\frac{c_i\tilde{L}_i z}{L^2}\right)\right)\Bigg|_{z_i(\lambda_{\min})}^{z_i(\lambda_{\max})}\end{aligned} \tag{4.32}$$

With λ integrated to the future, parameterization invariance requires $\mathrm{sign}(\mathcal{N}_i) = -1$ for null boundaries which are to the future of the bulk subregion, and $+1$ for past null boundaries.

4.7.5 $\mathcal{A}^T$: full WdW patch action

We first compute the full action on the WdW patch. Summing the bulk contributions from each quadrant we have

$$S_{\mathcal{V}}^T = -4\Delta x L^2\left(\frac{1}{\delta_L}+\frac{1}{\delta_R}-\frac{1}{z_F}-\frac{1}{z_P}\right)$$

where $z_F = z_P$ are the futuremost and pastmost joint location, given by eq. (4.27). The joint contributions amount to

$$S_J^T = 2\Delta x L^2 \Bigg(\frac{1}{z_F} \log\left(\frac{c_1 c_4 \, z_F^2 z_H^2}{L^2(z_F^2 - z_H^2)} \right) + \frac{1}{z_P} \log\left(\frac{c_2 c_3 \, z_P^2 z_H^2}{L^2(z_P^2 - z_H^2)} \right) - \frac{1}{\delta_R} \log\left(\frac{c_1 c_2 \, \delta_R^2 z_H^2}{L^2(z_H^2 - \delta_R^2)} \right) - \frac{1}{\delta_L} \log\left(\frac{c_3 c_4 \delta_L^2 z_H^2}{L^2(z_H^2 - \delta_L^2)} \right) \Bigg)$$

and the counterterms together give

$$\begin{aligned} \Delta S_{\mathcal{N}}^T = {} & 4\Delta x L^2 \left(\frac{1}{\delta_L} + \frac{1}{\delta_R} - \frac{1}{z_F} - \frac{1}{z_P} \right) \\ & + 2\Delta x L^2 \Bigg(\frac{1}{\delta_R} \log\left(\frac{c_1 c_2 \tilde{L}_1 \tilde{L}_2 \delta_R^2}{L^4} \right) + \frac{1}{\delta_L} \log\left(\frac{c_3 c_4 \tilde{L}_3 \tilde{L}_4 \delta_L^2}{L^4} \right) \\ & - \frac{1}{z_F} \log\left(\frac{c_1 c_4 \tilde{L}_1 \tilde{L}_4 z_F^2}{L^4} \right) - \frac{1}{z_P} \log\left(\frac{c_2 c_3 \tilde{L}_2 \tilde{L}_3 z_P^2}{L^4} \right) \Bigg) \end{aligned}$$

The cancellation of c_i constants from the joint terms after the inclusion of counterterms is evident from the above expressions. In the combined answers we impose that $c_1 = c_3 = c$, $c_2 = c_4 = \bar{c}$, $\tilde{L}_3 = \tilde{L}_1$, $\tilde{L}_4 = \tilde{L}_2$, as well as $z_P = z_F$. The total action, reported without ($\mathcal{A}^T$) and with ($\tilde{\mathcal{A}}^T$) the counterterms is therefore as follows.

$$\begin{aligned} \mathcal{A}^T = {} & \frac{\Delta x L^2}{8\pi G} \Bigg[\frac{2}{z_F} \left(2 + \log\left(\frac{c\bar{c} \, z_F^2 z_H^2}{L^2(z_F^2 - z_H^2)} \right) \right) - \frac{1}{\delta_R} \left(2 + \log\left(\frac{c\bar{c} \, \delta_R^2 z_H^2}{L^2(z_H^2 - \delta_R^2)} \right) \right) \\ & - \frac{1}{\delta_L} \left(2 + \log\left(\frac{c\bar{c} \, \delta_L^2 z_H^2}{L^2(z_H^2 - \delta_L^2)} \right) \right) \Bigg] \\ \tilde{\mathcal{A}}^T = {} & \frac{\Delta x L^2}{8\pi G} \Bigg[\frac{2}{z_F} \log\left(\frac{L^2 z_H^2}{\tilde{L}_1 \tilde{L}_2 (z_F^2 - z_H^2)} \right) - \frac{1}{\delta_R} \log\left(\frac{L^2 z_H^2}{\tilde{L}_1 \tilde{L}_2 (z_H^2 - \delta_R^2)} \right) \\ & - \frac{1}{\delta_L} \log\left(\frac{L^2 z_H^2}{\tilde{L}_1 \tilde{L}_2 (z_H^2 - \delta_L^2)} \right) \Bigg] \end{aligned} \tag{4.33}$$

4.7.6 Subregion Action

We now compute the right subregion action, defined by restricting the Wheeler-deWitt patch to the entanglement wedge of the boundary subregion, which for the right boundary is simply the full right-side exterior of the black hole. In most respects the right subregion computation follows the same procedure as the previous section. The bulk contribution is given by equation (4.28) as

$$S_{\mathcal{V}}^{R} = -4L^2\Delta x\left(\frac{1}{\delta_R} - \frac{1}{z_H}\right)$$

However, evaluating joints directly on the horizon would naively give divergent results. We follow [4], by first setting null surfaces just outside the past and future horizons and taking the limit that they coincide with the horizons. More precisely, we define null boundaries $\mathcal{N}_3$ and $\mathcal{N}_4$ to pass through a joint just off the bifurcation surface: $t = 0, z = zH - \epsilon$ in the right quadrant (a different t would not affect the result). We then let $\epsilon \to 0$, which ultimately leaves a finite result for the total joint contribution. Because of the simplicity of the $z^*(z)$ function in equation (4.30), this procedure can be carried out exactly for any δ_R.

Before setting the c_i constants to c and $\bar{c}$, the contribution from joints $\mathcal{J}_1$, $\mathcal{J}_3$, and $\mathcal{J}_4$ is

$$S_{\mathcal{J}_1}^{R} + S_{\mathcal{J}_3}^{R} + S_{\mathcal{J}_4}^{R} = \frac{2L^2\Delta x}{z_H}\left(\log\left(\frac{c_1c_2z_H^2(z_H+\delta_R)}{4L^2(z_H-\delta_R)}\right)\right).$$

Adding the contribution from $\mathcal{J}_2$ and replacing $c_1 \to c$ and $c_2 \to \bar{c}$, the total

joint contribution to the subregion action is

$$S^R_{\mathcal{J}} = 2L^2\Delta x\left(\frac{1}{z_H}\log\left(\frac{c\bar{c}\,z_H^2(z_H+\delta_R)}{4L^2(z_H-\delta_R)}\right)-\frac{1}{\delta_R}\log\left(\frac{c\bar{c}\,\delta_R^2 z_H^2}{L^2(z_H^2-\delta_R^2)}\right)\right).$$

The counterterm contributions from null boundaries $\mathcal{N}_3$ and $\mathcal{N}_4$ vanish and the remaining pieces give:

$$\Delta S^R_{\mathcal{N}_1}+\Delta S^R_{\mathcal{N}_2} = 4L^2\Delta x\left(\frac{1}{\delta_R}-\frac{1}{z_H}\right)+2L^2\Delta x\left(\frac{1}{\delta_R}\log\left(\frac{c\bar{c}\,\tilde{L}_1\tilde{L}_2\delta_R^2}{L^4}\right)-\frac{1}{z_H}\log\left(\frac{c\bar{c}\,\tilde{L}_1\tilde{L}_2 z_H^2}{L^4}\right)\right).$$

Combining the previous expressions we find the total result for the subregion action without ($\mathcal{A}^R$) and with ($\tilde{\mathcal{A}}^R$) the counterterms:

$$\begin{aligned}\mathcal{A}^R &= \frac{L^2\Delta x}{8\pi G}\left(\frac{1}{z_H}\left(2+\log\left(\frac{c\bar{c}\,z_H^2(z_H+\delta_R)}{4L^2(z_H-\delta_R)}\right)\right)-\frac{1}{\delta_R}\left(2+\log\left(\frac{c\bar{c}\,\delta_R^2 z_H^2}{L^2(z_H^2-\delta_R^2)}\right)\right)\right)\\ \tilde{\mathcal{A}}^R &= \frac{L^2\Delta x}{8\pi G}\left(\frac{1}{z_H}\log\left(\frac{L^2(z_H+\delta_R)}{4\tilde{L}_1\tilde{L}_2(z_H-\delta_R)}\right)-\frac{1}{\delta_R}\log\left(\frac{L^2 z_H^2}{\tilde{L}_1\tilde{L}_2(z_H^2-\delta_R^2)}\right)\right)\end{aligned} \tag{4.34}$$

In the main text, our discussion centers on the result with counterterms included (reported there in a somewhat different form, see section 4.5.2).

Bibliography

[1] J. Couch, S. Eccles, W. Fischler and M.-L. Xiao, *Holographic complexity and noncommutative gauge theory*, *Journal of High Energy Physics* **2018** (2018) .

[2] J. Couch, S. Eccles, T. Jacobson and P. Nguyen, *Holographic complexity and volume*, *Journal of High Energy Physics* **2018** (2018) .

[3] E. Caceres, J. Couch, S. Eccles and W. Fischler, *Holographic purification complexity*, *Physical Review D* **99** (2019) .

[4] C.A. Agón, M. Headrick and B. Swingle, *Subsystem Complexity and Holography*, `1804.01561`.

[5] J.M. Maldacena, *The Large N limit of superconformal field theories and supergravity*, *Int. J. Theor. Phys.* **38** (1999) 1113 [`hep-th/9711200`].

[6] S.S. Gubser, I.R. Klebanov and A.M. Polyakov, *Gauge theory correlators from noncritical string theory*, *Phys. Lett.* **B428** (1998) 105 [`hep-th/9802109`].

[7] E. Witten, *Anti-de Sitter space and holography*, *Adv. Theor. Math. Phys.* **2** (1998) 253 [`hep-th/9802150`].

[8] L. Susskind, *Computational Complexity and Black Hole Horizons*, *Fortsch. Phys.* **64** (2016) 44 [1403.5695].

[9] L. Susskind, *Entanglement is not enough*, *Fortsch. Phys.* **64** (2016) 49 [1411.0690].

[10] D. Stanford and L. Susskind, *Complexity and Shock Wave Geometries*, *Phys. Rev.* **D90** (2014) 126007 [1406.2678].

[11] L. Susskind and Y. Zhao, *Switchbacks and the Bridge to Nowhere*, 1408.2823.

[12] A.R. Brown, D.A. Roberts, L. Susskind, B. Swingle and Y. Zhao, *Complexity, action, and black holes*, *Phys. Rev.* **D93** (2016) 086006 [1512.04993].

[13] J. Maldacena, *Eternal black holes in anti-de sitter*, *Journal of High Energy Physics* **2003** (2003) 021–021.

[14] J. Maldacena and L. Susskind, *Cool horizons for entangled black holes*, *Fortschritte der Physik* **61** (2013) 781–811.

[15] J. Watrous, *Quantum computational complexity*, 2008.

[16] T.J. Osborne, *Hamiltonian complexity*, *Reports on Progress in Physics* **75** (2012) 022001.

[17] S. Gharibian, Y. Huang, Z. Landau and S.W. Shin, *Quantum hamiltonian complexity*, *Foundations and Trends® in Theoretical Computer Science* **10** (2015) 159–282.

[18] G. Fubini, *Sulle metriche definite da una forme hermitiana*, *Atti del Reale Instituto Veneto di Scienze, Lettre ed Art* **63** (1904) 502.

[19] E. Study, *Kurzeste wege im komplexen gebiet*, *Mathematische Annalen* **60** (1905) .

[20] R.A. Jefferson and R.C. Myers, *Circuit complexity in quantum field theory*, *Journal of High Energy Physics* **2017** (2017) .

[21] S. Chapman, M.P. Heller, H. Marrochio and F. Pastawski, *Toward a definition of complexity for quantum field theory states*, *Physical Review Letters* **120** (2018) .

[22] L. Hackl and R.C. Myers, *Circuit complexity for free fermions*, *Journal of High Energy Physics* **2018** (2018) .

[23] A. Bhattacharyya, A. Shekar and A. Sinha, *Circuit complexity in interacting qfts and rg flows*, *Journal of High Energy Physics* **2018** (2018) .

[24] M. Guo, J. Hernandez, R.C. Myers and S.-M. Ruan, *Circuit complexity for coherent states*, *Journal of High Energy Physics* **2018** (2018) .

[25] R. Khan, C. Krishnan and S. Sharma, *Circuit complexity in fermionic field theory*, *Physical Review D* **98** (2018) .

[26] A.R. Brown, L. Susskind and Y. Zhao, *Quantum complexity and negative curvature*, *Physical Review D* **95** (2017) .

[27] A.R. Brown and L. Susskind, *Second law of quantum complexity*, *Physical Review D* **97** (2018) .

[28] M.A. Nielsen, *Quantum computation as geometry*, *Science* **311** (2006) 1133–1135.

[29] M.R. Dowling and M.A. Nielsen, *The geometry of quantum computation*, .

[30] A.R. Brown, D.A. Roberts, L. Susskind, B. Swingle and Y. Zhao, *Holographic Complexity Equals Bulk Action?*, *Phys. Rev. Lett.* **116** (2016) 191301 [1509.07876].

[31] J. Couch, W. Fischler and P.H. Nguyen, *Noether charge, black hole volume, and complexity*, *JHEP* **03** (2017) 119 [1610.02038].

[32] Z.-Y. Fan and M. Guo, *On the Noether charge and the gravity duals of quantum complexity*, 1805.03796.

[33] S. Lloyd, *Ultimate physical limits to computation*, *Nature* **406** (2000) 1047.

[34] S.P. Jordan, *Fast quantum computation at arbitrarily low energy*, *Physical Review A* **95** (2017) .

[35] W. Cottrell and M. Montero, *Complexity is simple!*, *Journal of High Energy Physics* **2018** (2018) .

[36] D. Carmi, S. Chapman, H. Marrochio, R.C. Myers and S. Sugishita, *On the Time Dependence of Holographic Complexity*, 1709.10184.

[37] D. Carmi, S. Chapman, H. Marrochio, R.C. Myers and S. Sugishita, *On the time dependence of holographic complexity*, *Journal of High Energy Physics* **2017** (2017) .

[38] B. Czech, J.L. Karczmarek, F. Nogueira and M. Van Raamsdonk, *The Gravity Dual of a Density Matrix*, *Class. Quant. Grav.* **29** (2012) 155009 [1204.1330].

[39] A. Almheiri, X. Dong and D. Harlow, *Bulk Locality and Quantum Error Correction in AdS/CFT*, *JHEP* **04** (2015) 163 [1411.7041].

[40] X. Dong, D. Harlow and A.C. Wall, *Reconstruction of Bulk Operators within the Entanglement Wedge in Gauge-Gravity Duality*, *Phys. Rev. Lett.* **117** (2016) 021601 [1601.05416].

[41] M. Alishahiha, *Holographic Complexity*, *Phys. Rev.* **D92** (2015) 126009 [1509.06614].

[42] M. Alishahiha, K. Babaei Velni and M.R. Mohammadi Mozaffar, *Subregion Action and Complexity*, 1809.06031.

[43] E. Caceres and M.-L. Xiao, *Complexity-action of singular subregions*, 1809.09356.

[44] K. Hashimoto, N. Iizuka and S. Sugishita, *Time Evolution of Complexity in Abelian Gauge Theories - And Playing Quantum Othello Game* -, 1707.03840.

[45] P. Caputa, N. Kundu, M. Miyaji, T. Takayanagi and K. Watanabe, *Liouville action as path-integral complexity: from continuous tensor networks to ads/cft*, *Journal of High Energy Physics* **2017** (2017) .

[46] B. Czech, *Einstein equations from varying complexity*, *Phys. Rev. Lett.* **120** (2018) 031601.

[47] R.-Q. Yang, *Complexity for quantum field theory states and applications to thermofield double states*, *Physical Review D* **97** (2018) .

[48] N. Margolus and L.B. Levitin, *The Maximum speed of dynamical evolution*, *Physica* **D120** (1998) 188 [quant-ph/9710043].

[49] N. Seiberg and E. Witten, *String theory and noncommutative geometry*, *JHEP* **09** (1999) 032 [hep-th/9908142].

[50] J.M. Maldacena and J.G. Russo, *Large N limit of noncommutative gauge theories*, *JHEP* **09** (1999) 025 [hep-th/9908134].

[51] A. Hashimoto and N. Itzhaki, *Noncommutative Yang-Mills and the AdS / CFT correspondence*, *Phys. Lett.* **B465** (1999) 142 [hep-th/9907166].

[52] R.-G. Cai and N. Ohta, *On the thermodynamics of large N noncommutative superYang-Mills theory*, *Phys. Rev.* **D61** (2000) 124012 [hep-th/9910092].

[53] M. Alishahiha, Y. Oz and M.M. Sheikh-Jabbari, *Supergravity and large N noncommutative field theories*, *JHEP* **11** (1999) 007 [hep-th/9909215].

[54] D.S. Berman, V.L. Campos, M. Cederwall, U. Gran, H. Larsson, M. Nielsen et al., *Holographic noncommutativity*, *JHEP* **05** (2001) 002 [hep-th/0011282].

[55] M. Edalati, W. Fischler, J.F. Pedraza and W. Tangarife Garcia, *Fast Scramblers and Non-commutative Gauge Theories*, *JHEP* **07** (2012) 043 [1204.5748].

[56] W. Fischler, A. Kundu and S. Kundu, *Holographic Entanglement in a Noncommutative Gauge Theory*, *JHEP* **01** (2014) 137 [1307.2932].

[57] J.L. Karczmarek and C. Rabideau, *Holographic entanglement entropy in nonlocal theories*, *JHEP* **10** (2013) 078 [1307.3517].

[58] W. Fischler, E. Gorbatov, A. Kashani-Poor, R. McNees, S. Paban and P. Pouliot, *The Interplay between theta and T*, *JHEP* **06** (2000) 032 [hep-th/0003216].

[59] L. Lehner, R.C. Myers, E. Poisson and R.D. Sorkin, *Gravitational action with null boundaries*, *Phys. Rev.* **D94** (2016) 084046 [1609.00207].

[60] A.R. Brown and L. Susskind, *The Second Law of Quantum Complexity*, 1701.01107.

[61] A.R. Brown, L. Susskind and Y. Zhao, *Quantum Complexity and Negative Curvature*, *Phys. Rev.* **D95** (2017) 045010 [1608.02612].

[62] M. Alishahiha, H. Ita and Y. Oz, *Graviton scattering on d6 branes with b fields*, *Journal of High Energy Physics* **2000** (2000) 002–002.

[63] T. Araujo, I. Bakhmatov, E.O. Colgain, J. Sakamoto, M.M. Sheikh-Jabbari and K. Yoshida, *Yang-baxter sigma-models, conformal twists, and noncommutative yang-mills theory*, *Physical Review D* **95** (2017) .

[64] T. Araujo, I. Bakhmatov, E.O. Colgain, J. Sakamoto, M.M. Sheikh-Jabbari and K. Yoshida, *Conformal twists, yang–baxter sigma-models and holographic noncommutativity*, *Journal of Physics A: Mathematical and Theoretical* **51** (2018) 235401.

[65] I. Bakhmatov, O. Kelekci, E.O. Colgain and M.M. Sheikh-Jabbari, *Classical yang-baxter equation from supergravity*, *Physical Review D* **98** (2018) .

[66] M. Headrick and V.E. Hubeny, *Riemannian and Lorentzian flow-cut theorems*, 1710.09516.

[67] R. Cleve, *An introduction to quantum complexity theory*, *Quantum Computation and Quantum Information Theory* (2001) 103–127.

[68] S. Aaronson, *The complexity of quantum states and transformations: From quantum money to black holes*, 2016.

[69] M. Moosa, *Evolution of Complexity Following a Global Quench*, 1711.02668.

[70] M. Moosa, *Divergences in the rate of complexification*, 1712.07137.

[71] I. Bengtsson and J.M.M. Senovilla, *The Region with trapped surfaces in spherical symmetry, its core, and their boundaries*, *Phys. Rev.* **D83** (2011) 044012 [1009.0225].

[72] V. Balasubramanian, A. Bernamonti, J. de Boer, N. Copland, B. Craps, E. Keski-Vakkuri et al., *Thermalization of Strongly Coupled Field Theories*, *Phys. Rev. Lett.* **106** (2011) 191601 [1012.4753].

[73] V. Balasubramanian, A. Bernamonti, J. de Boer, N. Copland, B. Craps, E. Keski-Vakkuri et al., *Holographic Thermalization*, *Phys. Rev.* **D84** (2011) 026010 [1103.2683].

[74] M. Banados, C. Teitelboim and J. Zanelli, *The Black hole in three-dimensional space-time*, *Phys. Rev. Lett.* **69** (1992) 1849 [hep-th/9204099].

[75] R. Emparan, *AdS / CFT duals of topological black holes and the entropy of zero energy states*, *JHEP* **06** (1999) 036 [hep-th/9906040].

[76] R.M. Wald, *General Relativity*, Chicago Univ. Pr., Chicago, USA (1984), 10.7208/chicago/9780226870373.001.0001.

[77] S. Chapman, H. Marrochio and R.C. Myers, *Holographic Complexity in Vaidya Spacetimes I*, 1804.07410.

[78] S. Chapman, H. Marrochio and R.C. Myers, *Holographic Complexity in Vaidya Spacetimes II*, 1805.07262.

[79] R. Bousso and N. Engelhardt, *New area law in general relativity*, *Physical Review Letters* **115** (2015) .

[80] R. Bousso and N. Engelhardt, *Proof of a new area law in general relativity*, *Physical Review D* **92** (2015) .

[81] N. Engelhardt and A.C. Wall, *Decoding the apparent horizon: Coarse-grained holographic entropy*, *Physical Review Letters* **121** (2018) .

[82] N. Engelhardt and A.C. Wall, *Coarse graining holographic black holes*, *Journal of High Energy Physics* **2019** (2019) .

[83] Y. Zhao, *Uncomplexity and Black Hole Geometry*, 1711.03125.

[84] V.E. Hubeny and H. Maxfield, *Holographic probes of collapsing black holes*, *JHEP* **03** (2014) 097 [1312.6887].

[85] I. Bengtsson and E. Jakobsson, *Black holes: Their large interiors*, *Modern Physics Letters A* **30** (2015) 1550103.

[86] M.J. Duncan, *Maximally slicing a black hole with minimal distortion*, *Physical Review D* **31** (1985) 1267.

[87] B. Czech, J.L. Karczmarek, F. Nogueira and M. Van Raamsdonk, *Rindler Quantum Gravity*, *Class. Quant. Grav.* **29** (2012) 235025 [1206.1323].

[88] M. Parikh and P. Samantray, *Rindler-AdS/CFT*, 1211.7370.

[89] H. Casini, M. Huerta and R.C. Myers, *Towards a derivation of holographic entanglement entropy*, *JHEP* **05** (2011) 036 [1102.0440].

[90] A.C. Wall, *Maximin Surfaces, and the Strong Subadditivity of the Covariant Holographic Entanglement Entropy*, *Class. Quant. Grav.* **31** (2014) 225007 [1211.3494].

[91] M. Headrick, *General properties of holographic entanglement entropy*, *JHEP* **03** (2014) 085 [1312.6717].

[92] E. Witten, "Canonical quantization in anti de sitter space, conference talk at 20 years later: The many faces of ads/cft." 2017.

[93] F. Estabrook, H. Wahlquist, S. Christensen, B. Dewitt, L. Smarr and E. Tsiang, *Maximally Slicing a Black Hole*, *Physical Review D* **7** (1973) 2814.

[94] I. Gelfand and S. Fomin, *Calculus of Variations*, Dover Books on Mathematics, Dover Publications (2012).

[95] D. Carmi, R.C. Myers and P. Rath, *Comments on Holographic Complexity*, *JHEP* **03** (2017) 118 [1612.00433].

[96] Z. Fu, A. Maloney, D. Marolf, H. Maxfield and Z. Wang, *Holographic complexity is nonlocal*, *JHEP* **02** (2018) 072 [1801.01137].

[97] H. Stoltenberg, *Properties of the (Un)Complexity of Subsystems*, 1807.05218.

[98] K. Umemoto and T. Takayanagi, *Entanglement of purification through holographic duality*, *Nature Phys.* **14** (2018) 573 [1708.09393].

[99] P. Nguyen, T. Devakul, M.G. Halbasch, M.P. Zaletel and B. Swingle, *Entanglement of purification: from spin chains to holography*, *JHEP* **01** (2018) 098 [1709.07424].

[100] N. Bao and I.F. Halpern, *Holographic Inequalities and Entanglement of Purification*, *JHEP* **03** (2018) 006 [1710.07643].

[101] V. Balasubramanian, M. DeCross, A. Kar and O. Parrikar, *Binding Complexity and Multiparty Entanglement*, 1811.04085.

[102] M. Headrick, V.E. Hubeny, A. Lawrence and M. Rangamani, *Causality & holographic entanglement entropy*, *JHEP* **12** (2014) 162 [1408.6300].

[103] D.R. Brill, *Multi - black hole geometries in (2+1)-dimensional gravity*, *Phys. Rev.* **D53** (1996) 4133 [gr-qc/9511022].

[104] S. Aminneborg, I. Bengtsson, D. Brill, S. Holst and P. Peldan, *Black holes and wormholes in (2+1)-dimensions*, *Class. Quant. Grav.* **15** (1998) 627 [gr-qc/9707036].

[105] D.R. Brill, *Black holes and wormholes in (2+1)-dimensions*, gr-qc/9904083.

[106] D. Marolf, H. Maxfield, A. Peach and S.F. Ross, *Hot multiboundary wormholes from bipartite entanglement*, *Class. Quant. Grav.* **32** (2015) 215006 [1506.04128].

[107] V. Balasubramanian, P. Hayden, A. Maloney, D. Marolf and S.F. Ross, *Multiboundary Wormholes and Holographic Entanglement*, *Class. Quant. Grav.* **31** (2014) 185015 [1406.2663].

[108] R. Abt, J. Erdmenger, H. Hinrichsen, C.M. Melby-Thompson, R. Meyer, C. Northe et al., *Topological Complexity in AdS3/CFT2*, 1710.01327.